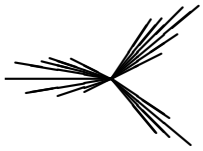

Instituto de Física Teórica
Universidade Estadual Paulista

DOCTORAL THESIS IFT–T.010/17

Symmetry-preserving contact interaction model for hadron structure and quark matter

FERNANDO ENRIQUE SERNA ALGARIN

Advisor

Dr. Gastão Inácio Krein

Co-Advisor

Dr. Bruno El-Bennich

October/2017

Acknowledgements

- First of all, special thanks must go to my advisor, Gastão Inácio Krein, for providing me with the opportunity to work with him on this subject. I am eternally grateful for his continued help and guidance during these 4 years. I also want to thank my co-advisor and friend Bruno El-Bennich for his continuous motivation and interest in this work and helpful discussions.

- I would like to thank my family, in special my mother Ilse, my father Taurino and my two sisters Merlys and Mildreth, who have always supported me in my studies and have given me much encouragement.

- I must also thank my friends: Indira, Melissa, Andrés, Rodolfo, Carlos and Jeiner, with whom I shared many pleasant moments. Also must thank to all my new friends accumulated during my time in the IFT-UNESP: Jose David, Adriana, Segundo, Jhon and Jhosep.

- This thesis was supported by Conselho Nacional de Desenvolvimento Científico e Tecnologico, CNPq.

Resumo

Nesta tese empregamos um modelo de interação de contato que preserva simetrias para estudar estrututura hadrônica e matéria de quarks. A interação de contato é uma representação de kernels não perturbativos usados em equações de Dyson-Schwinger e Bethe-Salpeter da Cromodinâmica Quântica (QCD). A ideia básica do modelo está baseada num esquema de subtração que evita passos tradicionais no cálculo de de integrais divergentes que invariavelmente levam a violações de simetrias. Em temperatura zero, as equações de Dyson-Schwinger para os propagadores dos quarks u, d, s and c são resolvidas e amplitudes de estado ligado de Bethe-Salpeter, que respeitam a invariância sob translações espaço-temporais e as identidades de Ward-Takahashi associadas com simetrias globais da QCD, são obtidas para calcular as massas e as constantes de decaimento eletrofracas dos mésons pseudoscalares π, K, D e D_s e dos mésons vetorias ρ, K^*, D^* e D_s^*. As predições do modelo estão em bom acordo com dados experimentais e da QCD na rede. Em adição, estendemos o modelo para temperaturas diferentes de zero; neste caso, o problema de violação de simetrias está restrito apenas às partes puramente divergentes porque os termos que dependem das distribuições térmicas são finitas e não requerem regularização. Finalmente, investigamos a dependência com a temperatura das contribuições das flutuações quânticas quark-π e quark-σ aos coeficientes de transporte de viscosidade de cisalhamento η e volumétrica ζ e as suas razões com a densidade de entropia s. As larguras térmicas originárias dessas fluctuações são calculadas com o formalismo de teoria de campos a temperatura finita de tempo real. Para esse cálculo, empregamos os resultados obtidos com as equações de Dyson-Schwinger e Bethe-Salpeter para a dependência com a temperatura das massas dos mésons e as contantes de acoplamento quark-méson. Os resultados para as razões η/s and ζ/s estão em bom acordo com resultados com a literatura obtidos com modelos e técnicas diferentes. Em particular, nossos resultados para η/s possuem um mínimo muito próximo ao limite inferior da conjectura AdS/CFT, $\eta/s = 1/4\pi$.

Palavras chaves: Cromodinâmica quântica, interação de contato, violao de simetrias, identidades de Ward-Takahashi,coeficientes de transporte, AdS/CFT.

Areas: Física de Hadrons, materia nuclear, plasma de quark e glúons.

Abstract

In thesis, a symmetry-preserving contact interaction model is used to study hadron structure and quark matter. The contact interaction is a representation of nonperturbative kernels used in Dyson-Schwinger and Bethe-Salpeter equations of Quantum Chromodynamics (QCD). The basic idea of the model is based on a subtraction scheme that avoids standard steps in the evaluation of divergent integrals that invariably lead to symmetry violation. At zero temperature, the Dyson-Schwinger equation is solved for the u, d, s and c quark propagators and the bound-state Bethe-Salpeter amplitudes respecting spacetime-translation invariance and the Ward-Green-Takahashi identities associated with global symmetries of QCD are obtained to calculate masses and electroweak decay constants of the pseudoscalar π, K, D and D_s and vector ρ, K^*, D^*, and D_s^* mesons. The predictions of the model are in good agreement with available experimental and lattice QCD data. In addition, we extend the model to nonzero temperature; here, the problem of symmetry violation is associated only with the purely divergent parts because the effects due to the thermal distributions are finite and do not need regularization. We compute the temperature dependence of the masses and decay constants of the pseudoscalar mesons considered here. Finally, we have investigated the temperature dependence of the contributions of quark-π and quark-σ quantum fluctuations to the transport coefficients of shear η and bulk ζ viscosities and their ratios to the entropy density s. The quark thermal widths originating those fluctuations are calculated with the formalism of real-time thermal field theory. For these calculations, we have used the results obtained via Dyson-Schwinger and Bethe-Salpeter equations for the temperature dependence of constituent quark and meson masses and quark-meson couplings. The results for the ratios η/s and ζ/s are in fair agreement with results of the literature obtained from different models and techniques. In particular, our result for η/s has a minimum very close to the conjectured AdS/CFT lower bound, $\eta/s = 1/4\pi$.

Key words: Quantum Chromodynamics, contact interaction, symmetry violation, Ward-Green-Takahashi identities, transport coefficients, AdS/CFT.

Areas: Hadron Physics, Nuclear matter, Quark gluon plasma.

Contents

Chapter 1

Introduction

Almost all of the visible matter in the universe is trapped in atomic nuclei. At the most fundamental level, that matter consists of quarks and gluons that are permanently confined in the interior of hadrons, a class of subatomic particles that interact via the strong force, like the proton and neutron. Quantum Chromodynamics (QCD) is the quantum field theory that describes the dynamics of quarks and gluons, it is the strongly interacting piece of the Standard Model. QCD describes strongly interacting matter under the extreme conditions reached in high energy particle collisions, but not much is known on how precisely quarks and gluons are kept permanently confined in the interior of hadrons.

It is a well established fact that hadronic processes at large momentum transfers are well described with perturbative calculations in quantum chromodynamics (QCD). The basic reason for the applicability of perturbative calculations in a theory meant to describe the strong interactions is asymptotic freedom [1,2], in that the interaction strength of QCD becomes weak at the small distances probed with large-momentum transfer processes. The smallness of the coupling is a prerequisite for a calculation based on an expansion in the coupling constant. Moreover, the calculations can be implemented in a systematic and well controlled fashion. But at small momentum transfers, or large distances, the QCD coupling is not small and one reaches the realm of strong QCD, where perturbation theory as an expansion in the coupling constant is not valid. Moreover, at such scales, the prominent nonperturbative phenomena of color confinement and dynamical chiral symmetry breaking set in. Confinement refers to the experimental fact that quarks and gluons are confined within hadrons; they do not appear in nature as asymptotic states like electrons and photons, for example. Dynamical chiral symmetry breaking (DχSB) refers to the

phenomenon of mass generation, in that from essentially massless quarks, hadrons masses are generated by the fundamental quark-gluon interaction. Nevertheless, there are a number of approaches for investigating this nonperturbative regime. Those methods are for example QCD sum rules, lattice QCD, AdS/CFT correspondence, chiral perturbation theory as well as the framework of Dyson-Schwinger and Bethe-Salpeter equations. This thesis we will concentrate only to the latter.

Dyson-Schwinger equations (DSEs) are the equations of motion of correlation functions of quark and gluon fields. Hadron bound states of quarks and gluons are identified as poles in the correlation functions; the amplitudes describing projections onto Fock-space components of the constituents are described by Bethe-Salperter equations (BSEs). Because of the infinite hierarchy of the equations, truncation schemes must be devised to obtain a tractable problem. Systematic, symmetry-preserving, nonpertubatively renormalizable truncation schemes, continuously developed since the 1990s, reached a high degree of sophistication and have proven very successful in describing and correlating a great variety of phenomena in the light-quark sector of QCD [3,4]. Symmetry-preserving schemes make use, in an essential way, of the Ward-Green-Takahashi (WGT) identities reflecting global symmetries and their explicit breaking; they impose stringent relationships between the interaction kernels entering DSEs for quark and gluon propagators and quark-gluon vertices and those entering BSEs for bound states [5].

Notwithstanding the advances and successes, challenges still remain in describing simultaneously the masses and decay constants of light- and heavy-flavored mesons within a single interaction-truncation scheme [6,7,8,9,10,11,12,13,14,15,16,17]; in particular, the disagreements with lattice QCD data for the electroweak decay constants of heavy-light mesons are substantial. Although one can expect that the challenges will be overcome in a foreseeable future, there is a pressing need for different pieces of information on the structure and interactions of such mesons for guiding new experiments at existing and forthcoming facilities, aiming at e.g. production of exotic hadrons like the X,Y,Z hadrons in heavy-ion collisions and creation of exotic nuclear bound states with charmed hadrons [18,19]. Predictions for masses, strong couplings, decay rates, and interaction cross sections are needed as functions of external parameters like temperature, baryon density and magnetic field, delivered in a form that can be used efficiently in transport and hydrodynamic simulation codes of

such complex experiments. Given these circumstances and demands, in the present thesis we explore the effectiveness in describing properties of D mesons of a simpler alternative based on a four-fermion contact interaction (CI) model embedded in a symmetry-preserving scheme [20].

Fermionic contact interactions find widespread applications in hadron physics as evidenced by the popular use of models inspired by the Nambu-Jona-Lasinio (NJL) [21]. A great deal of qualitative insight on the phenomenon of hadron mass generation via DχSB and the role of the π^0, $\pi^\pm$, K^0, $\bar{K}^0$, $K^\pm$, and η mesons as the associated (pseudo-)Goldstone bosons has been gleaned from such models—for reviews, see Refs. [22,23,24,25]. On the other hand, the lack of confinement and non-renormalizabilty are the major weaknesses of these CI models. The non-renormalizability, notably, carries along the danger of introducing gross violations of global symmetries due to the regularization procedure; ambiguities arising from momentum shifts in divergent integrals and severe dependence of results on choices of momentum sharing between a heavy and a light quark in a bound state are the main causes of the problems.

A new perspective, however, has recently emerged with the implementation by Gutiérrez-Guerrero, Bashir, Cloët and Roberts [125] (GBCR henceforth) of a confining, symmetry-preserving treatment of a vector-vector CI as a simplified *ansatz* for the gluon's two-point Schwinger function commonly employed in the kernel of the quark's DS equation [26,27,28,10]. By introducing a mechanism that ensures the absence of quark production thresholds [29], a feature of a confining theory, and embedding the interaction in a global-symmetry-preserving, rainbow-ladder (RL) truncation framework of the DS and BS equations [30,31], the GBCR scheme has enhanced the CI's capacity to describe in a unified manner a diverse array of phenomena that include the light-quark meson and baryon spectra as well as their electroweak, elastic and transition form factors [32,33,34,35,36,37,38,39,40] in appropriate kinematic regimes. Very recently, the scheme has been extended to calculate ground-state masses and weak decay constants of heavy charmonia [41], and also elastic and transition form factors of $\eta_c(1S)$ [42].

In this thesis, we examine the GBCR approach within the perspective of a subtraction scheme that allows one to isolate symmetry-violating contributions in BS amplitudes for arbitrary momentum routing in occurring divergent integrals. The

scheme has been employed in NJL model calculations in vacuum [43,44] and at finite temperature and baryon density [139,126,135,136], and very recently to investigate the critical behavior of quark matter in presence of a chiral imbalance [45]. The scheme is inspired in the method introduced in Ref. [46], the aim of which is the treatment of divergent Feynman integrals without specification of an explicit regulator; it shares similarities [47] with the Bogoliubov, Parasiuk, Hepp, Zimmermann (BPHZ) renormalization subtraction scheme [48], which uses systematic subtractions of momentum space integrals to isolate divergences.

We here take advantage of the strengths of the subtraction scheme and apply it to heavy-light mesons within the CI approach. Heavy-light $Q\bar{q}$ (and $\bar{Q}q$) mesons, such as the B and the D, are interesting bound states of QCD. They are interesting because they are composed of quarks belonging to two limiting mass sectors of QCD with associated emergent approximate symmetries: the sector of light quarks $q = (u, d, s)$, with masses $m_q \ll \Lambda_{\rm QCD}$, and the sector of heavy quarks $Q = (c, b, t)$, with masses $m_Q \gg \Lambda_{\rm QCD}$, where $\Lambda_{\rm QCD}$ is the energy scale at which the theory becomes strongly coupled, thereby implying that the characteristic size of a typical hadron is $\Lambda_{\rm QCD}^{-1}$. In the $m_q \to\ 0$ limit, QCD acquires an $SU(3)_L \times SU(3)_R$ chiral symmetry that is dynamically broken by the strong QCD interactions to an $SU(3)_V$ flavor symmetry; the eight pseudoscalar mesons π^0, $\pi^\pm$, K^0, $\bar{K}^0$, $K^\pm$, and η are identified with the (pseudo-)Goldstone bosons associated with the dynamical breaking of the symmetry. In the $m_Q \to \infty$ limit, the interactions of a heavy quark, regardless of its flavor, within a heavy-light meson become independent of its spin, a feature that gives rise to a spin-flavor heavy quark $U(2N_h)$ symmetry—$2N_h = 2\,(\text{spin}) \times N_h\,(\text{heavy flavors})$. Moreover, since the average velocity v of the heavy quark in a $Q\bar{q}$ bound state is changed very little by the interactions, as $\Delta v = \Delta p/m_Q \sim \Lambda_{\rm QCD}/m_Q \ll 1$, the light quark dynamics occurs in the background of a strong color field of an essentially static spectator. Therefore, heavy-light mesons offer a unique opportunity to learn about features of (DχSB) in a spin- and flavor-independent environment provided by the heavy quark.

Heavy-light mesons were studied previously in the NJL model using a traditional cutoff regularization [49]. However, a wrong pattern in the ordering of the pseudoscalar decay constants, $f_D < f_\pi$ was found—the experimental pattern is $f_\pi < f_K < f_D$. More recently, a similar incorrect ordering in the decay constants

was encountered within the CI framework for heavy charmonia in Ref. [41]. In addition, as already mentioned, even implementing a more realistic interaction in the RL truncation of the DS and BS equations, the weak decay constants of heavy-light mesons compare unfavorably [7] with predictions of lattice-QCD and the D to D_s mass difference is vanishingly small [12]. Possible causes for the failure of this truncation in heavy-light systems have been put forward in Ref. [50]. While not being a substitute for a full-fledged QCD-based DS-BS framework currently under intense development, it is nonetheless legitimate to expect that the capacity of a CI scheme in providing useful insight on heavy-light mesons is enhanced when it respects fundamental spacetime and internal symmetries of QCD.

There is also pressing need for different pieces of information on properties of such mesons both in vacuum and at finite T for guiding experimental proposals at existing and forthcoming facilities. Examples are charmed-hadron production via $\bar{p}p$ annihilation processes [51,52,53], J/Ψ-nuclear bound states [54,55], production in heavy-ion collisions of exotic molecules like the $\Delta\bar{D}^*$ [56]. Having this in mind, we we extend to finite T the CI model developed for the vacuum. We extend the subtraction scheme to finite T; the situation is more complicated than in the vacuum because Lorentz covariance is broken at finite $T$and special care must be exercised to separate purely divergent contributions from thermal distribution functions, which are finite and do not need regularization. After setting up the scheme, we calculate the masses of π, K, D and D_s at finite T.

On the other hand, due to asymptotic freedom, at sufficiently high temperature and/or densities, the hadronic matter undergoes a phase transition into a new state of matter, the quark-gluon plasma (QGP). This new phase is composed of weakly interacting quarks and gluons. This fact leads to gain more interest to investigate properties of QCD at finite temperature and density. For example physics of the early universe just after the Big Bang can almost be described by a hot quark-gluon plasma with low density, while high matter density conditions can be found in the interior of neutron stars. A high-temperature, weakly interacting medium is naturally expected to be produced in heavy ion collision (HIC) experiments at high energies. However, the experimental finding of elliptic flow in HICs at the Relativistic Heavy Ion Collider (RHIC) leads to the interpretation that the medium produced in the collisions is actually a strongly interacting liquid, instead of a weakly interacting

gas. Therefore, this state is not accessible by perturbation theory and nonperturbative methods are necessary. This interpretation comes, in first place, from the ability of hydrodynamics to describe the RHIC data with a small value of the shear viscosity over entropy density ratio, η/s [57,58,59,60,61,62,63,64]. The shear viscosity coefficient η of a medium represents the ability of its constituents to transfer momentum over a distance comparable to their mean free path. When the interparticle coupling is strong, momentum transfer takes place easily and, therefore, the shear viscosity of the matter is small. Several theoretical studies have estimated the ratio η/s, at weak and strong couplings and for different temperature regimes a set of such studies is represented by Refs. [65,66,67,68,69,70]. An interesting feature of the results in Refs. [66,71,72,73] is that η/s reaches a minimum in the vicinity of a phase transition; the smallness of this minimum is significant in connection with a conjectured lower bound, $\eta/s = 1/4\pi$, known as the KSS bound, obtained in the context of AdS/CFT correspondence [74].

Similar to the shear viscosity, another transport coefficient is the bulk viscosity, ζ. It is defined as the proportionality constant between the non-zero trace of the viscous stress tensor to the divergence of the fluid velocity, and usually it appears associated with processes accompanied by a change in fluid volume or density. The bulk viscosity has received much less attention than the shear viscosity in hydrodynamical simulations because its numerical value is assumed to be very small, as it is directly proportional to the trace of the energy-momentum tensor which generally vanishes for conformally symmetric matter. However, lattice QCD simulations [75,76] have shown that the trace of the energy momentum tensor of hot and dense QCD might be large near the QCD phase transition, which in turn indicates a non-zero, and possibly large value of ζ as well as of ζ/s near the transition temperature. In the framework of pure-gauge lattice QCD, ζ/s near the transition temperature is estimated in Ref. [77]. Analytical calculations employing different techniques and models have been used for estimating ζ of strongly interacting matter, important references are for example [78,79,80]; some of those indicate a divergent behavior for ζ near the transition temperature.

In thesis also we employ the CI model to evaluate the temperature dependence of the shear and bulk viscosities in the vicinity of the crossover temperature. A practical and transparent way to evaluate the contributions of quark-meson fluctuations

to viscosities is to evaluate one-loop quark self-energy diagrams to obtain the quark relaxation time or, equivalently, the quark thermal width. Adopting this method, we first analyzed the detailed Landau cut structures of the quark self-energy for quark-π and quark-σ loops, where the temperature dependence of the quark and meson masses and their couplings plays an important role in its on-shell contributions. The present work explicitly demonstrates the nontrivial contributions of the temperature dependence and momentum dependence of the quark thermal width to the viscosities, in the kinematic domains where the quark pole remains within the regions of the Landau cut.

This thesis is organized as follows: In chapter. 2 we review some important aspects of QCD. We discuss its origins, passing by the experimental and theory facts that led to the establishment of QCD. We present some general features and properties of the QCD's action, local and internal symmetries are studied, specifically the consequence of the chiral symmetry in the hadronic spectrum. Aspects as quantization and renormalization of the QCD's action also are considered. In the last part of the chapter, two important nonperturbative methods of QCD are discussed; lattice QCD and DSEs. Here, we mainly concentrate on the quark DSE.

Chapter 3 we implement the functional formalism to derive the meson BSE. We obtain a normalization condition for the Bethe-Salpeter amplitudes, that are needed to compute meson properties. In addition, in this chapter, we introduce the axial-vector Ward-Green-Takahashi identity (WGTI). Finally, we discuss a little bit about the solution method for the BSE.

In chapter. 4 we introduce the CI approximation employed herein. After that, we introduce the subtraction scheme to deal with divergent integrals that occur in the Bethe-Salpeter kernels due to the simplification of the CI and discuss the consequences of the axial vector WGTI for these divergences. Then, we present the numerical results for masses and weak decay constant of the mesons of interest.

In chapter 5 we use the Matsubara formalism extend the CI approximation to finite temperature. Here we explain in detail how the subtraction scheme can be aplicated in this case of nonzero temperature. We compute the temperature dependence of the masses and decay constants of the pseudoscalar mesons considered here.

In chapter 6, we address the formalism of computing shear and bulk viscosities

in terms of the quark thermal width, which is deducted from the quark self-energy diagram in the framework of real-time thermal field (RTF) theory. Finally, we present the numerical results for the shear and bulk viscosities and their ratios to the entropy.

Chapter 2

Aspects of Strong QCD

Quantum Chromodynamics (QCD) is the fundamental theory that describes the strong interactions. The strong force which is the responsible to held neutron and proton inside the atomic nucleus is around 100 times stronger than the electromagnetic (which binds electrons into atoms). The typical energy scale of the strong force is the mass of the proton ($\sim$ 1 GeV).

QCD is a local, non-Abelian gauge theory whose basic degrees of freedom are quarks and gluons. This is a unique theory with peculiar features. At short distances quarks and gluons are asymptotically free, but they are confined at large distances: only their bound states, the hadrons, can be observed in particle detectors. QCD was developed in the early seventies and its construction is a culmination of a long series of attempts to construct a theory for the strong interactions based on the principles of quantum field theory.

In this chapter, we will introduce some general aspects of QCD. The next section is dedicated to a review of the remarkable experimental and theory facts that led to the construction of the strong interaction theory that we know today.

2.1 A review of hadron Spectroscopy

With the discovery of the neutron by James Chadwick in 1932 [81] started the long path in understanding the strong interactions that even today is not yet understood very well. The discovery of this newly particle indicated that the nuclei consist of protons and neutrons, with the strong force being the responsible for holding them together. In the same year, in order to explain why proton and neutron have approximately the same mass, Heisenberg introduced the notion of isospin symmetry

[82]*. Then in 1935, Yukawa proposed that the nuclear force could be generated by the exchange of a "hypothetical" bosonic particle with nonzero mass [83]. In 1947 the existence of such particle was confirmed with the discovery of the pion in cosmic rays [84].

During the years of 1935 and 1965 many attempts by formulating a theory of strong interaction based on local interactions of the Yukawa type, using perturbation theory were made. But the problem with those theories was principally the fact of that the coupling constants invariably turned out larger, so that perturbation methods become inapplicable. Despite this, there was many progress in the understanding the general principles of quantum theory.

After the pion discovery and with apparition of new particle accelerators, many other strongly interacting particles were discovered in the fifties leading to the question of how to explain this wide range of new particles detected in accelerator experiments. During the 1950s and 1962s, Gell-Mann and Ne'eman described this new zoo of particles in a symmetry scheme based on the group SU(3), which is the group of unitary 3×3 matrices with determinant 1. The scheme, that is an extension of isospin flavor symmetry, classified the hadrons into two main groups, in analogy to as the Periodic Table classifies the chemical elements. In this new scheme called of "eighfold way" [85,86,87], the observed hadrons were classified as a members of a specific representation of SU(3). The baryons with $J = 1/2$ were grouped into an octet while those baryons with $J = 3/2$ belonged in a decuplet. On the other hand, the mesons could be grouped into an octet and a singlet, see Fig. 2.1. From the figure we see that the baryon octet contains the two nucleon (proton and neutron), the three Σ hyperons, the Λ hyperon and two Ξ hyperons. In the meson octet one has three pions, the two η mesons, the two K kaons and the two antikaons $\bar{K}$. In 1961, nine baryons resonances were observed (the four $\Delta's$, the three $\Sigma^{*'}s$ and the two $\Xi^{*'}s$), but these could not be members of an octet. Gell-Mann and Ne'eman proposed that they could be described by a decuplet, but one particle was missing. With this, they had predicted the existence of a new particle, the Ω^-, which was discovered with a mass of 1680 MeV at the Brookhaven National Laboratory in 1964 [88].

*Proton and neutron are considered as different states of the same particle of isospin 1/2, with isospin projections $I_3 = \pm 1/2$.

At that time it was not very clear why members of a triplet which corresponds to the fundamental representation of SU(3) were not observed in experiments. This fact led to Gell-Mann to formulate that hadrons are composed of more elementary constituents, which he called quarks [89,90,91]. These hypothetical particles are spin-1/2 fermions with fractional charge and come in three different flavors: up (u) with $Q_u = 2/3\,e$, down (d) with $Q_d = 1/3\,e$ and strange (s) with $Q_s = -1/3\,e$.

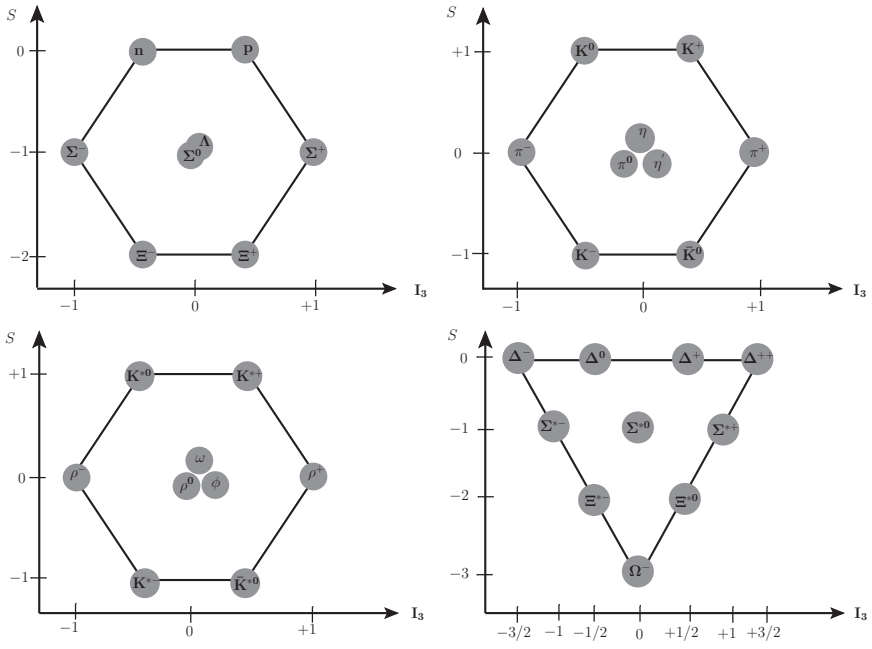

Figure 2.1: Hadrons in SU(3) representation within the "eighfold way".

In this scheme, baryons are made up of three valence quarks, while mesons can be made up by a quark and an antiquark. For example, the proton is a bound-state of two u quarks and one d quark (uud), while the positive pion is made up by one u quark and one $\bar{d}$ antiquark ($u\bar{d}$). In the fundamental representation $\mathbf{3}$ ($\bar{\mathbf{3}}$), baryons and mesons are a the direct product

$$\begin{aligned} \text{Barion} &= \mathbf{3} \otimes \mathbf{3} \otimes \mathbf{3} = \mathbf{10} \oplus \mathbf{8} \oplus \mathbf{8} \oplus \mathbf{1} \ , \\ \text{Meson} &= \mathbf{3} \otimes \bar{\mathbf{3}} = \mathbf{1} \oplus \mathbf{8} \ . \end{aligned} \tag{2.1}$$

In the following years, new hadrons were discovered and other quark flavors needed to be introduced. Today, we know that there are six flavors of quarks:

$$u \text{ (up)}, \ d \text{ (down)}, \ s \text{ (strange)}, \ c \text{ (charm)}, \ b \text{ (bottom)}, \text{ and } t \text{ (top)}. \tag{2.2}$$

In addition to the success of the quark model, also progress was made in the non-relativistic framework with the use of dynamical models [92]. In these models the effective degrees of freedom are the constituent quarks, whose origin is no explained and whose masses enter as parameters of the theory. The Hamiltonian of the system is composed by a kinetic part together a phenomenological potential for the inter-quark forces. Non-relativistically the Hamiltonian has the the form

$$H = \sum_i \left(\frac{\mathbf{p}_i^2}{2M_i} + M_i \right) + V(\mathbf{r}_1, \mathbf{r}_2, \mathbf{r}_3) \ , \tag{2.3}$$

where M_i are the constituent quark masses, $\mathbf{p}_i$ the momenta and $\mathbf{r}_i$ the individual quark coordinates. An example of a confining potential is that of a harmonic oscillator where the quark-antiquark potential has the form

$$V(\mathbf{r}_1, \mathbf{r}_2, \mathbf{r}_3) = \sum_{i<J} \frac{1}{2} K r_{ij}^2 \ , \tag{2.4}$$

where K is a constant and $r_{ij} = |\mathbf{r}_i - \mathbf{r}_j|$. There are of course many potential models which have been used to describe the spectrum of heavy hadrons like $c\bar{c}$ or $b\bar{b}$ [93,94,95,96,97].

On the other hand, to distinguish between the spin-1/2 and spin-3/2 baryons one combines the SU(3) flavour symmetry with the SU(2) of quark spin,

$$\begin{aligned} \mathbf{2} \otimes \mathbf{2} &= \mathbf{3} \oplus \mathbf{1} \ , \\ \mathbf{2} \otimes \mathbf{2} \otimes \mathbf{2} &= \mathbf{4} \oplus \mathbf{2} \oplus \mathbf{2} \ . \end{aligned} \tag{2.5}$$

Considering that $\Psi_{\text{spin}} \otimes \Psi_{\text{flavor}}$ is symmetric, the possible spin-flavor combinations produce a spin-1/2 octet $(\mathbf{2}, \mathbf{8})$ and a spin-3/2 decuplet $(\mathbf{4}, \mathbf{10})$, which correspond to the observed ground states in Figure 2.1. By the Pauli principle one needs that the overall baryon wave function given by

$$\Psi = \Psi_{\text{space}} \otimes \Psi_{\text{spin}} \otimes \Psi_{\text{flavor}} \ , \tag{2.6}$$

should be antisymmetric, which would imply that its spatial part is antisymmetric and thus not s-wave, contrary to our expectations for ground states. One could build antisymmetric spin-flavor combinations, although this would yield $(\mathbf{2}, \mathbf{8})$ and $(\mathbf{4}, \mathbf{1})$ and thus no decuplet baryons in orbital ground states (the Δ^{++} is a particularly apposite example). The situation can be remedied by introducing a new quantum

number for each quark named color charge, which is associated with the group SU(3) [98,99]. This color symmetry is exact, i.e. not broken like the flavor symmetry. Then, by adding an antisymmetric component $\Psi_{\rm color}$ to the total baryon wave function the Pauli principle is not violated because the total wave function is antisymmetric in the color indices denoted by red (r), green (g) and blue (b), namely one has

$$\Psi = \Psi_{\rm space} \otimes \Psi_{\rm spin} \otimes \Psi_{\rm flavor} \otimes \Psi_{\rm color} \ . \tag{2.7}$$

One of the experimental confirmation of the number of colors were provided by the famous ratio of the cross-section for electron-positron annihilation into hadrons

$$R = \frac{\sigma(e^+e^- \to \text{hadrons})}{\sigma(e^+e^- \to \mu^+\mu^-)} = N_c \left[\left(\frac{2}{3}\right)^2 + \left(-\frac{1}{3}\right)^2 + \left(-\frac{1}{3}\right)^2 \right] = 2 \ , \tag{2.8}$$

where $N_c = 3$. Without the colors this ratio would be 2/3, but the experimental data were in agreement with a ratio of 2.

2.2 QCD's action

Using Euclidean space conventions defined in Appendix A, the QCD classical action that describes the physics of the strong interaction is given by

$$S_{\rm QCD} = \int d^4x \, \bar{\psi}_f^c(x) \left(\gamma \cdot D^{cc'} + \delta^{cc'} m_f \right) \psi_f^{c'}(x) + S_{\rm YM} \ , \tag{2.9}$$

$$S_{\rm YM} = \int d^4x \frac{1}{4} F^a_{\mu\nu}(x) F^a_{\mu\nu}(x) \ , \tag{2.10}$$

being ψ_f, $\bar{\psi}_f$ the quark and antiquark fields, where $f = 1, \cdots, N_f$ is the quark flavor index (ψ_f : u, d, s, c, b, $\cdots$), the indices c, $c' = 1$, 2, 3 and $a = 1, \cdots, 8$ are the color indices in the fundamental and adjoint representation of SU(3) respectively, $m_f = \text{diag}(m_u, m_d, m_s, \cdots)$ is the quark mass matrix in flavor space, γ^μ are the Dirac matrices, $\mu, \nu = 0, \cdots 3$ are the Lorenz indices, and D_μ is the covariant derivative given by:

$$D^{cc'}_\mu = \delta^{cc'} \partial_\mu - ig \, t_a^{cc'} \, A^a_\mu \ , \tag{2.11}$$

where g is the strong coupling constant, $t^a = \lambda^a/2$ are the generators of SU(3) which satisfy the Lie-algebra $[t^a, t^b] = if^{abc}t^b$, being λ^a the Gell-Mann's matrices. In addition, A^a_μ are the gauge fields, gluons, which are the carrier of the SU(3)_c colors forces, and $F^a_{\mu\nu}$ is the gluon field strength tensor:

$$F^a_{\mu\nu} = \partial_\mu A^a_\nu - \partial_\nu A^a_\mu + g f^{abc} \, A^b_\mu A^c_\nu \ , \tag{2.12}$$

where the f^{abc} are the structure constants of SU(3). The Yang-Mills action $S_{\rm YM}$ can be written as

$$\begin{aligned} S_{\rm YM} &= \int d^4x \left[-\frac{1}{2} A^a_\mu (\partial^2 \delta_{\mu\nu} - \partial_\mu \partial_\nu) A^a_\nu - \frac{g}{2} f^{abc} (\partial_\mu A^a_\nu - \partial_\nu A^a_\nu) A^b_\mu A^c_\nu \right. \\ &+ \left. \frac{1}{4} f^{abe} f^{cde} A^a_\mu A^b_\nu A^c_\mu A^d_\nu \right] . \end{aligned} \tag{2.13}$$

From this explicit form of the Yang-Mills action we can see that the first term proportional to A^2 contains the inverse of the gluon propagator, which in momentum space it is proportional to a transverse projector that cannot be inverted. As we will see later, this problem will be solved by the introduction of the Gauge-fixing term into the QCD's action. The remaining terms proportional to A^3 and A^4 constitute the three and four gluon vertices respectively, which is represented in Fig. (2.2). This means that QCD's action exhibits the feature the self-interacting gauge field.

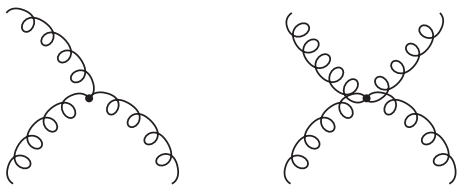

Figure 2.2: Gluon self-interactions generate by QCD's action.

The action given by Eq. (2.9) is constructed to be invariant under global and local transformations. Therefore, under local transformation the quarks and gluons fields transform as

$$\psi \to \psi' = U(\theta)\psi \ , \tag{2.14}$$

$$A^a_\mu \to A'^a_\mu = U(\theta) A^a_\mu U^{-1}(\theta) + \frac{i}{g} U(\theta) \partial_\mu U^{-1}(\theta) \tag{2.15}$$

where $U(\theta)$ is a local gauge transformation given by

$$U(\theta) = \exp(i\theta^a \cdot t_a) \ , \tag{2.16}$$

with θ^a being the space-time dependent parameters. On the other hand, the strength tensor (2.12) transform as

$$F'^a_{\mu\nu} = U(\theta) F^a_{\mu\nu} U^{-1}(\theta) \ . \tag{2.17}$$

From this, one notes that the contraction of two $F_{\mu\nu}$ are not invariant; only its the color contraction becomes invariant:

$$\begin{aligned} \mathrm{Tr}\left[F'_{\mu\nu}F'_{\mu\nu}\right] &= \mathrm{Tr}\left[U(\theta)F_{\mu\nu}U^{-1}(\theta)U(\theta)F_{\mu\nu}U^{-1}(\theta)\right] \\ &= \mathrm{Tr}\left[F_{\mu\nu}F_{\mu\nu}\right] \ . \end{aligned} \tag{2.18}$$

where we have used the cyclic property of the trace.

In addition to gauge symmetry, the classical QCD's action has a set of well-known strong-interaction symmetries. These include charge conjugation, parity, time reversal and all the flavor symmetries of the quark model. In the next section, we will focus on the two most important symmetries for the study of hadron physics in QCD: flavor and chiral symmetries.

2.3 Flavor and Chiral symmetries

If we consider the six quark flavors, the QCD's action exhibits an additional SU(6) flavor symmetry in the limit that the quark masses are equal. However, this symmetry is not realized in nature where we have

Light quark sector:

$$m_u \sim m_d \ \sim \ 2-6\,\mathrm{MeV}\ ,\ m_s \sim 150\,\mathrm{MeV}\ ,$$

Heavy quark sector:

$$m_c \sim 1200\,\mathrm{MeV}\ ,\ m_b \sim 4300\,\mathrm{MeV}\ ,\ m_t \sim 173000\,\mathrm{MeV}\ .$$

These masses are generate by the Higgs mechanism, but the origin of why are very different are still unknown and cannot be explained by the Standard Model of Fundamental Particles. The only source of flavor symmetry breaking in the QCD's action comes from the mass term. Therefore, in the light quark sector the flavor symmetry can be considered approximate, while in the heavy quark sector the flavor symmetry is severely broken.

In the limit of massless quarks $m_f = 0$, the QCD's action Eq. (2.9) is invariant under

$$U(1)_{\mathrm{V}} \otimes SU(6)_{\mathrm{V}} \otimes U(1)_{\mathrm{A}} \otimes SU(6)_{\mathrm{A}}\ ,$$

and by Noether's theorem we have a conserved vector and axial vector currents which are given by

$$J_a^\mu(x) = \bar{\psi}(x) i t^a \gamma_\mu \psi(x) \ , \quad J_{5\,a}^\mu(x) = \bar{\psi}(x) i t^a \gamma_5 \gamma_\mu \psi(x) \ , \tag{2.19}$$

where $t^a = \lambda^a/2$, with $a = 1, 2, \cdots 35$, are the generators of SU(6). For the case of two flavor we have $t^a = \tau^a/2$, with $a = 1, 2, 3$, and being τ^a the Pauli matrices and for three flavors t^a is related to the Gell-Mann matrices as previously we have mentioned. In addition, Noether's theorem states that there are also conserved charges which is this case are given by

$$Q_a(t) = \int d^3x J_a^0(x) \ , \quad Q_{5\,a}(t) = \int d^3x J_{5\,a}^0(x) \ . \tag{2.20}$$

In this limit, the QCD's action Eq. (2.9) can be separated into a sum of two actions for the left and right-handed Weyl-spinors:

$$S_{\rm QCD} = S_{\rm QCD}^L + S_{\rm QCD}^R \ , \tag{2.21}$$

with

$$\psi_L = \frac{1-\gamma_5}{2}\,\psi \ , \qquad \psi_R = \frac{1+\gamma_5}{2}\,\psi \ , \tag{2.22}$$

$$\bar{\psi}_L = \bar{\psi}\,\frac{1+\gamma_5}{2} \ , \qquad \bar{\psi}_R = \bar{\psi}\,\frac{1-\gamma_5}{2} \ . \tag{2.23}$$

In the general case of a non-vanishing mass matrix ($\mathbf{m} \neq 0$), this separation into two independent actions cannot be possible due to the mass term ($\bar{\psi}\mathbf{m}\psi$), which is not invariant under axial rotations. In this case, the divergences of the Noether's currents defined above are given by

$$\partial_\mu J_a^\mu(x) = i\bar{\psi}(x)\,[t^a, \mathbf{m}]\,\psi(x) \ , \quad \partial_\mu J_{5\,a}^\mu(x) = i\bar{\psi}(x)\,\{\gamma_5\, t^a, \mathbf{m}\}\,\psi(x) \ . \tag{2.24}$$

In the case of identical current-quark masses, the first relation states the vector current conservation, which describes the flavor symmetry of the light quark sector of QCD and the $U(1)_V$ symmetry corresponds to baryon number conservation. On the other hand, from the second relation we note that the axial symmetries $SU(6)_A$ and $U(1)_A$ are only conserved in the case of a vanishing mass term in the QCD's action. This situation is known as explicit chiral symmetry breaking.

2.4 Dynamical chiral symmetry breaking

Dynamical chiral symmetry breaking (DχSB) is the mechanism that transforms the bare quark in the QCD action into a "constituent quark". In general, the realization of the chiral symmetry is manifest as two possibilities: a Wigner-Weyl mode and Nambu-Goldstone mode. The broken symmetry indicates that the action or Lagrangian is invariant under all symmetries but the vacuum is not.

To see that, let consider the $SU(2)$ sector with the light quark u and d. In the chiral limit the QCD action is invariant under $SU(2)_L \otimes SU(2)_R$ transformations, whose generators are appropriate linear combinations of the vector and axial charges, Q_a and Q_{5a} defined in Eq. (2.20). Then, we can write these generators as

$$\begin{aligned} Q_a^L &= \frac{1}{2}(Q_a - Q_{5a}) \ , \\ Q_a^R &= \frac{1}{2}(Q_a + Q_{5a}) \ . \end{aligned} \tag{2.25}$$

These operators obey the following commutation relations

$$\begin{aligned} \left[Q_a^L(t), Q_b^L(t)\right] &= i\epsilon_{abc}\, Q_c^L(t) \ , \\ \left[Q_a^R(t), Q_b^R(t)\right] &= i\epsilon_{abc}\, Q_c^R(t) \\ \left[Q_a^L(t), Q_b^R(t)\right] &= 0 \ , \end{aligned} \tag{2.26}$$

which define the chiral $SU(2)_L \otimes SU(2)_R$ algebra, and the ordinary flavor transformations $SU(2)_V$, from a subgroup of chiral group. We have that the generators of the chiral group commute with the Hamiltonian of QCD,

$$[Q_a, H_{\rm QCD}] = [Q_{5a}, H_{\rm QCD}] = 0 \ . \tag{2.27}$$

Then, to see the implications of this symmetry in the hadronic spectrum, let us consider $|h, \pm\rangle$ to be an eigenstate of $H_{\rm QCD}$, which represents a hadron with mass M_h at rest. In the hadronic state $|h, \pm\rangle$, the $\pm$ labels refer to the intrinsic parity of the state, and spin labels have been omitted. Then, one has for example

$$H_{\rm QCD}|h, +\rangle = M_h|h, +\rangle \ , \tag{2.28}$$

where we have assumed that the above initial state has positive parity. The commutation relation given by Eq. (2.27) implies that the states $Q_a|h, +\rangle$ and $Q_{5a}|h, +\rangle$

are degenerate with the state $|h\rangle$. Explicitly this is,

$$H_{\rm QCD}(Q_a|h,+\rangle) = M_h(Q_a|h,+\rangle) \tag{2.29}$$

$$H_{\rm QCD}(Q_{5a}|h,+\rangle) = M_h(Q_{5a}|h,+\rangle) \ . \tag{2.30}$$

But the axial charges are pseudoscalar objects and change the parity of the state, namely

$$Q_{5a}|h,+\rangle = |h,-\rangle \ , \tag{2.31}$$

which leads to writhe Eq. (2.30) as

$$H_{\rm QCD}|h,-\rangle = M_h|h,-\rangle \ , \tag{2.32}$$

This implies that hadrons must manifest in isospin multiplets and for each multiplet there is the corresponding opposite parity multiplet. It is knows as Wigner-Weyl mode realization of the chiral symmetry. However, from the experimental hadron spectrum we only observe multiplets with near degenerate mass (for example the three pion, $\pi^0, \pi^\pm$). This means that in nature no parity doublets of massive particles with approximately equal masses are found in the hadronic spectrum.

The other alternative as we have said is the Nambu-Goldstone mode realization of the chiral symmetry. In the Wigner-Weyl mode, we have assumed that QCD vacuum, $|0\rangle$, (the ground state) is invariant under the symmetry group of transformations, namely

$$Q_a|0\rangle = 0 \ , \ \text{ and } \ Q_{5a}|0\rangle = 0 \ , \tag{2.33}$$

which means that the generators of the transformations annihilate the vacuum state. Nevertheless, the ground state may not be invariant under the continuous symmetry group of transformations, even if the action or Lagrangian is. The last conjecture is the so called Nambu-Goldstone chiral symmetry realization. In that case, the vacuum is not a symmetric state and the generators of the symmetry group do not annihilate it:

$$Q_{5a}|0\rangle \neq 0 \ . \tag{2.34}$$

It is said that the symmetry is dynamically (or spontaneously) broken and there exists massless Nambu-Goldstone bosons. Theses massless particles coupled to the

axial current, J^{μ}_{5a}, generating quantum numbers of the corresponding axial charges (pseudoscalar particles). For the case of three-flavor QCD, the massless Nambu-Goldstone bosons are identified with the eight light pseudoscalar mesons ($\pi^0, \pi^{\pm}$, $K^0, K^{\pm}$, $\bar{K}^0$ and η). However, in the real world, these hadrons have masses, but lightest compared with the masses of massive hadrons. They acquire small masses because an explicit broken symmetry which is due to the non-vanishing quark masses.

2.5 Correlation functions in QCD

The quantum field theory associated with the classical QCD's action Eq. (2.9) is defined by the path integral:

$$Z = \int \mathcal{D}[\Phi]\, e^{-S_{\rm QCD}[\Phi]} \ , \tag{2.35}$$

where $\Phi = \{\bar{\psi}, \psi, A, \bar{c}, c\}$ represents all (quarks, gluons, and ghosts) fields of the theory, $\mathcal{D}[\Phi] = \{\mathcal{D}\psi\mathcal{D}\bar{\psi}\mathcal{D}c\mathcal{D}\bar{c}\mathcal{D}A\}$ is the functional measure with respect to all fields included in the theory. In Eq. (2.41) $S_{\rm QCD}$ is given by

$$\begin{aligned} S_{\rm QCD}[\bar{\psi}, \psi, A, \bar{c}, c] &= \int d^4x\, \bar{\psi}_f(x)\, (\gamma\cdot D + m_f)\, \psi_f(x) \\ &+ S_{\rm YM}[A] + S_{\rm gf}[\bar{c}, c, A] \ , \end{aligned} \tag{2.36}$$

being $S_{\rm gf}$ the gauge-fixing action defined as

$$S_{\rm gf}[\bar{c}, c, A] = \int d^4x \left[\frac{1}{2\xi}\partial_\mu A^a_\mu(x)\partial_\nu A^a_\nu(x) - \partial_\mu \bar{c}^a(x) D^{ab}_\mu(x) c^b(x)\right] \ , \tag{2.37}$$

which is introduced to avoid the zero modes of the inverse of the gluon propagator. In Eq. (2.37) ξ is gauge- fixing parameter and D^{ab}_μ is the covariant derivative in the adjoint representation given by

$$D^{ab}_\mu(x) = \delta^{ab}\partial_\mu + g\, f^{abc} A^c_\mu(x) \ . \tag{2.38}$$

We note that the ghost fields only appear in the gauge fixing action and only interact with the gluon field. In addition, Eq. (2.37) is a consequence of the evaluation of the gauge fixing-condition in the path integral which involves the determinant of the Faddeev-Popov operator:

$$M^{ab}(x, y, A) = \partial_\mu D^{ab}_\mu(x)\delta^4(x - y) \ . \tag{2.39}$$

The physical properties of QCD can be extracted from Eq. (2.35) in term of correlation functions. For instance, the quark propagator is given by the expectation value of the operator $\mathcal{O} = \psi^c_\alpha(x)\bar{\psi}^{c'}_\beta(y)$, namely

$$\begin{aligned}\langle\psi^c_\alpha(x)\bar{\psi}^{c'}_\beta(y)\rangle &= \delta^{cc'}S_{\alpha\beta}(x-y) \\ &= \frac{1}{Z}\int \mathcal{D}[\Phi]\, e^{-S_{\rm QCD}[\Phi]}\psi^c_\alpha(x)\bar{\psi}^{c'}_\beta(y)\ . \end{aligned} \tag{2.40}$$

A more formal way to compute correlation functions can be made by the introduction of artificial sources into the path integral Eq. (2.35) via the addition of the term $\Phi\cdot J$:

$$Z[J] = \int \mathcal{D}[\Phi]\, e^{-S_{\rm QCD}[\Phi]+\Phi\cdot J}\ , \tag{2.41}$$

where $J = \{\eta, \bar{\eta}, J_\mu, \sigma, \bar{\sigma}\}$ representing the sources of the fields introduced above [†].

Correlation functions are obtained by taking functional derivatives of $Z[J]$ with respect to J and at the end set all the sources to zero. For example, the quark propagator Eq. (2.40) can be obtained by

$$S_{\alpha\beta}(x-y) = \frac{1}{Z[0]}\frac{\delta^2 Z[J]}{\delta\bar{\eta}_\alpha(x)\delta\eta_\beta(y)}\bigg|_{J=0}\ . \tag{2.42}$$

Usually, we are more interested in the connected and one-particle-irreducible (1PI) correlation functions (connected and amputated proper vertices). In fact, there is possible to generate connected correlation functions via the introduction of a new generating functional $W[J] = \ln Z[J]$. On the other hand, the proper vertices can be obtained by the introduction of the effective action $\Gamma[\Phi]$ via Legendre transformation

$$\Gamma_{\rm 1PI}[\Phi] = W[J] - \Phi\cdot J\ , \tag{2.43}$$

From the last equation we can derive the following relations:

$$\frac{\delta W[J_{\rm s}]}{\delta J^a_\mu(x)} = A^a_\mu(x)\ ,\ \frac{\delta W[J_{\rm s}]}{\delta\bar{\eta}_f(x)} = -\psi_f(x)\ ,\ \frac{\delta W[J_{\rm s}]}{\delta\eta_f(x)} = \bar{\psi}_f(x)\ , \tag{2.44}$$

where the external sources are not zero. Therefore, the effective action $\Gamma[\Phi]$ in Eq. (2.43) must satisfies

$$\frac{\delta\Gamma[\Phi]}{\delta A^a_\mu(x)} = J^a_\mu(x)\ ,\quad \frac{\delta\Gamma[\Phi]}{\delta\psi_f(x)} = -\bar{\eta}_f(x)\ ,\quad \frac{\delta\Gamma[\Phi]}{\delta\bar{\psi}_f(x)} = \eta_f(x)\ . \tag{2.45}$$

[†]Note that in Eq. (2.41), the quarks, ghosts and their respective sources are Grassmann c-munbers.

It is well known that correlation functions are not gauge invariance, but we can used the gauge invariance of the generating functional to derive the generalized Ward Takahashi identities for the non-Abelian case. These identities were first found by Slavnov and Taylor [100,101], but the full understanding of them was obtained by Becchi, Rouet, Stora and Tyutin, who discovered a new symmetry of the full QCD's action Eq. (2.36), called BRST symmetry [102,103].

The BRST symmetry is related to the infinitesimal gauge transformation, where the ghost field $c^a(x)$ is the gauge parameter:

$$\delta\psi(x) = i\epsilon\, c^a(x)\psi(x)\ ,\ \ \delta A^a_\mu(x) = \frac{1}{g}D^{ab}_\mu \epsilon\, c^b(x)\ ,\ \ \delta F^a_{\mu\nu} = it^b\epsilon\left[c^a(x), F^b_{\mu\nu}\right]\ , \quad (2.46)$$

where ϵ is an infinitesimal global parameter which is a Grassmann variable. The ghost fields transform as

$$\delta c^a(x) = -\frac{g}{2}\epsilon\, f^{abc}c^b(x)c^c(x)\ ,\ \ \delta\bar{c}^a(x) = \epsilon\, B^a(x)\ ,\ \ \delta B^a(x) = 0\ . \quad (2.47)$$

It is not difficult verify that the QCD's action Eq. (2.36) is BRST-invariant, up to a total derivative. The gauge-fixing action $S_{\rm gf}$ is a BRST variation itself and this means that $\delta S_{\rm gf} = 0$. This fact, is because a property of the BRST transformation, which states that applying successive BRST transformations to any field gives zero[‡].

Under a BRST transformation into Eq. (2.41) the only term that does not vanishes is the sources term. This implies that

$$\begin{aligned}\langle\delta\Phi\cdot J\rangle_J &= \int d^4x\, J_i\,\langle\delta\Phi_i\rangle_J \\ &= \int d^4x\,\frac{\delta\Gamma[\Phi]}{\delta\Phi_i}\langle\delta\Phi_i\rangle_J\ .\end{aligned} \quad (2.48)$$

where we have used the fact that functional integral of a total derivative vanish under appropriate boundary conditions and also in the second line we used a compact form of the relations given by Eq. (2.45). The last equation leads to the Slavnov-Taylor identities.

2.6 Renormalized QCD's action

The renormalizability of QCD allows us to define a well method for the calculations of correlation functions free of ultraviolet divergences at all orders in perturbation

[‡]This means that the BRST operator is nilpotent.

theory. In general, the procedure of eliminate divergences from a physical amplitude of a given renormalized quantum field theory can be achieved by adding the "counterterms action" to the bare action. The renormalized QCD's action $\tilde{S}_{\rm QCD}$ can be defined as [104]

$$\tilde{S}_{\rm QCD} = S_{\rm QCD} + S^{\rm ct}_{\rm QCD} \tag{2.49}$$

being $S_{\rm QCD}$ the bare QCD's action given by Eq. (2.36), and $S^{\rm ct}_{\rm QCD}$ is the counterterms action which is defined as

$$\begin{aligned} S^{\rm ct}_{\rm QCD} &= \int d^4x \Big\{ - C_{2F}\bar{\psi}_f(x)\gamma\cdot\partial\psi_f(x) + C_4\, m_f\bar{\psi}_f(x)\psi_f(x) \\ &+ ig\, C_{1F}\bar{\psi}_f(x)t^a\gamma\cdot A^a\psi_f(x) + \frac{C_6}{2\xi}A^a_\mu(x)\partial_\mu\partial_\nu A^a_\nu(x) \\ &- \frac{C_{3\,\rm YM}}{2}A^a_\mu(x)\left(-\delta_{\mu\nu}\partial^2 + \partial_\mu\partial_\nu\right)A^a_\nu(x) \\ &- \frac{C_{1\,\rm YM}\,g}{2}f^{abc}\left[\partial_\mu A^a_\nu(x) - \partial_\nu A^a_\nu(x)\right]A^b_\mu(x)A^c_\nu(x) \\ &- \frac{C_5\,g^2}{4}f^{abe}f^{cde}A^a_\mu(x)A^b_\nu(x)A^c_\mu(x)A^d_\nu(x) \\ &+ \tilde{C}_3\,\partial_\mu\bar{c}^a(x)\partial_\mu c^a(x) + g\,\tilde{C}_1\,f^{abc}\partial_\mu\bar{c}^a(x)c^b(x)A^c_\mu(x)\Big\}\,. \end{aligned} \tag{2.50}$$

The renormalizability of QCD implies that the coefficients, C_i, each understood as a power series in g^2, are the only additional terms necessary to remove all the ultraviolet divergences in the theory at every order in the perturbative expansion [§].

We note that the QCD's action (2.49) can be rewritten as

$$\begin{aligned} \tilde{S}_{\rm QCD} &= \int d^4x \Big\{ Z_{2F}\bar{\psi}_f(x)(\gamma\cdot\partial + Z_4Z_{2F}^{-1}\,m_f)\psi_f(x) \\ &- ig\,Z_{1F}\bar{\psi}_f(x)t^a\gamma\cdot A^a\psi_f(x) \\ &+ \frac{Z_{3\rm YM}}{2}A^a_\mu(x)\left[-\delta_{\mu\nu} + \left(1 - \frac{Z_6Z^{-1}_{3\rm YM}}{\xi}\right)\partial_\mu\partial_\nu\right]A^a_\nu(x) \\ &+ \frac{Z_{1\rm YM}\,g}{2}f^{abc}\left[\partial_\mu A^a_\nu(x) - \partial_\nu A^a_\nu(x)\right]A^b_\mu(x)A^c_\nu(x) \\ &+ \frac{Z_5\,g^2}{4}f^{abe}f^{cde}A^a_\mu(x)A^b_\nu(x)A^c_\mu(x)A^d_\nu(x) \\ &- \tilde{Z}_3\,\partial_\mu\bar{c}^a(x)\partial_\mu c^a(x) - g\,\tilde{Z}_1\,f^{abc}\partial_\mu\bar{c}^a(x)c^b(x)A^c_\mu(x)\Big\}\,. \end{aligned} \tag{2.51}$$

[§]For more details of renormalization of gauge theories see for example [105,106,107].

where we have introduced the renormalization constants Z_i as

$$Z_i = 1 - C_i \ , \tag{2.52}$$

We now introduce the bare fields, mass, coupling constant, and gauge fixing parameter:

$$\begin{aligned} \psi^c_{0f}(x) &= Z_{2F}^{1/2}\psi^c_f(x) \ , \quad A^{a\mu}_0(x) = Z_{3\mathrm{YM}}^{1/2} A^{a\mu}(x) \ , \\ c^a_0(x) &= \tilde{Z}_3^{1/2} c^a(x) \ , \qquad m_{0f} = Z_4\, Z_{2F}^{-1/2} m_f \ , \\ \xi_0 &= Z_6^{-1}\, Z_{3\,\mathrm{YM}}\xi \ , \qquad g_0 = Z_{1F}\, Z_{3\,\mathrm{YM}}^{-1/2}\, Z_{2F}^{-1} g \ . \end{aligned} \tag{2.53}$$

We have as a direct consequence of gauge invariance (Slavnov-Taylor identities) that these renormalization constants are not independent

$$\frac{Z_{3\,\mathrm{YM}}}{Z_{1\,\mathrm{YM}}} = \frac{\tilde{Z}_3}{\tilde{Z}_1} \ , \quad \frac{Z_{3\,\mathrm{YM}}}{Z_{1\,\mathrm{YM}}} = \frac{Z_{2F}}{Z_{1F}} \ , \quad Z_5 = \frac{Z^2_{1\,\mathrm{YM}}}{Z_{3\,\mathrm{YM}}} \ . \tag{2.54}$$

They guarantee the universality of the coupling constant and sometimes are called of Slavnov-Taylor identities.

2.7 Nonperturvative approaches of QCD

Confinement, dynamical chiral symmetry breaking and the formation of bound states are essentially nonperturbative phenomena and require an appropriate frameworks for their study. The are two famous framework, lattice QCD and Dyson-Schwinger equations; both methods are based on the functional formalism and in the last few years have shown to be successful in the description of the nonperturbative sector of QCD.

- **Lattice QCD:** The basic idea of lattice QCD is to extract QCDs correlation functions by formulating the theory on a discrete lattice of space-time points. The discretization of the lattice provide a regularization of the theory because naturally an ultraviolet momentum cut-off at the order π/a is introduced, being a the lattice spacing. The continuum QCD is recovered when the size of the lattice is taken infinitely large and its sites infinitesimally close to each other ($a \to 0$). Numerical simulations of lattice QCD are based on a Monte Carlo integration of the Euclidean path integral, consequently, the measurements have statistical errors in addition to the systematic errors due to lattice

discretization. These simulations can be extremely computationally intensive, requiring the use of the largest available supercomputers. For some review of Lattice QCD see Refs. [108,109,110].

- **Dyson-Schwinger equations:** In quantum field theory, Dyson-Schwinger equations (DSEs) are the quantum equations of motion of Green functions which describe the propagation and interaction of the fields. These are infinite tower of coupled equations which interrelating all the Green's functions of the theory [107,106,111,112,113]. Thus, the full solution of the system of DSEs provides a complete description of the theory. Therefore, DSEs is a powerful tool which can be used a to explore ultraviolet (UV) as well as the infrared (IR) regions of the theory. This fact is very important because them can help us to investigate the IR or strong coupling regime of QCD where perturbation theory does not work. In addition, DSEs can be also used to access at finite temperature and density without any problem [114], while using lattice QCD it is still difficult to access to finite density.

Here, we will focus on the DSEs and the next section is dedicated to introduce them, specifically for our interest the quark and gluon DSEs.

2.8 Quark and gluon Dyson-Schwinger equations

For the derivation of the quark DSE we will follow the same steps presented in Appendix B for the case of scalar field. The starting point is Eq. (B.8), which for the case of QCD is given by

$$\left[-\frac{\delta S_{\rm QCD}[\Phi]}{\delta\Phi}\left(\frac{\delta}{\delta J}\right)+J\right]Z[J] \;=\; 0 \tag{2.55}$$

where $Z[J]$ is the generating functional of the full correlation functions of QCD defined by Eq. (2.41). To obtain the quark DSE we have to choose $\Phi = \bar{\psi}$ in Eq. (2.55). By doing so, Eq. (2.55) leads to the following quantum equation of motion:

$$\left[-\frac{\delta S_{\rm QCD}}{\delta\bar{\psi}_f(x)}\left(\frac{\delta}{\delta\eta},\frac{\delta}{\delta\bar{\eta}},\frac{\delta}{\delta\sigma},\frac{\delta}{\delta\bar{\sigma}},\frac{\delta}{\delta J}\right)+\eta_f(x)\right]Z[J]=0\ , \tag{2.56}$$

or more explicit

$$\left\{\left[Z_{2F}(\gamma\cdot\partial+Z_m\,m_f)-ig\,Z_{1F}\,t^a\gamma_\mu\frac{\delta}{\delta J^a_\mu(x)}\right]\frac{\delta}{\partial\bar{\eta}_f(x)}-\eta_f(x)\right\}Z[J]=0\ , \tag{2.57}$$

where we have used the renormalized QCD's action given by Eq (2.51) and also defined $Z_m = Z_4\, Z_{2F}^{-1}$. The next step in the derivation of the quark DSE is to take another functional derivative, but now with respect to the source $\eta(y)$ and afterwards set $\bar{\eta} = \eta = 0$ to obtain

$$\begin{aligned}\delta^4(x-y) &= \Big[Z_{2F}(\gamma\cdot\partial + Z_m\, m_f) \\ &+ ig\, Z_{1F}\, t^a \gamma_\mu A^a_\mu(x;J) - ig\, Z_{1F}\, t^a\gamma_\mu \frac{\delta}{\delta J^a_\mu(x)}\Big] S_f(x,y;[A]). \quad (2.58)\end{aligned}$$

In the last equation we have introduced the connected and 1PI generating functionals via Eq. (2.43). In addition, we have defined $S_f(x,y;A^a_\mu)$ as

$$S_f(x,y;[A]) = \left(\frac{\delta^2\Gamma[\Phi]}{\delta\psi_f(x)\delta\bar{\psi}_f(y)}\bigg|_{\bar{\psi}=\psi=0}\right)^{-1} . \quad (2.59)$$

In similar way as in Eq. (B.25), we can write

$$\begin{aligned}\frac{\delta}{\delta J^a_\mu(x)} S_f(x,y,[A]) &= \int d^4z \frac{\delta A^b_\nu(z)}{\delta J^a_\mu(x)} \frac{\delta}{\delta A^b_\nu(z)} \left(\frac{\delta^2\Gamma[\Phi]}{\delta\psi_f(x)\delta\bar{\psi}_f(y)}\bigg|_{\bar{\psi}=\psi=0}\right)^{-1} \\ &= \int d^4z\, d^4u\, d^4v \frac{\delta A^b_\nu(z)}{\delta J^a_\mu(x)} S_f(x-u) \left(\frac{\delta^3\Gamma[\Phi]}{\delta A^b_\nu(z)\delta\psi_f(u)\delta\bar{\psi}_f(v)}\bigg|_{\bar{\psi}=\psi=0}\right) \\ &\times\ S_f(v-y) \\ &= -ig \int d^4z\, d^4u\, d^4v\, D^{ab}_{\mu\nu}(x-z) S_f(x-u) \\ &\times\ \Gamma^{bf}_\nu(u,v,z) S_f(v-y), \quad (2.60)\end{aligned}$$

where we have used (B.26), (2.59) and in the last line we set all the remaining sources to zero, and also we use

$$\begin{aligned}D^{ab}_{\mu\nu}(x-y) &= \frac{\delta A^b_\mu(y)}{\delta J^a_\mu(x)} \\ &= \frac{\delta^2 W[J_{\rm s}]}{\delta J^a_\mu(x)\delta J^b_\mu(y)}\bigg|_{J_{\rm s}=0} , \quad (2.61)\end{aligned}$$

and

$$-ig\Gamma^{bf}_\nu(x,y,z) = \frac{\delta^3\Gamma[\Phi]}{\delta A^b_\nu(z)\delta\bar{\psi}_f(x)\delta\psi_f(y)} . \quad (2.62)$$

In absence of external sources Eq. (2.58) can be rewritten as

$$\begin{aligned}Z_{2F}(\gamma\cdot\partial + Z_m\, m_f) S_f(x-y) &= \delta^4(x-y) \\ &+ Z_{1F} g^2 \int d^4z\, d^4u\, d^4v\, D^{ab}_{\mu\nu}(x-z) t^a\gamma_\mu S_f(x-u) \\ &\times\ \Gamma^{bf}_\nu(u,v,z) S_f(v-y) \quad (2.63)\end{aligned}$$

After a subsequent Fourier transformation, and the multiplication with the inverse propagator, we obtain

$$\begin{aligned} S_f^{-1}(p) &= Z_{2F}\,(i\gamma\cdot p + Z_m\, m_f) \\ &+ Z_{1F}\int^{\Lambda}\frac{d^4q}{(2\pi)^4}g^2 D^{ab}_{\mu\nu}(p-q)\frac{\lambda^a}{2}\gamma_\mu\,\tilde{S}_f(q)\Gamma^{bf}_{\nu}(p,q)\ . \end{aligned} \tag{2.64}$$

This is the Dyson-Schwinger equation for the renormalized quark propagator in momentum space, where m_f is the bare quark mass, Λ is a symmetry-preserving regularization mass scale, $D^{ab}_{\mu\nu} = \delta^{ab}D_{\mu\nu}$ is the renormalized dressed-gluon propagator, and $\Gamma^a_\nu = \lambda^a\Gamma_\nu/2$ is the renormalized dressed-quark-gluon vertex, which themselves satisfy their own Dyson-Schwinger equations respectively. The first term in the right-hand side of Eq. (2.64) is the inverse of the free propa-gator multiplied by the renormalization constant Z_{2F}, and the second one can be interpreted as the quark self-energy multiplied by the renormalization constant Z_{1F}. The diagrammatic representation of the quark DSE is displayed in Fig. 2.3.

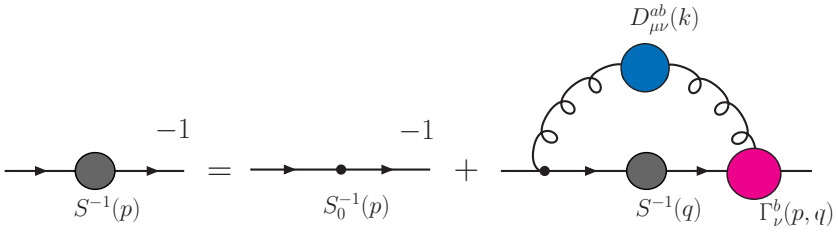

Figure 2.3: Diagrammatic representation of the Dyson-Schwinger equation for the quark propagator Eq. (2.64); filled circles mean fully dressed objects.

The derivation of the gluon DSE follows in the same way as for the case of the quark DSE just taking the functional derivative with respect to A^a_μ into the QCD generating functional, that means choose $\Phi = A^a_\mu$ in Eq. (2.55). Due to the complication with the large number of color and Dirac indices that will appear in the intermediate steps of the derivation of the gluon DSE, we just present the pictorial representation of this equation in Fig. 2.4. For details of its derivation see appendix C of Ref. [115]. The explicit form of the equation can be obtained from Fig. 2.4 via the application of the Feynman rules.

From Fig. 2.4, one notes that one of the graphs involves the full ghost propagator which satisfies its own DSE that also is displayed at the bottom of this figure.

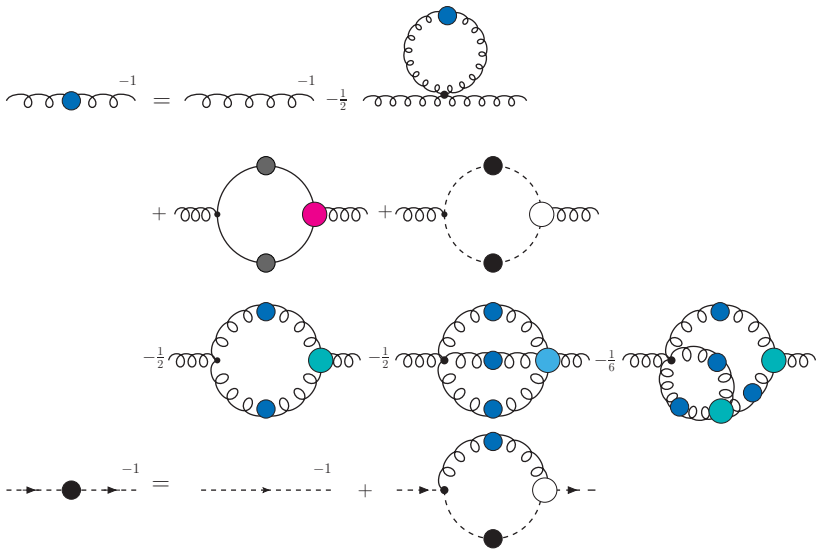

Figure 2.4: Pictorial representation of the gluon (at the top) and ghost Dyson-Schwinger equations (at the bottom).

Furthermore, one observes the appearance of the quark-gluon-vertex, the three-gluon vertex and the four-gluon vertex as well. Therefore, as one proceeds to correlation functions of hight order, new structures will appear with also satisfy their own DSEs. Obviously, it is impossible to solve this intricate, infinite tower of coupled correlation functions and truncations and approximations must be implemented.

2.9 Summary

In this chapter we have introduced some general aspects of QCD. We presented a little review of its history, emphasizing in the remarkable facts that led to the construction of the theory that we know today. We discussed some general features and properties of the classical QCD's action, for example its local and internal symmetries were studied and as well as their consequences. Aspects as quantization and renormalization of the QCD's action also were considered. Finally, we discussed about the importance of the nonperturbative methods that are needed to explain phenomenological aspects of QCD such as Dynamical chiral symmetry breaking and confinement. Here, we focused on the Dyson-Schwinger equations, DSEs, specifically the quark DSE was derived.

Chapter 3

Meson Bound-state Equation

Study of bound-states requires an appropriate relativistic covariant treatment. It is well known that in QCD, which a bound-state made of a quark and an antiquark (a meson), can be studied by solving the Bethe-Salpeter equation (BSE). It is a nonperturbative linear integral equation, which is analogous to the Lippmann-Schwinger equation of quantum mechanics [116]. Historically, the general form of the BSE appeared for first time in 1951 (sixty-six years ago) in the meeting of the American Royal Society, where Bethe and Salpeter presented their derivation using Feynman graphs [117]. In the following years new methods to derive this equation were appearing [118,119,120], but currently the most common is the functional method. The goal of this chapter is initially show how to extract the meson spectrum from QCD using the functional formalism.

3.1 Derivation of the Bethe-Salpeter equation

To extract the meson spectrum from QCD, we have to derive the respective meson bound-state equation, which is well known as Bethe-Salpeter equation. The derivation of this equation follows in the similar way as in the case of the quark DSE explained in the last chapter. The first step is to introduce the following generating functional

$$Z[J] = \int \mathcal{D}\Phi \, e^{-S_{\rm QCD}[\Phi]+\Phi\cdot J\cdot\Phi}, \tag{3.1}$$

with

$$\Phi\cdot J\cdot\Phi = \int d^4x \, d^4y \, \Phi_i(x) J_{ik}(x,y) \Phi_k(y) \ . \tag{3.2}$$

Note that we have introduced a new type of sources $J_{ik}(x,y)$ (bi-local), which is able to connect two fields.

The generating functional defined by Eq. (3.1) generates the full correlation function $S^{(2N)}$:

$$Z[J] = \sum_{N=0}^{\infty} \frac{1}{N!} S^{(2N)}(x_1, y_1; \cdots ; x_N, y_N) J(x_1, y_1) \cdots J(x_N, y_N) \ . \tag{3.3}$$

As before, we introduce the generating functionals, $W[J] = \ln Z[J]$, for connected (bi-locally) correlation functions, or

$$W[J] = \sum_{N=1}^{\infty} \frac{1}{N!} G_c^{(N)}(x_1, y_1; \cdots ; x_N, y_N) J(x_1, y_1) \cdots J(x_N, y_N) \ , \tag{3.4}$$

and the irreducible correlation functions by the bi-local Legendre transformation

$$\Gamma_{\rm 2PI}[B] \ = \ B \cdot J - W[J] \ , \tag{3.5}$$

with

$$B_{ij}(x, y) = \int d^4x \, d^4y \, B_{ij}(x, y) J_{ji}(y, x) \ , \tag{3.6}$$

where $B_{ij}(x, y)$ is the classical bi-local field corresponding to the source $J_{ji}(y, x)$:

$$B_{ij}(x, y) = \frac{\delta W[J]}{\delta J_{ij}(x, y)} \ . \tag{3.7}$$

$\Gamma_{\rm 2PI}[B]$ is the two-particle irreducible (2PI) effective action. Derivatives of Eq. (3.5) will be related to 2PI amputated correlation functions. From Eq. (3.5) we have the following bi-local relationship

$$\frac{\delta \Gamma_{\rm 2PI}[B]}{\delta B_{i,j}(x, y)} = J_{ij}(x, y) \ . \tag{3.8}$$

In order to obatain the two-particle propagator (quark-antiquark system) which is related to derivatives of $W[J]$, namely from Eq. (3.4) one has

$$G_c^{(2)} = \frac{\delta^2 W[J]}{\delta J_{\psi\bar{\psi}} \delta J_{\psi\bar{\psi}}} \ , \tag{3.9}$$

we need to separate the interacting and non-interacting parts. It is known [121] that the 2PI effective action can be written as

$$\Gamma_{\rm 2PI}[B] = {\rm Tr} \left[S_0^{-1} B \right] - {\rm Tr} \left[\ln(B) \right] + \tilde{\Gamma}[B] \ , \tag{3.10}$$

where $\tilde{\Gamma}[B]$ denotes the interacting contributions to the 2PI effective action. By expanding $e^{W[J]}$ and comparing with Eq. (3.4) and (3.3), we find for example

$$\begin{aligned} G_c^{(1)}(x,y) &= S^{(2)}(x-y) \ , \\ G_c^{(2)}(x_1,y_1;x_2,y_2) &= S^{(4)}(x_1,y_1,x_2,y_2) \\ &- S^{(2)}(x_1-y_1)S^{(2)}(x_2-y_2) \ , \\ &\vdots \end{aligned} \tag{3.11}$$

Therefore, from Eq. (3.3) and Eq. (3.7) one obtains

$$B(x,y)\Big|_{J=0} = S^{(2)}(x-y) \ . \tag{3.12}$$

which is the full propagator. In this case, the inverse two-particle propagator is

$$\begin{aligned} \left[G_c^{(2)}(x_1,y_1;x_2,y_2)\right]^{-1} &= \frac{\delta^2\Gamma_{\rm 2PI}[B]}{\delta B(x_1,y_1)\delta B(x_2,y_2)}\Big|_{B=G} \\ &= [S^{(2)}(x_1-y_1)]^{-1}[S^{(2)}(x_2-y_2)]^{-1} \\ &+ \frac{\delta^2\tilde{\Gamma}[S]}{\delta S(x_1,y_1)\delta S(x_2,y_2)} \ . \end{aligned} \tag{3.13}$$

From this equation we can define the interaction kernel

$$K(x_1,y_1,x_2,y_2) = \frac{\delta^2\tilde{\Gamma}[S]}{\delta S(x_1,y_1)\delta S(x_2,y_2)} \ . \tag{3.14}$$

With this, Eq. (3.13) can be written in a more familiar form

$$\begin{aligned} G_c^{(2)}(x_1,y_1;x_2,y_2) &= S(x_1,y_1)S(x_2,y_2) + \int d^4z_1 d^4z_2 d^4z_3 d^4z_4 S(x_1,y_1)S(x_2,y_2) \\ &\times K(z_1,z_1,z_3,z_4)G_c^{(2)}(z_3,y_1;z_4,y_2) \ . \end{aligned} \tag{3.15}$$

This is the inhomogeneous Bethe-Salpeter equation (BSE) for the propagator of the quark-antiquark system. The diagrammatic representation of Eq. (3.15) is displayed in Fig. 3.1

3.2 Homogeneous Bethe-Salpeter equation

Before deriving the homogeneous BSE from Eq. (3.15), it is more convenient to go to momentum space. The first step is to define the relative coordinate $x = x_1 - x_2$ (good for translational invariance requirement), which allows us introduce the arbitrary

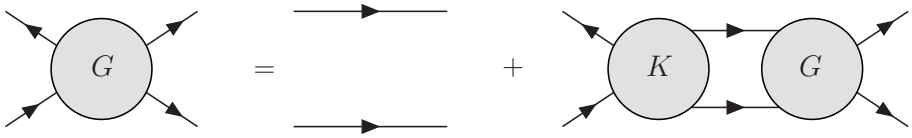

Figure 3.1: Diagrammatic representation of the inhomogeneous BSE equation Eq. (3.15).

parameters $\eta_\pm$, such that $\eta_+ + \eta_- = 1$. In addition, we defined the coordinate of the center of mass of the system by $X = \eta_+ x_1 + \eta_- x_2$, which in principle is arbitrary. Then, after transforming to momentum space, we obtain

$$k_+ = \eta_+ P + k, \quad k_- = \eta_- P - k \ , \tag{3.16}$$

$$P = k_+ + k_-, \quad k = \eta_- k_+ - \eta_+ k_- \ , \tag{3.17}$$

where P is the total momentum of the bound state and k the relative momentum. Therefore, after applying Fourier transformation into the quantities of Eq. (3.15), it becomes

$$\begin{aligned} G_c^{(2)}(k,p;P) &= S(k_+)S(k_-)\delta^4(k-p) \\ &+ S(k_+)S(k_-)\int \frac{d^4q}{(2\pi)^4} K(k,q;P) G_c^{(2)}(p,q;P) \ . \end{aligned} \tag{3.18}$$

The Eq. (3.18) has poles at energies where the system exhibits a bound state. The pole contribution to the two-particle propagator is [122]

$$G_c^{(2)}(k,p,P) = \sum_i \frac{\chi(k,P_i)\bar{\chi}(p,-P_i)}{P^2 - P_i^2} + R(p,q,P) \tag{3.19}$$

with $P_i^2 = -m_i^2$, where the index i labels the bound state, $R(p,q,P)$ are regular terms (no poles at $P_i^2 = -m_i^2$), and we have introduced the called the Bethe-Salpeter wave function $\chi(p,P_i)$

$$\chi(x_1,x_2) = \langle 0|\psi_1(x_1)\psi_2(x_2)|P\rangle \tag{3.20}$$

$$\bar{\chi}(x_1,x_2) = \langle 0|\bar{\psi}_1(x_1)\bar{\psi}_2(x_2)|P\rangle \tag{3.21}$$

and their Fourier transforms

$$\chi(x_1,x_2) = e^{-iP\cdot X}\int \frac{d^4p}{(2\pi)^4} e^{ip\cdot x}\chi(p,P) \tag{3.22}$$

$$\bar{\chi}(x_1,x_2) = e^{iP\cdot X}\int \frac{d^4p}{(2\pi)^4} e^{ip\cdot x}\bar{\chi}(p,P) \ . \tag{3.23}$$

Now, inserting Eq. (3.19) into Eq. (3.15) (written in a shorthand form), we have

$$\sum_i \frac{\chi\bar{\chi}}{P^2 - P_i^2} + R \;=\; S\,S + S\,S\,K\left(\sum_i \frac{\chi\bar{\chi}}{P^2 - P_i^2} + R\right), \tag{3.24}$$

and comparing the residues at the pole (multiplying the equation by $(P^2 - P_i^2)$ and afterwards take the limit $P^2 = P_i^2$), yields

$$\left[\Gamma_M^{lh}(k;P)\right]_{AB} = \int_q \left[K^{lh}(k,q;P)\right]_{AC,DB} \left[S_l(q_+)\Gamma_M^{lh}(q;P)S_h(q_-)\right]_{CD}, \tag{3.25}$$

where $\int_q \equiv \int d^4q/(2\pi)^4$. This is the so called homogeneous Bethe-Salpeter equation, which is valid only at discrete momenta $P^2 = -m_{\rm bs}^2$, being $m_{\rm bs}$ the meson bound-state mass. In Eq. (3.25), $K^{lh}(k,q;P)$ is the fully amputated quark-antiquark scattering kernel, $A, B, \cdots$ denote color and spinor indices only, l and h are flavor indices, M specifies the kind of meson (scalar, vector, pseudoscalar,...), $q_\pm = q \pm \eta_\pm P$, with q being the relative quark momentum. $S(k)$ is the dressed-quark propagator given by Eq. (2.64), and $\Gamma_M^{lh}(k;P)$ is the Bethe-Salpeter amplitude (BSA) which is defined by

$$\Gamma_M^{lh}(k;P) = S_l^{-1}(k_+)\chi_M(k;P)S_h^{-1}(k_-)\,. \tag{3.26}$$

The pictorial representation of Eq. (3.25) is given in Fig. 3.2.

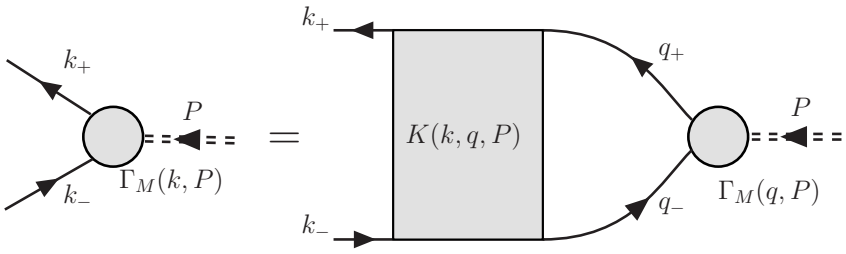

Figure 3.2: Pictorial representation of the homogeneous Bethe-Salpeter equation Eq. (3.25).

It is important to note that spacetime-translation invariance requires that no observable can depend on the choice of the momentum routing in quark propagators in Eq. (3.27); that is, physical results must be independent of $\eta_\pm$.

On the other hand, another important element that we are interested is the inhomogeneous BS vertex, which is given by

$$\left[\Gamma_{\mathcal{M}}^{lh}(k;P)\right]_{AB} = \mathcal{M}_{AB} + \int_q \left[K^{lh}(k,q;P)\right]_{AC,DB} \left[S_l(q_+)\Gamma_{\mathcal{M}}^{lh}(q;P)S_h(q_-)\right]_{CD}, \tag{3.27}$$

where $\mathcal{M}$ represents the Dirac spinor structure of the state. In general, we are interested in the flavor-nonsinglet axial-vector $\Gamma^{lh}_{5\mu}(k;P)$ and pseudoscalar $\Gamma^{lh}_{\rm PS}(k;P)$ amplitudes for a quark-antiquark pair, with $\mathcal{M}_{5\mu}=\gamma_5\gamma_\mu$ and $\mathcal{M}_{PS}=\gamma_5$ respectively.

Associated with $\Gamma^{fg}_{5\mu}$ is the Ward-Green-Takahashi (WGT) identity:

$$P_\mu\Gamma^{lh}_{5\mu}(k;P) \;=\; S_l^{-1}(k_+)i\gamma_5 + i\gamma_5 S_h^{-1}(k_-) - \, i\,(m_l+m_h)\,\Gamma^{lh}_{\rm PS}(k;P)\,, \quad (3.28)$$

where $\Gamma^{lh}_{PS}(k;P)$ is the pseudoscalar vertex; both $\Gamma^{lh}_{5\mu}(k;P)$ and $\Gamma^{lh}_{\rm PS}(k;P)$ obey the inhomogeneous BS equation (3.27).

3.3 Normalization condition

The homogeneous BSE Eq. (3.25) is equipped with an auxiliary normalization condition. This is an important component of the BS approach because it ensures the correct charge of a meson. This canonical normalization condition of the BSA follows from taking the derivative of the two-particle propagator, $G_c^{(2)}$ at $P^2=m_{\rm bs}^2$, and afterwards comparing the residues at the pole.

The one pole contribution to the two-particle propagator with residue r_i reads as

$$\begin{aligned} G_c^{(2)}(k,p,P) \;&\simeq\; r_i\,\frac{\chi(k,P_i)\bar\chi(p,-P_i)}{P^2-P_i^2} \\ &\simeq\; \frac{r_i}{P_\mu+(P_i)_\mu}\,\frac{\chi(k,P_i)\bar\chi(p,-P_i)}{P_\mu-(P_i)_\mu}\;, \end{aligned} \quad (3.29)$$

where we have neglected the regular terms. On the other hand, we can write Eq. (3.19) as

$$G_c^{(2)} \;=\; (S^{-1}\,S^{-1}-K)^{-1}\;. \quad (3.30)$$

From this equation one has

$$r_i\frac{\chi\bar\chi}{(P^2-P_i^2)}\left[\frac{\partial\,(S^{-1}\,S^{-1}-K)}{\partial P_\mu}\right] r_i\frac{\chi\bar\chi}{(P^2-P_i^2)} = 2P_\mu r_i\frac{\chi\bar\chi}{(P^2-P_i^2)^2}\;. \quad (3.31)$$

Then, after comparing the residue on both sides we obtain

$$\frac{2P_\mu}{r_i} = \bar\chi\left[\frac{\partial\,(S^{-1}\,S^{-1}-K)}{\partial P_\mu}\right]\chi\;, \quad (3.32)$$

which is the normalization condition for the BS wave-function. This equation can be rewritten in term of the BSA $\Gamma_M^{lh}(k;P)$

$$\begin{aligned}\frac{2P_\mu}{r_i} &= N_c\int\frac{d^4q}{(2\pi)^4}\mathrm{Tr}\Bigg[\bar{\Gamma}_M^{hl}(q;-P)\frac{\partial S_l(q_+)}{\partial P_\mu}\Gamma_M^{lh}(P)S_h(q_-)\\ &+ \bar{\Gamma}_M^{hl}(q;-P)S_l(q_+)\Gamma_M^{lh}(q;P)\frac{\partial S_h(q_-)}{\partial P_\mu}\Bigg]\\ &+ \int\frac{d^4q}{(2\pi)^4}\int\frac{d^4k}{(2\pi)^4}\bar{\chi}(q;-P)\frac{\partial K^{lh}(k,q;P)}{\partial P_\mu}\chi(k;P)\ . \end{aligned}\tag{3.33}$$

If $r_i = 1$, it is the canonical normalization condition for the BS amplitude.

3.4 Meson Bethe-Salpeter amplitudes

One notes that due to the quark dressed propagators in Eq. (3.25), the BSA $\Gamma_M(k;P)$ of a meson as a bound-state of a quark-antiquark pair carries Dirac indices. In addition, the BSA depends on two independent four-vector variables: the bound-state momenta P and the relative quark-antiquark momenta q. For mesons characterized by quantum numbers $J^{\mathcal{PC}}$ (being J the total angular momentum, $\mathcal{P}$ the parity and C charge parity), they are 4×4 matrices in Dirac space and for the case of $J>0$ they also carry Lorentz indices. Then, one can write the BSA as a sum over Dirac covariants T_i multiplied by Lorentz-invariant functions F_i in the form

$$[\Gamma_M(k;P)]_{AB} = \sum_i [T_i(\gamma;k,P)]_{AB}F_i(k;P)\ . \tag{3.34}$$

With $F_i(k;P)\equiv F_i(P^2;k^2,k\cdot P)$. For example, the BSA for the scalar meson with quantum numbers $J^{\mathcal{PC}}=0^{++}$, has four Dirac covariants and four Lorentz-invariant functions [123]:

$$\begin{aligned}\Gamma_{\mathrm{S}}(k;P) &= \mathbb{1}F_1(k;P) + i\,\gamma\cdot P F_1(k;P)\\ &+ i\,\gamma\cdot k\,F_3(k;P) + \sigma_{\mu\nu}k_\mu P_\nu F_4(k;P)\ , \end{aligned}\tag{3.35}$$

and for the case of the pseudoscalar meson ($J^{\mathcal{PC}}=0^{-+}$) which has negative parity, its BSA can be constructed from Eq. (3.35) by multiplication of each covariant by γ_5, namely

$$\begin{aligned}\Gamma_{\mathrm{PS}}(k;P) &= \gamma_5\big[iF_1(k;P) + \gamma\cdot P F_1(k;P)\\ &+ \gamma\cdot k\,F_3(k;P) + \sigma_{\mu\nu}k_\mu P_\nu F_4(k;P)\big]\ . \end{aligned}\tag{3.36}$$

Often these four Lorentz-invariant functions are denoted in the literature by the letters E, F, G and H [124].

For the case of vector mesons there are eight Dirac covariant and Lorentz-scalar amplitudes $F_i(k;P)$. Details about the construction of the BSAs are given in Appendix (C).

3.5 Solution Method

We can see that Eq. (3.25) is an eigenvalue equation with eigenvalue equal to 1. Then, the solution method can make use of the eigenvalue concept via introduction of an artificial eigenvalue $\lambda(P^2)$, namely

$$\lambda(P^2)[\Gamma_M^{lh}(k;P)] = \int \frac{d^4q}{(2\pi)^4}\,[K^{lh}(k,q,P)]_{AC,DB}[\chi_M(q;P)]_{CD}\ . \tag{3.37}$$

Therefore, for any given value of P^2 one can solve this eigenvalue equation and obtain a spectrum of eigenvalues $\lambda_1, \lambda_2, ...$ Thus, the only step left is to find those values of P^2 where $\lambda_i(P^2) = 1$ for each i, which restores Eq. (3.25) and in this way one can obtain the bound-state masses m_i of the system. This procedure is illustrated in Fig. 3.3

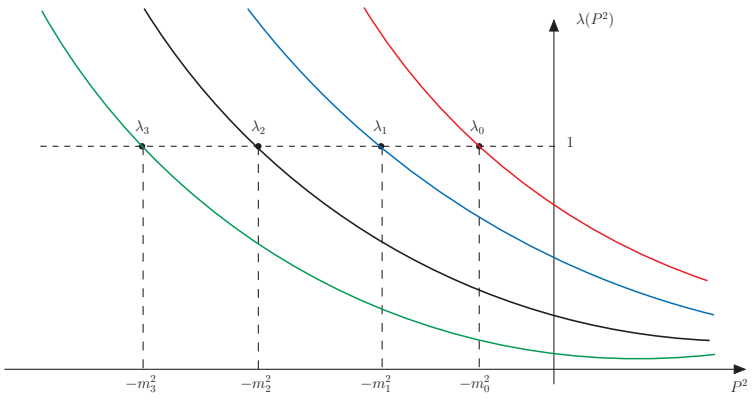

Figure 3.3: Illustration of the procedure to solve the homogeneous BSE.

Together with the mass $m_{\rm bs}$, we also obtain the BSA, which must be normalized in order to compute properties of the bound-state, such as decay constant or form factors.

3.6 Summary

In this chapter we have explored the Bethe-Salpeter equation, which together with the DSEs provide a means to study the nonperturbative properties of hadrons at the microscopic level. We have derived its inhomogeneous and homogeneous forms, where the last one was obtained considering the existence of a bound state by the occurrence of a pole in the four-point Greens function. In addition, a normalization condition for the meson BS amplitudes was derived. These normalized amplitudes are needed to compute meson properties. Finally, we discussed a little bit about the structure of the meson BSA and a method to solve the BSE based on the idea that the solution of the homogeneous BSE can be considered as an eigenvalue problem.

Chapter 4

Symmetry-Preserving Contact Interaction Model

The contact interaction of Ref. [125] is a representation of nonperturbative kernels used in Dyson-Schwinger and Bethe-Salpeter equations. However, as we have pointed out in the introduction of the thesis, the regularization procedure of divergent integrals of this kind of nonrenormalizable model, leads to symmetry violation. The aim of this chapter is to examine the contact-interaction model within the perspective of a regularization method which is based on a subtraction scheme that allows us to avoid standard steps in the evaluation of divergent integrals that invariably lead to symmetry violation. We will formulate the problem generically with the aim of using it for heavy-light mesons.

4.1 Contact interaction approximation

The CI scheme introduced in Ref. [125] amounts to the following replacement in Eq. (2.64)

$$\begin{aligned} g^2 D_{\mu\nu}(k-q)\Gamma^{af}_{\nu}(q,k) &\rightarrow \left(\frac{4\pi\alpha_{\rm IR}}{m_g^2}\right)^f \delta_{\mu\nu}\frac{\lambda^a}{2}\gamma_\nu \\ &\equiv \left(\frac{1}{m_{\rm G}^f}\right)^2 \frac{\lambda^a}{2}\gamma_\mu, \end{aligned} \tag{4.1}$$

which basically means that the dressed-gluon propagator is remplaced by a constant times a delta ($\delta_{\mu\nu}$). This is the four fermion interaction between two quarks where the gluon shrinks to a point and is integrated out. In Fig. 4.1 is depicted the contact interaction approximation.

In Eq. (4.1) m_g is a gluon mass scale and $\alpha_{\rm IR}$ is a coupling strength parameter. Note that a flavor dependence in the interaction strength is due to the flavor dependence of the full quark-gluon vertex Γ^{af}_{μ}. The flavor dependence is important to

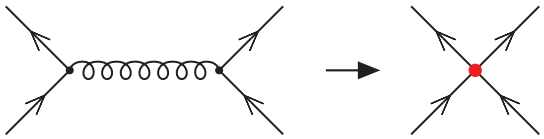

Figure 4.1: Contact interaction approximation.

accommodate the fact that heavy-flavor quarks probe shorter distances than light-flavor quarks at the corresponding quark-gluon vertices, thereby implying a smaller coupling strength for heavy-flavor quarks [50]. This fact was used previously in the NJL model to mimic the short-distance and weak-coupling physics in quark matter at high temperatures and baryon densities [126,127]. Very recently, Refs. [41,42] have shown that good agreement with experiment for heavy-charmonia masses can be obtained by using a weaker coupling strength and a simultaneous increase in the ultraviolet cutoff of the CI of Ref. [125]. We anticipate that the same turns out to be relevant for heavy-light mesons and write for the BS kernel

$$\left[K^{lh}(k,q;P)\right]_{AC,DB} = -\frac{1}{m_{\rm G}^{l} m_{\rm G}^{h}} \left(\frac{\lambda^a}{2}\gamma_\mu\right)_{AC} \left(\frac{\lambda^a}{2}\gamma_\mu\right)_{DB} . \tag{4.2}$$

A feature of the momentum independence of the CI is that the corresponding DS equation in Eq. (2.64) is nonrenormalizable. In addition, the BS equation in the CI acquires ultraviolet divergences and is also nonrenormalizable. This implies that mass-scale parameters introduced with the regularization of divergent integrals cannot be removed from the calculations and need to be fixed phenomenologically. Another feature, as previously mentioned, concerns the regularization of divergent integrals: they carry along the danger of symmetry violation, in particular the WGTI in Eq. (3.28) is not satisfied even when Poincaré-invariant regularization schemes are employed.

Let us consider the DS and the homogeneous pseudoscalar BS equations, Eqs. (2.64) and (3.25) respectively, with the CI approximation. Since the most general form of the dressed quark propagator is

$$S(p) = \frac{1}{i\gamma\cdot p\, A(p^2) + B(p^2)} = \frac{-i\gamma\cdot p\, A(p^2) + B(p^2)}{p^2 A^2(p^2) + B^2(p^2)} , \tag{4.3}$$

where $A(p^2)$ and $B(p^2)$ are Lorentz scalar functions, one has that the quark DSE

decouples in

$$A(p^2) = 1 + \frac{8}{3}\left(\frac{1}{m_G^f}\right)^2 \int \frac{d^4q}{(2\pi)^4} \frac{(p\cdot q)A(q^2)}{q^2A(q^2)+B(q^2)} \ , \tag{4.4}$$

$$B(p^2) = m_f + \frac{16}{3}\left(\frac{1}{m_{\rm G}^f}\right)^2 \int \frac{d^4q}{(2\pi)^4} \frac{B(q^2)}{q^2A(q^2)+B(q^2)} \ . \tag{4.5}$$

One note that the integral in Eq. (4.4) vanishes, since

$$\int d^4q\, f(q^2) p\cdot q \sim \int dq q^3 f(q^2) p\, q \int d\theta \sin^2\theta \cos\theta = 0 \ , \tag{4.6}$$

which implies in

$$A(p^2) = 1 \ . \tag{4.7}$$

Due that the right side of Eq. (4.5) is independent of p, we have that B a constant. Therefore defining $B(p^2) = M_f$ the solution of the gap equation becomes

$$S_f^{-1}(k) = i\gamma\cdot k + M_f \ , \tag{4.8}$$

with the momentum independent quark-mass function given by

$$M_f = m_f + \frac{16}{3}\left(\frac{1}{m_{\rm G}^f}\right)^2 \int \frac{d^4q}{(2\pi)^4} \frac{M_f}{q^2+M_f^2}. \tag{4.9}$$

It is remarkable that the nonrunning quark mass, M_f, is related to the commonplace constituent quark masses of quark and light-front models [128,129,130,131,132], yet it is dynamically generated. Such a momentum independent mass function is appropriate in the calculation of static observables, such as the meson mass spectrum, weak decay constants and charge radii, but leads to *hard* elastic and transition form factors that strongly depart from experimental data for $q^2 > \Lambda_{\rm QCD}^2$ [125,32,33,34,35,36,37,38,39,40,42,133,134].

In this same CI framework, the BSE Eq. (3.25) becomes

$$\Gamma^{lh}_{M^a}(P) = -\frac{4}{3\, m_{\rm G}^l m_{\rm G}^h} \int \frac{d^4q}{(2\pi)^4} \gamma_\mu\, S_l(q_+)\, \Gamma^{lh}_{M^a}(P)\, S_h(q_-)\, \gamma_\mu \ , \tag{4.10}$$

with $\Gamma^{lh}_{M^a}(P) = T^a\, \Gamma^{lh}_M(P)$, where for example in the case of pseudoscalar channel, T^a is given by

$$T^a = \begin{cases} \lambda^3, \text{ for } \pi^0 \\ \frac{1}{\sqrt{2}}(\lambda^1 \pm i\lambda^2), \text{ for } \pi^\pm \\ \frac{1}{\sqrt{2}}(\lambda^4 \pm i\lambda^5), \text{ for } K^\pm \\ \frac{1}{\sqrt{2}}(\lambda^6 \pm i\lambda^7), \text{ for } K^0, \bar{K}^0 \ . \end{cases} \tag{4.11}$$

The pseudoscalar BS amplitude is independent of the relative quark-antiquark momentum. As a consequence, $G^{lh}_{\rm PS} = H^{lh}_{\rm PS} = 0$, and Eq. (3.36) reduces to,

$$\Gamma^{lh}_{\rm PS}(P) = \gamma_5 \left[i E^{lh}_{\rm PS}(P) + \frac{1}{2M_{lh}} \gamma \cdot P \, F^{lh}_{\rm PS}(P) \right], \tag{4.12}$$

where $M_{lh} = M_l M_h/(M_l + M_h)$. Therefore, the BS equation can be written in the matrix form,

$$\begin{bmatrix} E^{lh}_{\rm PS}(P) \\ F^{lh}_{\rm PS}(P) \end{bmatrix} = \frac{1}{3 m^l_{\rm G} m^h_{\rm G}} \begin{bmatrix} \mathcal{K}^{EE}_{\rm PS} & \mathcal{K}^{EF}_{\rm PS} \\ \mathcal{K}^{FE}_{\rm PS} & \mathcal{K}^{FF}_{\rm PS} \end{bmatrix} \begin{bmatrix} E^{lh}_{\rm PS}(P) \\ F^{lh}_{\rm PS}(P) \end{bmatrix}, \tag{4.13}$$

where the kernel's matrix elements are given by,

$$\mathcal{K}^{EE}_{\rm PS}(P) = -\int_q {\rm Tr}\left[\gamma_5 \gamma_\mu S_l(q_+) \gamma_5 S_h(q_-) \gamma_\mu\right], \tag{4.14}$$

$$\mathcal{K}^{EF}_{\rm PS}(P) = \frac{i}{2M_{lh}} \int_q {\rm Tr}\left[\gamma_5 \gamma_\mu \, S_l(q_+) \gamma_5 \gamma \cdot P S_h(q_-) \gamma_\mu\right], \tag{4.15}$$

$$\mathcal{K}^{FE}_{\rm PS}(P) = \frac{2iM_{lh}}{P^2} \int_q {\rm Tr}\left[\gamma_5 \gamma \cdot P \gamma_\mu S_l(q_+) \gamma_5 S_h(q_-) \, \gamma_\mu\right], \tag{4.16}$$

$$\mathcal{K}^{FF}_{\rm PS}(P) = \frac{1}{P^2} \int_q {\rm Tr}\left[\gamma_5 \gamma \cdot P \gamma_\mu S_l(q_+) \gamma_5 \gamma \cdot P S_h(q_-) \, \gamma_\mu\right]. \tag{4.17}$$

In Eqs. (4.14)–(4.17) the traces are over Dirac indices. All integrals in Eq. (4.9) and Eqs. (4.14)–(4.17) are ultraviolet divergent; the divergences are quadratic and logarithmic. The vast majority of applications within NJL models ignore the pseudovector component $F^{lh}_{\rm PS}(P)$; in doing so leads to the random-phase-approximation (RPA) of the BS equation [22,23,24,25].

For vector mesons, the corresponding BS equation in the RL CI model is given by

$$\Gamma^{lh}_{\rm V}(P) = \gamma^\perp_\mu \, E^{lh}_{\rm V}(P) \ , \tag{4.18}$$

where

$$\gamma^\perp_\mu = \gamma_\mu - \frac{\gamma \cdot P}{P^2} P_\mu. \tag{4.19}$$

With only one Lorentz covariant the BS equation for the vector meson simplifies to

$$1 = \frac{1}{m^l_G \, m^h_G} K^{EE}_{\rm V}(P) \ , \tag{4.20}$$

with

$$K^{EE}_{\rm V}(P) = -\frac{1}{3} \int_q {\rm Tr}[\gamma^\perp_\nu \, \gamma_\mu \, S_l(q_+) \, \gamma^\perp_\nu \, S_h(q_-) \, \gamma_\mu]. \tag{4.21}$$

4.2 Symmetry-preserving subtraction scheme

The issue of symmetry violation can be exposed examining the momenta running in the quark propagators in the BS amplitudes in Eqs. (4.14)–(4.17); they are $q_+ = q + \eta_+ P$ and $q_- = q - \eta_- P$, where $\eta_\pm$ are arbitrary partition variables satisfying $\eta_+ + \eta_- = 1$. However, to maintain translational invariance, the results of the integrals can depend on the relative momentum $q_+ - q_-$ only, or, equivalently, they must not depend on $\eta_\pm$ individually but solely on the combination $\eta_+ + \eta_- = 1$. This dependence on the relative momentum is also crucial for preserving the WGTI in Eq. (3.28), as we discuss shortly ahead. Moreover, for very different values of M_h and M_l, the independence of the results on η_+ and η_- is a serious issue in RL finite-range models [14] which becomes exacerbated in nonrenormalizable CI models.

Within NJL models, the customary way of handling integrals, such as in Eqs. (4.14)–(4.17), is as follows [22,23,24,25]: after evaluating the traces, a choice for η_+ and η_- is made and Feynman parameters are used to combine in a single term the product $(q_+^2 + M_l^2)(q_-^2 + M_h^2)$ in the denominator. Thereafter a *momentum shift* is applied to eliminate the angle defined by the scalar product, $q\cdot P$, in the denominator and finally the integral over q is performed. In shifting the momentum, changes in the integration limits are ignored. Invariably, results depend upon the choices made for $\eta_\pm$; in particular, the value of the pion decay constant f_π, sensitive to the normalization of the pion BS equation, depends on the choices of the partition parameters. In some instances regularization-independent results can be obtained after using the gap equation to eliminate the quadratic divergences, like in the derivation of a Goldberg-Treiman relation at the quark level and the Gell-Mann–Oakes-Renner relationship, see for example the discussions around Eq. (4.27) in Ref. [23].

The subtraction scheme is based on the repeated use of the identity,

$$\begin{aligned} \frac{1}{q_\pm^2 + M_{l,h}^2} &= \left(\frac{1}{q_\pm^2 + M_{l,h}^2} - \frac{1}{q^2 + M^2} \right) + \frac{1}{q^2 + M^2} \\ &= \frac{1}{q^2 + M^2} - \frac{(q_\pm^2 - q^2 + M_{l,h}^2 - M^2)}{(q^2 + M^2)\,(q_\pm^2 + M_{l,h}^2)}\,, \end{aligned} \tag{4.22}$$

where M is an arbitrary subtraction mass-scale parameter. This mass scale plays a similar role to the μ scale in dimensional regularization and can be used to tune parameters of the model when applying it to explore physics at different scales. We do not trail this interesting possibility in this thesis and simply keep M arbitrary;

we comment on this further ahead in this section.

Assuming a Poincaré-invariant regularization for the integrals in Eqs. (4.14)-(4.17), subtractions are performed in each of the propagators, $S_l(q_+)$ and $S(q_-)$, the number of which is dictated by the requirement that a finite integral is obtained. Note that while the original denominator behaves as $1/q^2$ in the limit $q \to \infty$, the last term in Eq. (4.22) tends to $1/q^4$ for $q \to \infty$. We illustrate the procedure in detail for the $\mathcal{K}_{\rm PS}^{EE}(P)$ kernel. Evaluation of the trace in Eq. (4.14) leads to

$$\begin{aligned}\mathcal{K}_{\rm PS}^{EE}(P) &= 16\int_q^\Lambda \frac{q_+\cdot q_- + M_l M_h}{(q_+^2+M_l^2)(q_-^2+M_h^2)} \\ &= 8\int_q^\Lambda \left\{\frac{1}{q_+^2+M_l^2}+\frac{1}{q_-^2+M_h^2}-\frac{P^2+(\Delta M_{hl})^2}{(q_+^2+M_l^2)(q_-^2+M_h^2)}\right\}, \quad (4.23)\end{aligned}$$

where $\Delta M_{lh} = M_l - M_h$, and Λ denotes the ultraviolet mass scale associated with the regularization. By using three times the identity of Eq. (4.22), the first two terms can be rewritten as

$$\int_q^\Lambda \frac{1}{q_\pm^2+M_{l,h}^2} = I_{\rm quad}(M_{l,h}^2) + \eta_\pm^2\, P_\mu P_\nu A_{\mu\nu}(M^2), \quad (4.24)$$

where $A_{\mu\nu}(M^2)$ is the integral defined by

$$A_{\mu\nu}(M^2) = \int_q^\Lambda \frac{4q_\mu q_\nu - (q^2+M^2)\delta_{\mu\nu}}{(q^2+M^2)^3}, \quad (4.25)$$

which is the Euclidean space counterpart of the integral $\Delta_{\mu\nu}(M^2)$ in Minkowski space of Refs. [46,43,44]. Using Eq. (4.24) and subtracting each of the denominators in the third term in Eq. (4.23), one can write $\mathcal{K}_{\rm PS}^{EE}$ as a sum of three kinds of terms: (1) a finite integral independent of $\eta_\pm$; (2) quadratic and logarithmically divergent integrals that are also independent of $\eta_\pm$; and (3) a symmetry violating term proportional to η_+^2 and η_-^2, namely,

$$\begin{aligned}\mathcal{K}_{\rm PS}^{EE}(P) &= 8\Big\{-\left[P^2+(\Delta M_{hl})^2\right]\left[I_{\log}(M^2) - Z_0(M_l^2,M_h^2,P^2;M^2)\right] \\ &+ I_{\rm quad}(M_l^2) + I_{\rm quad}(M_h^2) + \left(\eta_+^2+\eta_-^2\right) A_{\mu\nu}(M^2)P_\mu P_\nu\Big\}, \quad (4.26)\end{aligned}$$

where $Z_0(M_l^2,M_h^2,P^2;M^2)$ is the finite integral

$$\begin{aligned}Z_0(M_l^2,M_h^2,P^2;M^2) &= \int_0^1 dz \int_q^\Lambda \left[\frac{1}{(q^2+M^2)^2} - \frac{1}{(q^2+H(z))^2}\right] \\ &= \frac{1}{(4\pi)^2}\int_0^1 dz\, \ln\left[\frac{H(z)}{M^2}\right], \quad (4.27)\end{aligned}$$

where $H(z)$ is the function

$$H(z) = z(1-z)P^2 - (M_l^2 - M_h^2)z + M_l^2. \tag{4.28}$$

Here $I_{\log}(M^2)$ and $I_{\rm quad}(M^2)$ are the logarithmically and quadratically divergent integrals,

$$I_{\log}(M^2) = \int_q^\Lambda \frac{1}{(q^2+M^2)^2}, \tag{4.29}$$

$$I_{\rm quad}(M^2) = \int_q^\Lambda \frac{1}{q^2+M^2}. \tag{4.30}$$

In the derivation of Eq. (4.26), we made use of the identity

$$I_{\rm quad}(M_{l,h}^2) = I_{\rm quad}(M^2) - (M_{l,h}^2 - M^2)I_{\log}(M^2) - \frac{1}{(4\pi)^2}\left[M_{l,h}^2 - M^2 - M_{l,h}^2 \ln\left(\frac{M_{l,h}^2}{M^2}\right)\right]. \tag{4.31}$$

We note that to arrive at these results, no momentum shift was made in the divergent integrals; if one had shifted the momenta without change in the integration limits, one would have missed the term proportional to $A_{\mu\nu}(M^2)$. We also note that the divergences in each of the integrals in the first equality of Eq. (4.27) cancel and the final result is finite. Therefore, there is no need for a regulator in Z_0. This feature, that one can remove the regulator in finite integrals, plays a very important role when considering high temperatures and densities in the NJL model [126,135,136,45]. It will play an important role also in the phenomenology of mesons with heavy quarks, as we discuss in the next section.

We stress that Eq. (4.26) is an exact result and no approximations were made in the derivation from Eq. (4.23). Moreover, as already mentioned, no momentum shifts were made in obtaining the symmetry-violating and divergent integrals. This is important, as a momentum shift in a divergent integral is a delicate process and in many instances is the source of symmetry violation. Note that whatever choice made for $\eta_\pm$ unavoidably implies translation symmetry breaking, *unless* the regularization scheme leads to $A_{\mu\nu}(M^2) = 0$. Momentum shifts were made only in the *finite integral* $Z_0(M_l^2, M_h^2, P^2; M^2)$; it can be integrated without imposing an ultraviolet cutoff. The integral develops an imaginary part that reflects the possibility of meson decay into a quark-antiquark pair when $P^2 < -(M_l + M_h)^2$; this is an unphysical feature that afflicts CI models. However, there is no difficulty in introducing an

infrared cutoff [29] in this and other finite integrals to avoid unphysical quark-antiquark thresholds in BS amplitudes. This will be implemented in Sec. 4.3. The expressions for the remaining kernels $\mathcal{K}^{EF}_{\rm PS}$, $\mathcal{K}^{FE}_{\rm PS}$, and $\mathcal{K}^{FF}_{\rm PS}$ contain the same terms as in Eq. (4.26) and an additional symmetry violation term—they are presented in Appendix D.

Let us next examine how choices of $\eta_\pm$ lead to violation of the WGT identity in Eq. (3.28) in the case of CI. In the chiral limit, $m^h = m^l = 0$, combining Eq. (3.28) with Eq. (3.25), straightforward manipulations lead to two equations (for the light-light case):

$$0 = M_l - \frac{8}{3}\left(\frac{1}{m^l_{\rm G}}\right)^2 \int_q^\Lambda \left(\frac{M_l}{q_+^2 + M_l^2} + \frac{M_l}{q_-^2 + M_l^2}\right), \tag{4.32}$$

$$0 = \int_q^\Lambda \left(\frac{q_+ \cdot P}{q_+^2 + M_l^2} - \frac{q_- \cdot P}{q_-^2 + M_l^2}\right). \tag{4.33}$$

Using Eq. (4.24) in Eq. (4.32), one obtains

$$\begin{aligned} 0 \;\; = \;\; & M_l - \frac{16}{3}\left(\frac{1}{m^l_{\rm G}}\right)^2 \Big[M_l I_{\rm quad}(M_l^2) \\ & + M_l \left(\eta_+^2 + \eta_-^2\right) A_{\mu\nu}(M^2) P_\mu P_\nu \Big]. \end{aligned} \tag{4.34}$$

The last terms, being proportional to η_+^2 and η_-^2 are symmetry violating. The subtractions in Eq. (4.33) lead to new symmetry violating terms, in addition to terms proportional to $A_{\mu\nu}(M^2)$:

$$\begin{aligned} \int_q^\Lambda \frac{q_\mu}{q_\pm^2 + M_l^2} \;\; = \;\; & \mp \eta_\pm P_\mu \, I_{\rm quad}(M_l^2) \mp \eta_\pm P_\alpha B_{\alpha\mu}(M^2) \\ & \pm \eta_\pm \left(\eta_\pm^2 P^2 + M^2 - M_l^2\right) P_\alpha A_{\alpha\mu}(M^2) \\ & \mp \frac{1}{2}\eta_\pm^3 P_\alpha A_{\alpha\beta}(M^2) \left(P_\mu P_\beta + P^2 \delta_{\beta\mu}\right) \\ & \mp \frac{1}{3}\eta_\pm^3 P_\alpha P_\beta P_\rho \, C_{\alpha\beta\rho\mu}(M^2), \end{aligned} \tag{4.35}$$

where $B_{\mu\nu}(M^2)$ and $C_{\mu\nu\rho\sigma}(M^2)$ are new tensor structures,

$$B_{\mu\nu}(M^2) \;\; = \;\; \int_q^\Lambda \frac{2q_\mu q_\nu - (q^2 + M^2)\delta_{\mu\nu}}{(q^2 + M^2)^2}, \tag{4.36}$$

$$C_{\mu\nu\rho\sigma}(M^2) \;\; = \;\; \int_q^\Lambda \frac{c_{\mu\nu\rho\sigma}(q, M^2)}{(q^2 + M^2)^4}, \tag{4.37}$$

with

$$\begin{aligned} c_{\mu\nu\rho\sigma}(q^2, M^2) &= 24 q_\mu q_\nu q_\rho q_\sigma - 4(q^2 + M^2) \\ &\times \ (\delta_{\mu\nu} q_\rho q_\sigma + \text{perm. } \nu\sigma\rho). \end{aligned} \tag{4.38}$$

The $B_{\mu\nu}(M^2)$ and $C_{\mu\nu\rho\sigma}(M^2)$ integrals are the Euclidean space counterparts of the Minkowski space integrals $\nabla_{\mu\nu}(M^2)$ and $\Box_{\mu\nu\rho\sigma}(M^2)$ of Refs. [46,43,44]. Using Eq. (4.35) in Eq. (4.33), we obtain

$$\begin{aligned} 0 &= \int_q^\Lambda \left(\frac{q_+ \cdot P}{q_+^2 + M_l^2} - \frac{q_- \cdot P}{q_-^2 + M_l^2} \right) \\ &= \text{terms proportional to } \ \eta_\pm \left(A_{\mu\nu}, B_{\mu\nu}, C_{\mu\nu\rho\sigma} \right). \end{aligned} \tag{4.39}$$

We observe that for arbitrary momentum routing in the loop integrals, the subtraction scheme allows one to systematically identify symmetry violating terms; they are proportional to the integrals $A_{\mu\nu}$, $B_{\mu\nu}$ and $C_{\mu\nu\rho\sigma}$ in Eqs. (4.25), (4.36) and (4.37). A consistent regularization scheme must make the integrals vanish automatically. Otherwise, the vanishing of the integrals must be imposed; in doing so, the regularization scheme becomes a central part of the model. Dimensional regularization and Pauli-Villars regularization are examples of schemes that lead to $A_{\mu\nu} = 0$, $B_{\mu\nu} = 0$, and $C_{\mu\nu\rho\sigma} = 0$. Removing the symmetry-violating terms, Eq. (4.34) becomes nothing else than the gap equation of Eq. (4.9).

Let us make contact with the GBCR scheme [125]. For a proper comparison, we need to take $\eta_+ = 1$ and $\eta_- = 0$, the choice made in that reference. For this choice, Eq. (4.33) becomes

$$\int_q^\Lambda \left(\frac{q_+ \cdot P}{q_+^2 + M_l^2} - \frac{q \cdot P}{q^2 + M_l^2} \right) = 0, \tag{4.40}$$

which is Eq. (15) of Ref. [125]. Using Eq. (4.35) for this integral, one obtains:

$$\begin{aligned} 0 &= \int_q^\Lambda \left(\frac{q_+ \cdot P}{q_+^2 + M^2} - \frac{q \cdot P}{q^2 + M^2} \right) \\ &= P_\mu \big[B_{\mu\nu}(M^2) + \frac{1}{3} C_{\mu\nu\rho\sigma}(M^2) P_\rho P_\sigma \\ &\quad + \frac{1}{3} P_\mu A_{\rho\nu}(M^2) P_\rho - \frac{4}{3} P^2 A_{\mu\nu}(M^2) \big] P_\nu, \end{aligned} \tag{4.41}$$

that is, the M_l dependence cancels and the remaining divergent terms depend on

M only:

$$B_{\mu\nu}(M^2) \;+\; \frac{1}{3}C_{\mu\nu\rho\sigma}(M^2)P_\rho P_\sigma + \frac{1}{3}P_\mu A_{\rho\nu}(M^2)P_\rho - \frac{4}{3}P^2 A_{\mu\nu}(M^2) = 0. \tag{4.42}$$

In the chiral limit, this is equal to

$$B_{\mu\nu}(M^2) = 0 = \delta_{\mu\nu}\int_q^\Lambda \frac{\frac{1}{2}q^2 + M^2}{(q^2+M^2)^2}, \tag{4.43}$$

which is Eq. (17) of Ref. [125]. This result makes it clear that our scheme, besides being in agreement with Ref. [125] for the particular choice of $\eta_\pm$, it is also more general as is valid for *arbitrary* values of $\eta_\pm$. The independence of the results on $\eta_\pm$ is particularly important when $M_h \gg M_l$. Reference [124] has analyzed this issue studying the pion and kaon using a finite-range interaction model in the RL approximation and found essentially no $\eta_\pm$ dependence. In a more recent study, still within a RL framework but using a different interaction model, Ref. [14] finds agreement with the conclusions of Ref. [124] for the pion and kaon, but for heavy-light mesons, it finds that the results are very sensitive on choices for $\eta_\pm$. The same sensitivity to $\eta_\pm$ is also seen in the simpler heavy-light meson models of Refs.[137,138], where only the leading covariant of the Bethe-Salpeter amplitude is retained. In the subtraction scheme, this issue simply does not appear as the results are independent of $\eta_\pm$ by construction.

Here, we take the opportunity to comment on the role played by the subtraction mass M. As mentioned previously, it shares similarities with the mass scale μ that appears in dimensional regularization. Indeed, suppose one uses dimensional regularization in the model. Besides removing automatically all potential symmetry-violating terms, dimensional regularization introduces an arbitrary mass scale μ that comes with the replacement $D = 4 \to D = 4-2\epsilon$ in the integrals. On the other hand, in the subtraction scheme one introduces the arbitrary mass M and prescribes that symmetry-violating terms vanish. In addition, one also obtains divergent integrals depending on M, like $I_{\log}(M^2)$ and $I_{\rm quad}(M^2)$ of Eqs. (4.29) and (4.30), that need a regularization that cannot be removed because the model is nonrenormalizable. Applying dimensional regularization in those integrals, one introduces two arbitrary

dimensionful parameters, M and μ:

$$\begin{aligned} I_{\log}(M^2) &= (\mu)^{2\epsilon} \int \frac{d^D q}{(2\pi)^D} \frac{1}{(q^2+M^2)^2} \\ &= \frac{1}{(4\pi)^2}\left[\frac{1}{\epsilon} - \ln\left(\frac{M^2}{\bar{\mu}^2}\right)\right], \end{aligned} \tag{4.44}$$

where $\bar{\mu}^2 = 4\pi e^{-\gamma}\mu^2$. Choosing $\bar{\mu} = M$, the integral is scale independent; likewise for $I_{\rm quad}(M^2)$, it depends only on M. Alternatively, there is no need for evaluating these integrals with an explicit regulator, since M can be set by fitting the parameters of the model to physical quantities [43,44,139]. Through relations like that in Eq. (4.31), one obtains the divergent integrals at any other scale in terms of the physical quantities fitted at the scale M. As said, we do not trail this interesting possibility in this thesis and simply keep M arbitrary and use a second scale that is an ultraviolet cutoff. As we shall discuss in the next section, our results are essentially independent of M; small differences in the results caused by using different values can be absorbed by refitting parameters.

The masses of the mesons are obtained from Eq. (4.13) and as we have seen in the Chapter. 3, the equation defines an eigenvalue problem with solutions for the masses $P^2 = -m_{\rm PS}^2$, namely,

$$\lambda(P^2)\,\Gamma_{\rm PS}(P^2) = \mathcal{K}(P^2)\,\Gamma_{\rm PS}(P^2), \tag{4.45}$$

where $\mathcal{K}(P^2)$ is the 2×2 matrix defined in Eq. (4.13), and $\lambda(-m_{\rm PS}^2) = 1$. Then, from Eq. (4.13) one has

$$\begin{aligned} F(m_{\rm ps}^2) &= 1 - G_{lh}K_{\rm PS}^{EE}(-m_{\rm PS}^2) - G_{lh}K_{\rm PS}^{FF}(-m_{\rm PS}^2) \\ &- G_{lh}^2\left[K_{\rm PS}^{EE}(-m_{\rm PS}^2)K_{\rm PS}^{FF}(-m_{\rm PS}^2) + K^{EF}(-m_{\rm PS}^2)_{\rm PS}K_{\rm PS}^{FE}(-m_{\rm PS}^2)\right] , \end{aligned} \tag{4.46}$$

where we have defined G_{lh} as

$$G_{lh} = \frac{1}{3m_{\rm G}^l m_{\rm G}^h} . \tag{4.47}$$

The root of Eq. (4.46) give us the pseudoscalar meson mass. The derivation of the subtracted kernels is detailed in Appendix D.

The weak decay constant of the PS meson, $f_{\rm PS}$, can be extracted from

$$\begin{aligned} P_\mu f_{\rm PS} &= \langle 0|\bar{\psi}_l(0)\gamma_\mu\gamma_5\psi_h(0)|\Phi(P)\rangle \\ &= N_c\int_q {\rm Tr}\left[\gamma_5\,\gamma_\mu S_l(q_+)\Gamma_{\rm PS}^{lh}(P)S_h(q_-)\right], \end{aligned} \tag{4.48}$$

where ψ_l and ψ_h are quark field operators and $|\Phi(P)\rangle$ is the state of the PS meson with momentum P. Also, the trace in Eq. (4.48) is over Dirac indices. Inserting Eq. (4.12) into Eq. (4.48) and evaluating the trace leads to

$$f_{\rm PS} = \frac{N_c}{4M_{lh}} \left[E_{\rm PS}(P)\mathcal{K}^{FE}_{\rm PS} + F_{\rm PS}(P)\mathcal{K}^{FF}_{\rm PS} \right]_{P^2=-m^2_{\rm PS}} , \tag{4.49}$$

where, we recall, $M_{lh} = M_l M_h/(M_l + M_h)$. The eigenvalue equation Eq. (4.45) does not fix the amplitudes $E_{\rm PS}(P)$ and $F_{\rm PS}(P)$ separately; for that, one needs a normalization condition, which in the CI approximation Eq. (3.33) reduces to

$$\begin{aligned} 2P_\mu &= N_c \int \frac{d^4q}{(2\pi)^4} {\rm Tr} \Bigg[\bar{\Gamma}^{hl}_{\rm PS}(-P) \frac{\partial S_l(q_+)}{\partial P_\mu} \Gamma^{hl}_{\rm PS}(P) S_h(q_-) \\ &\quad + \bar{\Gamma}^{hl}_{\rm PS}(-P) S_l(q_+) \Gamma^{hl}_{\rm PS}(P) \frac{\partial S_h(q_-)}{\partial P_\mu} \Bigg], \end{aligned} \tag{4.50}$$

evaluated at $P^2 = -m^2_{\rm PS}$, where the charge conjugated pseudoscalar BSA is defined as $\bar{\Gamma}^{hl}_{\rm PS}(-P) = \left[C^{-1}\Gamma^{hl}_{\rm PS}(-P)C \right]^T = \Gamma^{hl}_{\rm PS}(-P)$. We note that with this convention, the experimental value of the pion decay constant is $f_\pi \simeq 130$ MeV [140]. For the case of the pion , where we have $M_l = M_h = M$, the psudoscalar kernels reduce to

$$\mathcal{K}^{EE}_\pi(P) = 8 \left\{ 2I_{\rm quad}(M^2) - P^2 \left[I_{\log}(M^2) - Z_0(M^2, P^2) \right] \right\} , \tag{4.51}$$

$$\mathcal{K}^{EF}_\pi(P) = 16P^2 \left[I_{\log}(M^2) - Z_0(M^2, P^2) \right] , \tag{4.52}$$

$$\mathcal{K}^{FE}_\pi(P) = \frac{M^2}{2P^2} \mathcal{K}^{EF}_\pi(P) , \tag{4.53}$$

$$\mathcal{K}^{FF}_\pi(P) = -2\mathcal{K}^{FE}_\pi(P) , \tag{4.54}$$

which are the equivalent to the equations (32)-(35) of Ref. [32]. The pion decay constant is given by

$$f_\pi = \frac{N_c}{2M} \left[E_\pi(P) - 2F_\pi(P) \right] \mathcal{K}^{FE}_\pi(P) \Big|_{P^2=-m^2_\pi} , \tag{4.55}$$

that is the equivalent to the equation (40) of Ref. [32]. Now, for example in the chiral limit, it is easy to see that $\mathcal{K}^{EE}_\pi = 8\, I_{\rm quad}(M^2)$, $\mathcal{K}^{EF}_\pi = 0$, $\mathcal{K}^{FE}_\pi = 8M^2 I_{\log}(M^2)$ and $\mathcal{K}^{FF}_\pi = -2\mathcal{K}^{FE}_\pi$. Therefore, the pion decay constant Eq. (4.55) in the chiral limit (f^0_π) can be written as

$$f^0_\pi = 4N_c M \left[E^0_\pi - 2F^0_\pi \right] I_{\log}(M^2) . \tag{4.56}$$

On the other hand, in the neighborhood of $P^2 = 0$, the solution of the axial-vector vertex, $\Gamma_{5\nu}(k_+, k_-)$, has the form [141,142]

$$\Gamma_{5\mu}(k_+, k_-) = \frac{P_\mu}{P^2} 2 f_\pi^0 \Gamma_\pi(P) + \gamma_5 \gamma_\mu F_R(P) \ , \tag{4.57}$$

where $\Gamma_\pi(P)$ is the normalized pion BSA and F_R is regular as $P^2 = 0$. Then, from the axial-vector WGT identity in the chiral limit one has

$$f_\pi^0 E_\pi^0 = M \ , \tag{4.58}$$

$$2\frac{F_\pi^0}{E_\pi^0} + F_R = 1 \ , \tag{4.59}$$

which are the generalized Goldberger-Treiman relations [141].

The normalization condition Eq. (D.22), in the case of the pion in the chiral limit reduces to

$$1 = 4 N_c E_\pi^0 \left[E_\pi^0 - 2 F_\pi^0 \right] I_{\log}(M^2) \ . \tag{4.60}$$

Thus, taking the ratio between Eq. (4.56) and Eq. (4.60) one obtains again the Goldberger-Treiman relation Eq. (4.58), which implies that in the chiral limit the pion normalization constant, $\mathcal{N}_\pi$, is equal to the pion decay constant because $E_\pi^0 = \bar{E}_\pi^0 / \mathcal{N}_\pi = M / \mathcal{N}_\pi$, where $\bar{E}_\pi^0$ is the unnormalized pion BSA.

To close this section, we comment on the regularization procedure. On computing the masses and the decay constants of the pseudoscalar mesons, the first step is to obtain the constituent quark masses, M_f, from the gap equation, Eq. (4.9), and then solve the eigenvalue problem, Eq. (4.45). Both equations contain the ultraviolet divergent integrals $I_{\rm quad}$ and $I_{\log}$ that need regularization and, in addition, Eq. (4.45) contains also the finite integral Z_0-function (and the Z_1 that appears in the other kernels). As briefly discussed in Sec. 4.2, Z_0 develops thresholds as it can acquire an imaginary part when $P^2 < -(M_l + M_h)^2$. We avoid the possibility of unphysical thresholds in hadron decay into quarks by eliminating this branch cut with an infrared cutoff. Both ultraviolet and infrared cutoffs can be introduced using a proper-time regularization [29] as follows. All integrals, finite and divergent, contain integrands of the form $1/(q^2 + a^2)^n$, where $n = 1, 2$ and a^2 is independent of q. The imaginary part in Z_0 happens when $q^2 \to -a^2$; to avoid this happening,

one then rewrites the integrands as

$$\begin{aligned}\frac{1}{(q^2+a^2)^n} &= \frac{1}{(n-1)!}\int_0^\infty d\tau\,\tau^{n-1}\,e^{-\tau(q^2+a^2)} \\ &\to \frac{1}{(n-1)!}\int_{\tau_{\rm uv}}^{\tau_{\rm ir}} d\tau\,\tau^{n-1}\,e^{-\tau(q^2+a^2)},\end{aligned} \tag{4.61}$$

with $\tau_{\rm uv}=1/\Lambda_{\rm uv}^2$ and $\tau_{\rm ir}=1/\Lambda_{\rm ir}^2$, where $\Lambda_{\rm uv}$ and $\Lambda_{\rm ir}$ are the ultraviolet and infrared cutoffs respectively. For the Z_0 integral, $\tau_{\rm uv}$ is not needed, as the integral is finite; therefore

$$\frac{1}{(q^2+a^2)^2} \to \frac{1-\left[1+(q^2+a^2)\,\tau_{\rm ir}\right]e^{-\tau_{\rm ir}(q^2+a^2)}}{(q^2+a^2)^2}, \tag{4.62}$$

which is finite when $q^2\to -a^2$, as can be verified very easily. The final result for Z_0 can be written as

$$\begin{aligned}Z_0(M_l^2,M_h^2,P^2;M^2) &= \frac{1}{(4\pi)^2}\int_0^1 dz\int_0^{\tau_{\rm ir}^2}\frac{d\tau}{\tau}e^{-\tau M^2} \\ &\quad\times\left(1-e^{-\tau[H(z)-M^2]}\right),\end{aligned} \tag{4.63}$$

which is clearly finite when $\tau\to 0$. Unphysical thresholds in the function Z_1 are eliminated using its relation to Z_0, given in Eq. (D.14).

Although $\tau_{\rm ir}$ is not needed for $I_{\rm quad}$ and $I_{\rm log}$, we keep it in those integrals to compare results with Ref. [125]. Therefore

$$I_{\rm quad}(M_f^2)=\frac{1}{(4\pi)^2}\int_{\tau_{\rm uv}^2}^{\tau_{\rm ir}^2}\frac{d\tau}{\tau^2}\,e^{-\tau M_f^2}. \tag{4.64}$$

The logarithmically divergent integral $I_{\rm log}(M_f^2)$ can be derived from $I_{\rm quad}(M_f^2)$ by a simple differentiation:

$$I_{\rm log}(M_f^2) = -\frac{\partial I_{\rm quad}(M_f^2)}{\partial M_f^2}. \tag{4.65}$$

Using (4.64) the gap equation Eq. (4.9) can be rewitten as

$$M_f = m_f + \frac{M_f\,G}{3\pi^2}\int_{\tau_{\rm uv}^2}^{\tau_{\rm ir}^2}\frac{d\tau}{\tau^2}\,e^{-\tau M_f^2}\ , \tag{4.66}$$

where we have introduced the coupling $G=(1/m_G^f)^2$. We see from Eq. (4.66) that there is a trivial solution when $G=0$, but a solution also exists at large G. In the chiral limit the critical coupling, $G_{\rm cr}$, has the form

$$G_{\rm cr}=\frac{3\pi^2}{(\Lambda_{\rm uv}^2-\Lambda_{\rm ir}^2)}\ . \tag{4.67}$$

Therefore, in chiral limit the constituent quark mass has non-trivial solution where $M \neq 0$ provided by $G < G_{\rm cr}$. This result is shown in Fig. 4.2 and we see that the constituent quark mass is zero when $x < 1$, being $x = G/G_{\rm cr}$; above that value the chiral symmetry is dynamically broken. The results for the dynamical quark mass

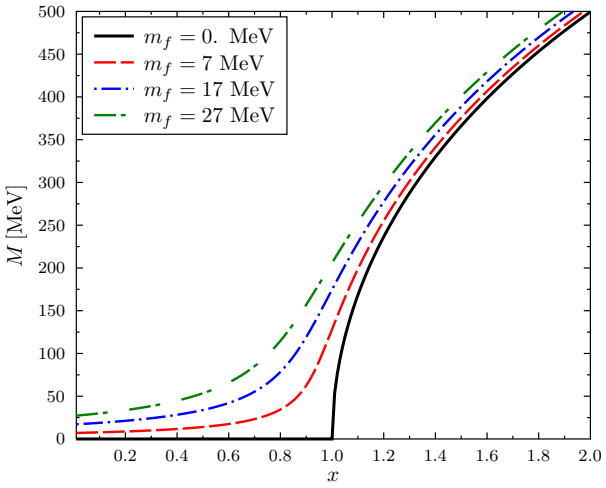

Figure 4.2: Solution of the gap equation as a function of x. Solid line is the solution in the chiral limit $m_f = 0$ and the dashed lines show the solution for $m_f \neq 0$.

presented in Fig. 4.2 was found using the infrared and ultraviolet cutoffs of Ref. [36]: $\Lambda_{\rm ir} = 240$ MeV and $\Lambda_{\rm uv} = 905$ MeV.

4.3 Numerical Results

We start considering the $f = \{u, d, s\}$ quark flavors and compare results from the CI subtraction and GBCR schemes [125]. More specifically, we compare results with Ref. [36] that extended the GBCR CI to the strange flavor sector. We recall the differences that mark both approaches: in the subtraction scheme the results are independent of $\eta_\pm$, while those in Refs. [125,36] are for $\eta_+ = 1$ and $\eta_- = 0$. The finite integrals Z_0 and Z_1 in the BS amplitudes that appear in the subtraction scheme can be integrated without imposing ultraviolet or infrared cutoffs, though we removed the thresholds of these functions by means of infrared cutoff as discussed in the previous section. As shown in Sec. 4.2, for $\eta_+ = 1$ and $\eta_- = 0$ and neglecting symmetry violating terms and using the same ultraviolet and infrared cutoffs, both approaches lead to identical results for the gap equation. There will be differences, that we quantify in the following, in the numerical values for meson observables due

to the different treatment of the BS amplitudes, in that in the subtraction scheme no regulator is used in the finite integrals Z_0 and Z_1.

The free parameters are the quark masses m_u, m_d and m_s, the coupling strength $\alpha_{\rm IR}$, the gluon-mass scale m_g, and the cutoffs $\Lambda_{\rm ir}$ and $\Lambda_{\rm uv}$. For a proper comparison, we use the parameter set of Ref. [36]: $m_u = m_d = m = 7$ MeV, $m_s = 165$ MeV, $\alpha_{\rm IR} = 0.93\pi$, $m_g = 800$ MeV, $\Lambda_{\rm ir} = 240$ MeV, and $\Lambda_{\rm uv} = 905$ MeV. The ultraviolet cutoff is used in the divergent integrals $I_{\rm log}$ and $I_{\rm quad}$ only. These parameters give for the constituent masses, solutions of the gap equation in Eq. (4.9): $M_u = M_d = 367$ MeV and $M_s = 523$ MeV.

In Table 4.1 we present the BS amplitudes $(E, F)_{\rm PS}$ and masses and decay constants $(m, f)_{\rm PS}$ of π and K from both approaches. Here, we use the natural value for the subtraction mass M in the calculation for both π and K properties, namely the light constituent quark mass, $M = M_u$; choosing $M = M_s$, or any other value between M_u and M_s, does not change the results for the properties of π and K, as expected. Table 4.1 informs that the results in both approaches compare very well, and are in good agreement with experimental data. The particular choice of momentum partitioning and use or not of an ultraviolet cutoff in finite integrals does not affect the results in this case. While the first conclusion is consistent with the findings in Ref. [124] in a finite-range RL model, the second means that the momentum integrands that give rise to the finite functions Z_0 and Z_1 have integrands well concentrated within the momentum range extending from $\Lambda_{\rm ir}$ to $\Lambda_{\rm uv}$.

Table 4.1: BS amplitudes $(E, F)_{\rm PS}$ and masses and decay constants $(m, f)_{\rm PS}$ of π and K from the CI subtraction scheme and CI GBCR of Ref. [36]. The amplitudes are dimensionless and masses and decay constants are listed in MeV.

	$(E,F)_\pi$	$(E,F)_K$	$(m,f)_\pi$	$(m,f)_K$
Data (PDG)	—	—	(139, 131)	(494, 156)
CI-subtr	(5.10, 0.67)	(5.64, 0.85)	(139, 144)	(502, 153)
GBCR [36]	(5.09, 0.68)	(5.40, 0.83)	(140, 141)	(500, 156)

Next, we include the charm quark and calculate properties of heavy-light mesons. The issue on the necessity for a flavor dependence of the effective coupling is exposed:

using the same parameters as in the light quark sector and adjusting the charm quark mass to fit the mass of the $D-$meson, the decay constant f_D turns out smaller than f_K. The same feature is also present in Ref. [49] within the NJL model. Like in the extension of the NJL model made in Refs. [127,126] to high temperatures and densities, and also in the extension of the GBCR CI model in Refs. [41,42] to charmonium, one can readjust the effective coupling $m_{\rm G}^h$ and the ultraviolet cutoff $\Lambda_{\rm uv}$ in our model. In the light quark sector, we used $m_g = 800$ MeV and $\alpha_{\rm IR} = 0.93\pi$, which imply $m_{\rm G}^l = 132$ MeV. We set $m_c = 1454$ MeV, and reset $\Lambda_{\rm uv} = 1290$ MeV and $m_{\rm G}^h = 3.5\, m_{\rm G}^l = 462$ MeV—see Eq. (4.2). We stress that the new value of $\Lambda_{\rm uv}$ is used in the gap and BS equation involving the charm quark only. Regarding the subtraction mass M, we use for it the light quark mass; more on this at the end of this section. From the gap equation, we obtain $M_s = 529$ MeV and $M_c = 1490$ MeV, which shows that there is very little dressing of the charm quark.

Table 4.2 presents our results for the masses and decay constants of pseudoscalar mesons. We have also readjusted the strange quark mass to $m_s = 165$ MeV to obtain a perfect fit to m_K. For orientation and comparison, we have listed in the table the results from the GBCR CI and from several representative studies employing finite-range interactions treated within the RL framework of the DS and BS equations in QCD. The latter are identified in the table by NST1 and NST2 from Ref. [7], REBM from Ref. [12], HK from Ref. [15], and HGKL1 and HGKL2 from Ref. [17]. The first observation one can draw from Table 4.2 is that, once the parameters of CI subtraction model are fixed to obtain an almost perfect agreement with experiment for the $m_{\rm PS}$ masses, the model predicts for the decay constants, $f_\pi < f_K < f_D < f_{D_s}$, a pattern that is corroborated by realistic DS-BS and lattice-QCD calculations. Moreover, the individual values of $f_{\rm PS}$ are in very good agreement with the experimental and lattice data collected by the PDG [140], the discrepancies being at the level of a few percent. It is also remarkable that the CI subtraction model gives a much better description for $(m, f)_{\rm PS}$ than finite-range models within the RL framework, in which the discrepancies with the PDG values for the decay constants can reach up to 40% in some cases.

Regarding the very small value of f_D in the NJL model, one may reasonably object that it is due to the inadequate use of parameters adjusted to the light mesons. Although it is true that one can remedy this situation adjusting the coupling

Table 4.2: Masses and decay constants of the pseudoscalar mesons (in MeV). Parameters of the CI subtraction model are given in the main text. NST1, NST2, REBM, HGKL1 and HGKL2 are results from representative studies employing finite-range interactions treated within the RL framework of the DS and BS equations in QCD.

	$(m, f)_{\rm PS}$			
	π	K	D	D_s
Data (PDG)	(139, 131)	(494, 156)	(1864, 212)	(1968, 249)
CI-subtr	(139, 143)	(494, 153)	(1869, 207)	(1977, 240)
GBCR [34]	(140, 141)	(500, 156)	—	—
NJL [49]	(135, 131)	(498, 135)	(1869, 113)	—
NST1 [7]	(138, 131)	(497, 155)	(1850, 222)	(1970, 197)
NST2 [7]	—	—	(1880, 260)	(1900, 275)
REBM [12]	(138, 139)	(493, 164)	(2115, 204)	(2130, 249)
HK [15]	(137, 129)	(499, 157)	(1868, 268)	(1888, 268)
HGKL1 [17]	(137, 133)	(492, 155)	(1868, 323)	(1872, 269)
HGKL2 [17]	(137, 128)	(489, 150)	(1869, 960)	(1802, 295)

and cutoff in the NJL model, one still faces the problem that the results become unacceptably dependent on the choices for $\eta_\pm$. This means that for any new choice of $\eta_\pm$, new values for the parameters of the model are required to fit observables; the situation is even more dramatic, in that no solutions for the BS equation can be found for some choices of $\eta_\pm$. The subtraction scheme solves this problem.

We have also calculated masses and decay constants of vector mesons with the same parameter set used for the pseudoscalar mesons; the results are listed in Table 4.3. There is fairly good experimental information on their masses but not on their decay constants. The values quoted in Table 4.3 for the masses are taken from PDG [140] and those for the decay constants of ρ and K^* are extracted indirectly [143] from τ decays, whereas those for D^* and D_s^* are from a recent lattice calculation [144]. The CI predictions for the masses, $m_{\rm V}$, agree very well with ex-

periment but less well for $f_{\rm V}$, as there is a wrong ordering between f_ρ and f_{K^*} and between f_{D^*} and $f_{D_s^*}$.

Table 4.3: Masses and decay constants of vector mesons (in MeV). Parameters of the CI subtraction model are the same as in Table 4.2. The entries for Reference values are explained in the text.

	$(m,f)_V$			
	ρ	K^*	D^*	D_s^*
Reference values	(775, 212)	(892, 225)	(2010, 278)	(2112, 322)
CI-subt	(776, 205)	(881, 195)	(2011, 281)	(2098, 276)
GBCR [36]	(930, —)	(1030, —)	—	—
GBCR [32]	(928,182)	—	—	—
NST1 [7]	(742, 207)	(936, 241)	(2040, 160)	(2170, 180)
HGKL1 [17]	(758, 219)	(946, 247)	—	(2175, 178)
HGKL2 [17]	(725, 203)	(919, 237)	—	—

On the other hand, inspection of Table 4.3 reveals that finite-range RL models also have difficulties in the vector sector; for instance, $f_{D_s^*} < f_{K^*}$ in all of those models. In this connection, also calculated charmonium properties: in the same vein of Ref. [41], by a further increase of m_G^h and $\Lambda_{\rm uv}$, the CI subtraction model predicts similar results to those of the GBCR model, including the wrong ordering between the vector and pseudoscalar decay constants, $f_{J/\Psi} < f_{\eta_c}$. This is an additional indication that the vector channels pose a challenge for CI models, possibly reflecting in this context the limitations of the RL framework exposed in finite-range models [4,5,6,10].

4.4 Summary

A symmetry-preserving treatment of a vector-vector contact interaction was used to study charmed heavy-light mesons. The contact interaction is a representation of nonperturbative kernels used in Dyson-Schwinger and Bethe-Salpeter equations

of QCD. The Dyson-Schwinger equation was solved for the u, d, s and c quark propagators and the bound-state Bethe-Salpeter amplitudes respecting spacetime-translation invariance and the Ward-Green-Takahashi identities associated with global symmetries of QCD were obtained to calculate masses and electroweak decay constants of the pseudoscalar π, K, D and D_s and vector ρ, K^*, D^*, and D_s^* mesons. We have found that the predictions of the model are in good agreement with available experimental and lattice QCD data.

Chapter 5

Contact Interaction at Finite Temperature

So far, we have used the CI approximation to compute meson properties in the vacuum. The goal of this chapter is to extend the subtraction scheme introduced in the last chapter to finite temperature. In this case the situation is more complicated than in the vacuum because Lorentz covariance is broken at finite T and special care must be exercised to separate purely divergent contributions from thermal effects, which are finite and do not need regularization. In the next section, we will introduce some basic aspects of finite temperature, and afterwards will use with the CI. An extensive discussion of of thermal quantum field theory is given in Ref. [145,146].

5.1 Finite temperature-Matsubara formalism

The starting point of the thermal field theory is to couple the system to a heat bath at fixed temperature T. In equilibrium statistical physics, the partition function is the most important object because all the thermodynamic quantities can be calculated from it. In the grand canonical ensemble it takes the form

$$Z = \mathrm{Tr}\left[e^{-\beta\hat{H}}\right] = \sum_n \langle n|e^{-\beta\hat{H}}|n\rangle \ , \tag{5.1}$$

being $|n\rangle$ a complete set of orthonormal states, $\hat{H}$ the Hamiltonian and the temperature T enters by $\beta = 1/T$. The partition function can be written as a path integral and for the case of QCD one has

$$Z_\beta[\Phi] = \int_{\mathrm{periodic}} \mathcal{D}[\Phi] e^{-S_{\mathrm{QCD}}} \ , \tag{5.2}$$

where

$$S_{\mathrm{QCD}} = \int_0^\beta d\tau \int d^3x \left[\bar{\psi}_f(x)\left(\gamma\cdot D + m_f\right)\psi_f(x) + \frac{1}{4}F_{\mu\nu}F_{\mu\nu}\right] \ . \tag{5.3}$$

Here, we have that the time variable of the Minkowski space is changed to a complex, namely instead of real time t we have to use $t \to \tau := it$, with $\tau \in [0, \beta]$.

The integral measure $\mathcal{D}[\Phi]$ in Eq. (5.2) correspond to that Eq. (2.35), but with the restriction of the following boundary conditions in time for the fields

$$\begin{aligned} \psi_f(\tau, \mathbf{x}) &= -\psi_f\left(\tau + \frac{1}{T}, \mathbf{x}\right) \ , \quad \text{for a fermion field} \ , \\ A_\mu(\tau, \mathbf{x}) &= +A_\mu\left(\tau + \frac{1}{T}, \mathbf{x}\right) \ , \quad \text{for a boson field.} \end{aligned} \tag{5.4}$$

This means that the fermion fields are antiperiodic and boson fields are periodic. Thermodynamic variables are obtained as derivatives of ln $\mathcal{Z}$; thermal expectation values of other observables can be obtained by inserting the relevant expression for the operator into the path integral.

The Fourier transformations of the fields introduce the Matsubara formalism

$$\begin{aligned} \psi_f(\tau, \mathbf{x}) &= \sqrt{\frac{\beta}{V}} \sum_{n=-\infty}^{\infty} \sum_{\mathbf{p}} e^{i(\omega_n \tau + \mathbf{p}\cdot\mathbf{x})} \psi_{f\,n}(p) \ , \\ A_\mu(\tau, \mathbf{x}) &= \sqrt{\frac{\beta}{V}} \sum_{n=-\infty}^{\infty} \sum_{\mathbf{p}} e^{i(\nu_n \tau + \mathbf{p}\cdot\mathbf{x})} A_{\mu,n}(p) \ , \end{aligned} \tag{5.5}$$

where ω_n and ν_n are the fermionic and bosonic Matsubara frequencies given by

$$\nu_n = \frac{2n\pi}{\beta} \ , \quad \text{for bosons} \tag{5.6}$$

$$\nu_n = \frac{(2n+1)\pi}{\beta} \ , \quad \text{for fermions} \tag{5.7}$$

with n integer valued. Therefore, the integral over the energy has to be replaced by a sum over Matsubara frequencies, namely

$$\int \frac{d^4q}{(2\pi)^4} F(q) \to \frac{1}{\beta} \sum_{m=-\infty}^{\infty} \int \frac{d^3q}{(2\pi)^3} F(\omega_m, \mathbf{q}) \ , \tag{5.8}$$

As we have said before, the system has been coupled to an external heat bath. Therefore, at finite temperature there is a preferred rest frame which is specified by the heat bath. In other words this means that the direction of Euclidean time corresponds to the rest frame of the heat bath, that is defined by the four vector u_μ.

Now with this additional vector, the general structure of the quark propagator at finite temperature is [147]

$$\begin{aligned} S^{-1}(p, u) &= i\gamma \cdot p A(p^2, u^2, p\cdot u) + B(p^2, u^2, p\cdot u) \\ &+ i\gamma \cdot u \, p \cdot u \, C(p^2, u^2, p\cdot u) + i\sigma_{\mu\nu} p_\mu u_\nu \, D(p^2, u^2, p\cdot u) \ . \end{aligned} \tag{5.9}$$

By choosing $u_\mu = (0,0,0,1)$ and $p_\mu = (\omega_n, \mathbf{p})$, the last equation can be rewritten as

$$S_f^{-1}(\mathbf{p},\omega_n) = i\boldsymbol{\gamma}\cdot\mathbf{p}\,A(\mathbf{p}^2,\omega_n) + i\gamma_4\,\omega_n C(\mathbf{p}^2,\omega_n) + B(\mathbf{p}^2,\omega_n)\ , \tag{5.10}$$

where we have neglected the dressing function D because in the UV it does not contribute [147]. The three scalar dressing functions $\mathcal{F} = A,\ B,\ C$ are complex and satisfy

$$\mathcal{F}(\mathbf{p}^2,\omega_n)^* = \mathcal{F}(\mathbf{p}^2,\omega_{-n-1})\ . \tag{5.11}$$

On the other hand, similar to the quark propagator, at finite temperature the general structure of the gluon propagator changes and acquires a longitudinal and transverse parts, namely

$$D_{\mu\nu}(\mathbf{k},\nu_n) = P^L_{\mu\nu}(\mathbf{k},\nu_n)G(k,\nu_n) + P^T_{\mu\nu}(\mathbf{k},\nu_n)F(\mathbf{k},\nu_n)\ , \tag{5.12}$$

where $P^T_{\mu\nu}$ and $P^L_{\mu\nu}$ are projectors which are given by

$$P^T_{\mu\nu}(\mathbf{k},\nu_n) := \begin{cases} 0\ , & \text{for } \mu \text{ and/or } \nu = 4 \\ \delta_{ij} - \frac{k_i k_j}{\mathbf{k}^2}\ , & \text{for } \mu,\,\nu = i,j = 1,2,3\ \ , \end{cases} \tag{5.13}$$

and

$$P^L_{\mu\nu}(\mathbf{k},\nu_n) := \left(\delta_{\mu\nu} - \frac{k_\mu k_\nu}{k^2}\right) - P^T_{\mu\nu}\ . \tag{5.14}$$

5.2 DS and BS equations at finite temperature

At nonzero temperature the quark propagator with the CI approximation is given by

$$S^{-1}(\mathbf{p},\omega_n) = i\boldsymbol{\gamma}\cdot\mathbf{q} + i\gamma_4\,\omega_n + \frac{4}{3}\left(\frac{1}{m^f_{\rm G}}\right)^2 \frac{1}{\beta}\sum_{m=-\infty}^{\infty}\int\frac{d^3q}{(2\pi)^3}\,\gamma_\mu S(\mathbf{q},\omega_m)\,\gamma_\mu\ , \tag{5.15}$$

where we have omitted the temperature-induced separation of the gluon propagator into a transverse and longitudinal parts discussed in the previous section. Using the general form of the quark propagator Eq. (5.10) the last equation reads as

$$\begin{aligned} i\boldsymbol{\gamma}\cdot\mathbf{q}A + i\gamma_4\,\omega_n C + B &= i\boldsymbol{\gamma}\cdot\mathbf{q} + i\gamma_4\,\omega_n \\ &+ \frac{4}{3}\left(\frac{1}{m^f_{\rm G}}\right)^2 \frac{1}{\beta}\sum_{m=-\infty}^{\infty}\int\frac{d^3q}{(2\pi)^3}\,\gamma_\mu S(\mathbf{q},\omega_m)\,\gamma_\mu\ . \end{aligned} \tag{5.16}$$

After projecting to separate the scalar functions we obtain as before in the vacuum case that $A = 1$ and $B = M_f$ and for the case of C we obtain

$$C = 1 - \frac{8}{3\,\omega_n}\left(\frac{1}{m_{\rm G}^f}\right)^2 \int \frac{d^3q}{(2\pi)^3}\,\frac{1}{C}\left[\frac{1}{\beta}\sum_{m=-\infty}^{\infty}\frac{\omega_m}{\omega_m^2+\epsilon_f^2(\mathbf{q})}\right] \,, \tag{5.17}$$

where we have defined $\epsilon_f(\mathbf{q}) = E_f(\mathbf{q})/C$, with $E_f(\mathbf{q}) = \sqrt{\mathbf{q}^2 + M_f^2}$. In the last equation the sum over Matsubara frequencies vanishes and one finds $C = 1$, for details of evaluation of Matsubara sums see Appendix. E. Again, this means that at finite temperature we obtain a momentum independent solution for the quark propagator

$$S_f^{-1}(\mathbf{q},\omega_n) = i\boldsymbol{\gamma}\cdot\mathbf{q} + i\gamma_4\,\omega_n + M_f \,, \tag{5.18}$$

where the quark mass $M_f \equiv M_f(T)$ is given by

$$M_f = m_f + \frac{16}{3}\left(\frac{1}{m_{\rm G}^f}\right)^2 \frac{1}{\beta}\sum_{m=-\infty}^{\infty}\int \frac{d^3q}{(2\pi)^3}\frac{M_f}{\mathbf{q}^2+\omega_m^2+M_f^2} \,. \tag{5.19}$$

For the last equation we have to evaluate the sum over Matsubara frequencies and for this we write this equation in the form

$$\begin{aligned} M_f &= m_f + \frac{16}{3}\left(\frac{1}{m_{\rm G}^f}\right)^2 \int \frac{d^3q}{(2\pi)^3}\frac{M_f}{2E_f(\mathbf{q})} \\ &\times \frac{1}{\beta}\sum_{m=-\infty}^{\infty}\left[\frac{1}{i\omega_m + E_f(\mathbf{q})} - \frac{1}{i\omega_m - E_f(\mathbf{q})}\right], \end{aligned} \tag{5.20}$$

In this form, we can use the following relation to evaluate the sum over Matsubara frequencies

$$\frac{1}{\beta}\sum_{m=-\infty}^{\infty}\frac{1}{i\omega_m - E} = f(E) \,. \tag{5.21}$$

Using this the quark mass can be written as

$$M_f = m_f + \frac{16}{3}\left(\frac{1}{m_{\rm G}^f}\right)^2 \left\{ I_{\rm quad}(M_f^2) - \int \frac{d^3q}{(2\pi)^3}\frac{M_f}{E_f(\mathbf{q})} f(E_f(\mathbf{q}))\right\} \,, \tag{5.22}$$

with $f(E)$ being the the Fermi-Dirac distribution defined as

$$f(E) = \frac{1}{1+e^{\beta E}} \,. \tag{5.23}$$

In Eq. (5.22) $I_{\rm quad}$ is quadratically divergent integral given by Eq. (4.30), but being the quark mass M_f temperature dependent. Using the scale relation given by

Eq. (4.31) we can rewrite Eq. (5.22) in term of the vacuum quark mass M_{0f}, namely

$$\begin{aligned} M_f &= m_f + \frac{16}{3}\left(\frac{1}{m_{\rm G}^f}\right)^2 \Big\{ I_{\rm quad}(M_{0f}^2) - (M_f^2 - M_{0f}^2) I_{\log}(M_{0f}^2) \\ &- \frac{1}{(4\pi)^2}\left[M_f^2 - M_{0f}^2 - M_f^2 \ln\left(\frac{M_f^2}{M_{0f}^2}\right)\right] - \int \frac{d^3q}{(2\pi)^3}\frac{M_f}{E_f(\mathbf{q})} f(E_f(\mathbf{q}))\Big\}. \end{aligned} \tag{5.24}$$

This means that in the last equation we have not introduced divergent integrals which dependent on the temperature.

On the other hand, the BSE Eq. (4.10) reads as

$$\Gamma_M^{lh}(\mathbf{P},\nu_n) = -\frac{4}{3\, m_{\rm G}^l m_{\rm G}^h}\frac{1}{\beta}\sum_{m=-\infty}^{\infty}\int_{\mathbf{q}} \gamma_\mu S_l(\mathbf{q}_+,\omega_+)\Gamma_M^{lh}(\mathbf{P},\nu_n) S_h(\mathbf{q}_-,\omega_-)\gamma_\mu \ , \tag{5.25}$$

where $\mathbf{q}_\pm = \mathbf{q} \pm \eta_\pm \mathbf{P}$ and $\omega_\pm = \omega_m \pm \chi_\pm \nu_n$, with $\chi_\pm \in \mathbb{Z}$, and $\nu_n = 2n\pi/\beta$ are the bosonic Matsubara frequencies. If we consider the pseudoscalar channel the BSA is

$$\Gamma_{\rm PS}^{lh}(\mathbf{P},\nu_n) = \gamma_5\left[iE_{\rm PS}^{lh}(\mathbf{P},\nu_n) + \frac{1}{2M_{lh}}\gamma\cdot P\, F_{\rm PS}^{lh}(\mathbf{P},\nu_n)\right] \ . \tag{5.26}$$

For the scalar channel there is only a component for its BSA, namely in the CI approximation Eq. (3.35) reduces to

$$\Gamma_{\rm S}(\mathbf{P},\nu_n) = \mathbb{1} E_{\rm S}(\mathbf{P},\nu_n) \ , \tag{5.27}$$

where there is not a F component because charge conjugation requirement.

5.3 Subtraction scheme at finite temperature

In order to apply the subtraction scheme to finite temperature we will consider again the case of the pseudoscalar mesons. Therefore, at finite temperature Eq. (4.14) reads as

For this kernel we have to evaluate the following sums over Matsubara frequencies

$$S_\pm = \frac{1}{\beta}\sum_{m=-\infty}^{\infty}\frac{1}{\omega_\pm^2 + E_{l,h}^2(\mathbf{q}_\pm)} \ , \tag{5.28}$$

$$S_{+-} = \frac{1}{\beta}\sum_{m=-\infty}^{\infty}\frac{1}{[\omega_+^2 + E_l^2(\mathbf{q}_+)][\omega_-^2 + E_h^2(\mathbf{q}_-)]} \ . \tag{5.29}$$

After doing so, the kernel $\mathcal{K}_{\rm PS}^{EE}(\mathbf{P},\nu_n)$ can be written as

$$\mathcal{K}_{\rm PS}^{EE}(\mathbf{P},\nu_n) = \mathcal{K}_{\rm PS}^{EE}(\mathbf{P},\nu_n)|_{\rm div} + \mathcal{K}_{\rm PS}^{EE}(\mathbf{P},\nu_n)|_{\rm fin} \ , \tag{5.30}$$

where $\mathcal{K}^{EE}_{\rm PS}(\mathbf{P},\nu_n)|_{\rm div}$ and $\mathcal{K}^{EE}_{\rm PS}(\mathbf{P},\nu_n)|_{\rm fin}$ are given by

$$\begin{aligned}\mathcal{K}^{EE}_{\rm PS}(\mathbf{P},\nu_n)|_{\rm div} &= 8\int_{\mathbf{q}}\Bigg\{\frac{1}{2E_l(\mathbf{q}_+)}+\frac{1}{2E_h(\mathbf{q}_-)}\\ &- \frac{\left[\mathbf{P}^2+\nu_n^2+(\Delta M_{hl})^2\right]}{2E_l(\mathbf{q}_+)E_h(\mathbf{q}_-)}\frac{[E_l(\mathbf{q}_+)+E_h(\mathbf{q}_-)]}{[[E_l(\mathbf{q}_+)+E_h(\mathbf{q}_-)]^2-(i\nu_n)^2]}\Bigg\},\end{aligned} \tag{5.31}$$

$$\begin{aligned}\mathcal{K}^{EE}_{\rm PS}(\mathbf{P},\nu_n)|_{\rm fin} &= -8\int_{\mathbf{q}}\Bigg\{\frac{f(E_l(\mathbf{q}_+))}{2E_l(\mathbf{q}_+)}+\frac{f(E_h(\mathbf{q}_-))}{2E_h(\mathbf{q}_-)}+\frac{\left[\mathbf{P}^2+\nu_n^2+(\Delta M_{hl})^2\right]}{4E_l(\mathbf{q}_+)E_h(\mathbf{q}_-)}\\ &\times \left[\frac{2E_h(\mathbf{q}_-)f(E_l(\mathbf{q}_+))}{[i\nu_n+E_l(\mathbf{q}_+)]^2-E_h^2(\mathbf{q}_-)}+\frac{2E_h(\mathbf{q}_-)f(E_l(\mathbf{q}_+))}{[i\nu_n-E_l(\mathbf{q}_+)]^2-E_h^2(\mathbf{q}_-)}\right.\\ &+ \left.\frac{2E_l(\mathbf{q}_+)f(E_h(\mathbf{q}_-))}{[i\nu_n+E_h(\mathbf{q}_-)]^2-E_l^2(\mathbf{q}_+)}+\frac{2E_l(\mathbf{q}_+)f(E_h(\mathbf{q}_-))}{[i\nu_n-E_h(\mathbf{q}_-)]^2-E_l^2(\mathbf{q}_+)}\right]\Bigg\}.\end{aligned} \tag{5.32}$$

The details to arrive at these results are given in Appendix. (F). One notes that Eq. (5.31) is exactly the vacuum contributions Eq. (4.23) after integrating in the time variable in the complex plane. Therefore, for the kernel $K^{EE}_{\rm PS}(\mathbf{P},\nu_n)$ we have separated the purely divergent contributions from thermal effects, which are finite and do not need regularization. Thus, we note that at finite temperature the problem with symmetry violations comes from the divergent part $K^{EE}_{\rm PS}(\mathbf{P},\nu_n)|_{\rm div}$, which we have handled in the previous chapter by using the subtraction scheme.

The result for Eq. (5.31) after using Eq. (4.26) and taking the analytic continuation $i\nu_n \to \omega+\eta$ is given by

$$\begin{aligned}\mathcal{K}^{EE}_{\rm PS}(\mathbf{P},-i\omega)|_{\rm div} &= 8\Big\{I_{\rm quad}(M_l^2)+I_{\rm quad}(M_h^2)-\left[\mathbf{P}^2+\omega^2+(\Delta M_{hl})^2\right]\\ &\times \left[I_{\log}(M_0^2)-Z_0(M_l^2,M_h^2,\left(\mathbf{P}^2+\omega^2\right);M_0^2)\right]\Big\},\end{aligned} \tag{5.33}$$

and the finite part Eq. (5.32) which is in terms of the Fermi-Dirac distributions after the analytic continuation reads as

$$\begin{aligned}\mathcal{K}^{EE}_{\rm PS}(\mathbf{P},-i\omega)|_{\rm fin} &= -8\int_{\mathbf{q}}\Bigg\{\frac{f(E_l(\mathbf{q}_+))}{2E_l(\mathbf{q}_+)}+\frac{f(E_h(\mathbf{q}_-))}{2E_h(\mathbf{q}_-)}+\frac{\left[\mathbf{P}^2+\omega^2+(\Delta M_{hl})^2\right]}{4E_l(\mathbf{q}_+)E_h(\mathbf{q}_-)}\\ &\times \left[\frac{2E_h(\mathbf{q}_-)f(E_l(\mathbf{q}_+))}{[\omega+E_l(\mathbf{q}_+)]^2-E_h^2(\mathbf{q}_-)}+\frac{2E_h(\mathbf{q}_-)f(E_l(\mathbf{q}_+))}{[\omega-E_l(\mathbf{q}_+)]^2-E_h^2(\mathbf{q}_-)}\right.\\ &+ \left.\frac{2E_l(\mathbf{q}_+)f(E_h(\mathbf{q}_-))}{[\omega+E_h(\mathbf{q}_-)]^2-E_l^2(\mathbf{q}_+)}+\frac{2E_l(\mathbf{q}_+)f(E_h(\mathbf{q}_-))}{[\omega-E_h(\mathbf{q}_-)]^2-E_l^2(\mathbf{q}_+)}\right]\Bigg\}.\end{aligned} \tag{5.34}$$

Note that in Eq. (5.33) we have already neglected the symmetry violating term $A_{\mu\nu}(M_0^2)$, where M_0 is the vacuum subtraction mass used for the results reported

in the previous chapter. For the other pseudoscalar kernels also we can separate the purely divergent part from thermal effects and the results for them are given in Appendix. (F). Again, we can compute the pseudoscalar meson mass and the BS amplitudes by solving the eigenvalue problem defined by Eq. (4.45), but now using the 2×2 matrix defined by Eq. (F.1) evaluated at the rest frame of the meson $\mathbf{P} = 0$, and taking $\omega = m_{\rm PS}$. For the case of the scalar mesons the BSE at finite temperature is given by

$$1 \;=\; \frac{1}{m_G^l\, m_G^h} K_{\rm S}^{EE}\left(\mathbf{P}=0, -i\omega = i m_{\rm S}\right), \tag{5.35}$$

where the explicit expression the scalar kernel is given in Appendix. (F).

5.4 Numerical results

We start with the solution of the gap equation Eq. (5.24) using the same set vacuum parameters of Ref. [36] which were used in the previous chapter. At the top panel of Fig. 5.1 we present the results of the solution of the gap equation for the case of the chiral limit $m_f = 0$ and for $m_f = 7$ MeV, which in the vacuum generate the dynamical quark masses $M_{0f} = 359$ MeV and $M_{0f} = 368$ MeV respectively. From the figure we can see that the chiral solution (black curve) corresponds to a second-order transition, where the chiral symmetry is restored at the critical temperature $T_{\rm c} = 217$ MeV. The other solution (red-dashed curve) for a small but finite value of current quark mass corresponds to a crossover transition, which means a first-order transition, where we note that the chiral symmetry is partially restored above a pseudocritical temperature $T_{\rm pc} \approx 220$ MeV associated with the crossover. At the bottom panel, we present the results for the chiral susceptibility defined as the derivative of quark mass with respect of the temperature, $\chi = -dM/dT$, for both case. From the figure we see that in the chiral limit, the chiral susceptibility diverges at the critical temperature $T_c = 217$ MeV.

In Fig. 5.2 we depict the results for the temperature dependence of M_u, M_s and M_c. Here, one notes that as the current quark mass increases, the effect of the temperature becomes less important, even close to and above the pseudocritical temperature. We stress that for the case of the solution of the heavy quark mass M_c was found using the new values of $\Lambda_{\rm uv}$ and $m_{\rm G}^h$ that were readjusted in the previous chapter.

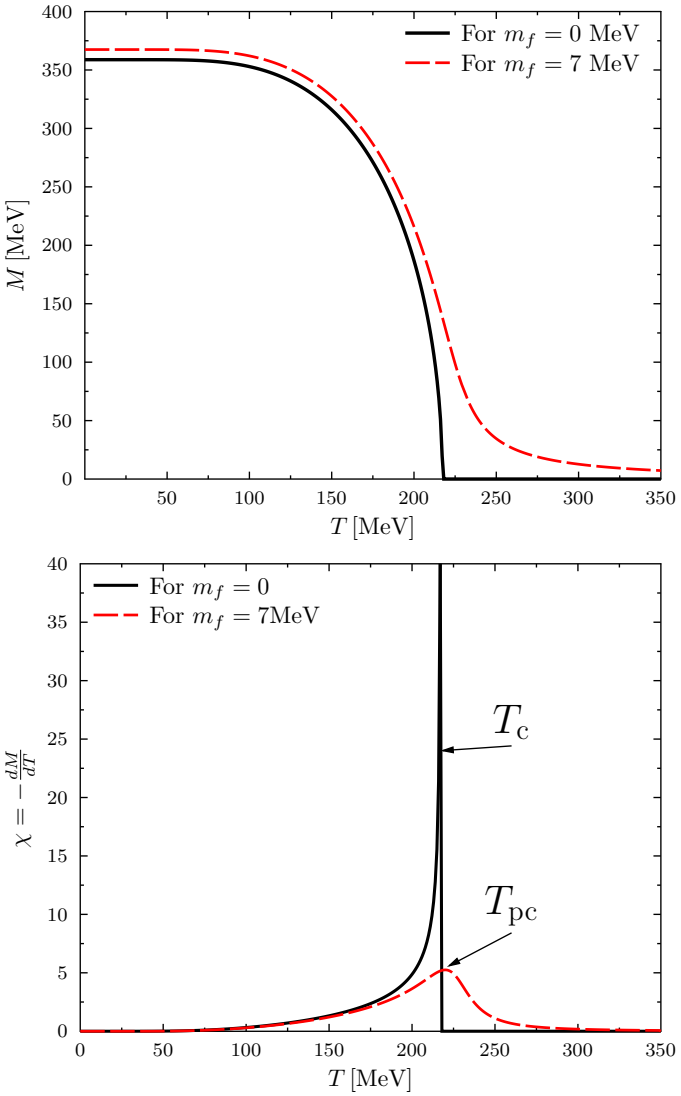

Figure 5.1: Temperature dependence of the solution of the gap equation. Top panel: the solution in the chiral limit $m_f = 0$ and for $m_f = 7$ MeV. Bottom panel: Chiral susceptibility $\chi = -dM/dT$ as a function of the temperature.

Now, we present the results for the mass spectrum of the mesons at finite temperature. We start considering the pion and the sigma mesons. For example, using Eq. (5.33) and Eq. (5.34) with $M_l = M_h = M$ and setting $\mathbf{P} = 0$, we obtain that the pion kernel $K_\pi^{EE}(0, -i\omega)$ can be written as

$$\begin{aligned} \mathcal{K}_\pi^{EE}(\mathbf{0}, -i\omega) &= 8\Bigg\{ \frac{1}{8G_\pi}\left(1 - \frac{m}{M}\right) + \omega^2 \Bigg[I_{\log}(M_0^2) - Z_0(M, \omega^2; M_0^2) \\ &- \frac{1}{4\pi^2}\int_0^\infty dq\, q^2 \frac{1}{E(\mathbf{q})} \frac{f(E(\mathbf{q}))}{[E^2(\mathbf{q}) - \omega^2/4]} \Bigg] \Bigg\} , \end{aligned} \tag{5.36}$$

where we have used the gap equation, Eq. (5.24), and also defined $G_\pi = 1/m_{\rm G}^2$. The

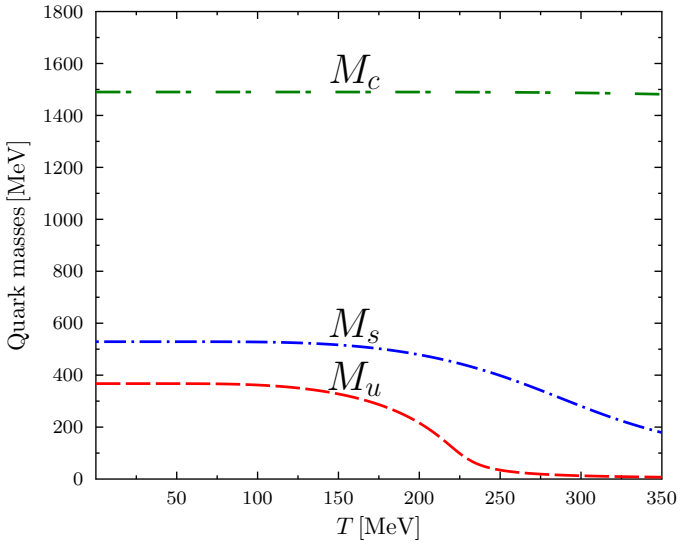

Figure 5.2: Temperature dependence of M_u, M_s and M_c generate by the current quark masses $m_u = 7$ MeV, $m_s = 165$ MeV and $m_c = 1454$ MeV.

other pion kernels can be obtained from Eqs. (F.54), (F.55), (F.56) and (F.57)

$$\begin{aligned}\mathcal{K}_\pi^{EF}(\mathbf{0},-i\omega) &= -16\omega^2\Big[I_{\log}(M_0^2) - Z_0(M,\omega^2;M_0^2) \\ &- \frac{1}{4\pi^2}\int_0^\infty dq\, q^2 \frac{1}{E(\mathbf{q})}\frac{f(E(\mathbf{q}))}{[E^2(\mathbf{q})-\omega^2/4]}\Big]\,, \qquad (5.37)\\ \mathcal{K}_\pi^{FE}(\mathbf{0},-i\omega) &= -\frac{M^2}{2\omega^2}\mathcal{K}_\pi^{EF}(\mathbf{0},-i\omega)\,, \qquad (5.38)\\ \mathcal{K}_\pi^{FF}(\mathbf{0},-i\omega) &= -2\mathcal{K}_\pi^{FE}(\mathbf{0},-i\omega)\,. \qquad (5.39)\end{aligned}$$

The normalization of the pion BS amplitudes, $E_\pi(\mathbf{0},-i\omega)$ and $F_\pi(\mathbf{0},-i\omega)$, are obtained via Eq. (D.22) and Eq. (D.28), using the pion kernels defined above.

In the previous chapter we have introduced an infrared cutoff into Z_0 integral in order to removed the thresholds in this function when $P^2 < -2M^2$. However, it is known that at finite temperature the production thresholds reappears when $T = T_d$ being T_d the deconfinement temperature [148]. From Eq. (5.36), one notes that the integral in the last term which is proportional to the Fermi-Dirac distribution diverges at $q = \pm\sqrt{\omega^2 - 4M^2}/2$, which means that the integral gets an imaginary part when $\omega^2 > 4M^2$. Here, for numerical calculations below $T_{\rm ps}$ we introduce a temperature dependent infrared cutoff $\tau_{\rm ir}(T)$ into Z_0 and the last integral in Eq. (5.36).

For us, the form of this cutoff is

$$\tau_{\rm ir}(T) = \frac{\tau_{\rm ir}}{\left|1-\frac{T}{T_{\rm pc}}\right|^{\alpha}} \ , \tag{5.40}$$

where α is a constant to be fixed. Therefore, when $T = T_{\rm pc}$ the cutoff defined by Eq. (5.40) goes to infinity and thus the pion kernel Eq (5.36) acquires an imaginary part. When this happens one can write an analytic expression for Z_0, namely

$$\begin{aligned} Z_0(M,\omega^2;M_0^2) &= \frac{1}{(4\pi)^2}\Bigg\{2+\sqrt{\frac{\omega^2-4M^2}{\omega^2}}\ln\left[\frac{\omega-\sqrt{\omega^2-4M^2}}{\omega+\sqrt{\omega^2-4M^2}}\right] \\ &- \ln\left(\frac{M^2}{M_0^2}\right)+i\pi\sqrt{\frac{\omega^2-4M^2}{\omega^2}}\Bigg\} \ , \end{aligned} \tag{5.41}$$

and for the other integral can be written as

$$\begin{aligned} \int_0^\infty dq\, q^2 \frac{1}{E(\mathbf{q})}\frac{f(E(\mathbf{q}))}{[E^2(\mathbf{q})-\omega^2/4]} &= \mathcal{P}\int_0^\infty dq\, q^2 \frac{h(q^2)}{q^2-k_0^2} \\ &+ 2\pi\, i\sqrt{\frac{\omega^2-4M^2}{\omega^2}} f\left(\frac{\omega}{2}\right) \ , \end{aligned} \tag{5.42}$$

where $\mathcal{P}$ denotes the Cauchy principal value [149], and we have defined $k_0^2 = (\omega^2 - 4M^2)/4$ and $h(q^2) = f(E(\mathbf{q}))/E(\mathbf{q})$. On the other hand, from Eq. (5.35) one has that the BSE for the sigma meson is

$$1 - G_\pi\, \mathcal{K}_\sigma(\mathbf{0},-i\omega)\Big|_{\omega^2=m_\sigma^2} = 0 \ , \tag{5.43}$$

with the sigma kernel given by

$$\begin{aligned} \mathcal{K}_\sigma(\mathbf{0},-i\omega) &= 8\Bigg\{\frac{1}{8G_\pi}\left(1-\frac{m}{M}\right)+(\omega^2-4M^2)\Bigg[I_{\log}(M_0^2)-Z_0(M,\omega^2;M_0^2) \\ &- \frac{1}{4\pi^2}\int_0^\infty dq\, q^2\frac{1}{E(\mathbf{q})}\frac{f(E(\mathbf{q}))}{[E^2(\mathbf{q})-\omega^2/4]}\Bigg]\Bigg\} \ , \end{aligned} \tag{5.44}$$

which allows us to write Eq. (5.43) in the form

$$m_\sigma^2 = 4M^2 + \frac{m}{8G_\pi M I(M,m_\sigma^2;M_0^2)} \ , \tag{5.45}$$

where we have defined the integral $I(M,m_\sigma^2;M_0^2)$ as

$$\begin{aligned} I(M,m_\sigma^2;M_0^2) &= I_{\log}(M_0^2) - Z_0(M,m_\sigma^2;M_0^2) \\ &- \frac{1}{4\pi^2}\int_0^\infty dq\, q^2\frac{1}{E(\mathbf{q})}\frac{f(E(\mathbf{q}))}{[E^2(\mathbf{q})-m_\sigma^2/4]} \ , \end{aligned} \tag{5.46}$$

and the normalization condition for the scalar BSA, $E_\sigma(\mathbf{0}, -i\omega)$, leads to

$$\frac{1}{E_\sigma^2} = \frac{3}{2}\frac{\partial \mathcal{K}_\sigma(\mathbf{0}, -i\omega)}{\partial \omega^2}\bigg|_{\omega^2 = m_\sigma^2} . \tag{5.47}$$

At $T = 0$, the sigma mass is obtained from Eq. (5.45), where the last integral in Eq. (5.46) vanishes in this limit and we obtain $m_\sigma = 741$ MeV in the vacuum. The result for the pion mass is reported in Table. 4.1. In the chiral limit the pion mass is zero and we note from Eq. (5.45) that the sigma mass is $m_\sigma = 2M$. For the case of $T \neq 0$, in Fig. 5.3 we depict the numerical results for the temperature dependence of the pion and sigma masses as well as the temperature evolution of the pseudovector component of the pion BSA, $F_\pi(T)$, and the pion decay constant $f_\pi(T)$ *. From the top panel of Fig. 5.3, we observe the following: First, below the pseudocritical temperature $T_{\rm pc}$ the pion mass remains constant (small T-dependence), while the sigma mass decreases and it is almost equal to $2M(T)$. Second, above the pseudocritical temperature at $T \sim 1.12\, T_{\rm pc}$ the masses of the pion and sigma start to be degenerate and to increase linearly with the temperature. Above the pseudocritical temperature, we can neglect the pseudovector component of the pion BSA, F_π, and the pion mass equation is exactly the second term in Eq. (5.45), which means that $m_\sigma^2 = 4M^2 + m_\pi^2$. Thus, when the symmetry is partially restored ($M \to m$) we obtain $m_\sigma(T) \simeq m_\pi(T)$, which is the behavior reported at the top panel of Fig. (5.3). These features are in agreement for example with the references [23,38,150,151,152].

Now, at the bottom panel of Fig. (5.3), we have reported the results for $F_\pi(T)$ and $f_\pi(T)$. From this figure, we note that as the temperature increases, the strength of these quantities begin to decreases and above the pseudocritical temperature they practically disappear. These results are also in according with Fig. (5) of Ref. [38], where the authors extend the GBCR schemes of Refs. [36,125] to finite temperature. Again, we point out some differences between both approaches. First, we have separated the thermal contributions from the BS kernels, which are finite, while in Ref. [38] the thermal parts are handled together with the divergent parts. Second, due to the form of handled the purely divergent parts into the BS kernels, we do not have temperature dependent symmetry violating terms. However, in Ref. [38] a temperature dependent integral is fixed to be zero to guarantee the vector and axial-vector WGTI.

*The results presented in Fig. (5.3) were obtained by fixing $\alpha = 0.5$ in Eq. (5.40). Above $T_{\rm ps}$ we have taken the real parts of Eqs. (5.41) and (5.42).

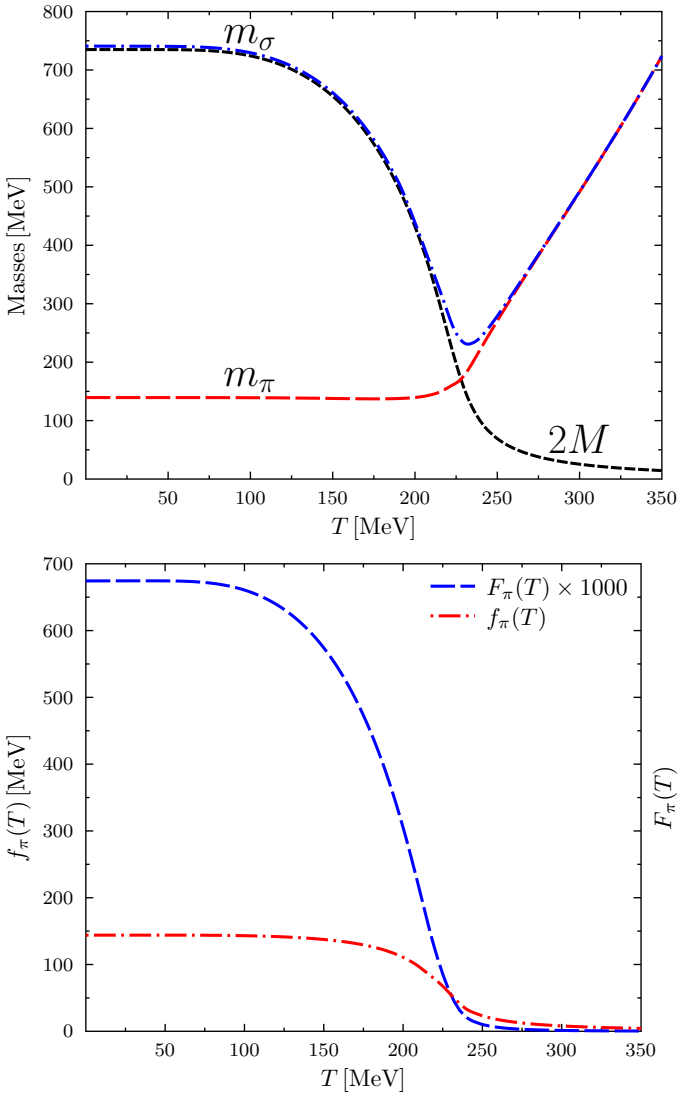

Figure 5.3: Top panel: Temperature dependence of the pion (red-dashed curve) and sigma (blue-dashed curve) masses for $m = 7$ MeV. In the graph the black-solid line represents the trajectory of $2M$. Bottom panel: Temperature dependence of pseudovector component of the pion BSA (blue-dashed curve), $F_\pi(T)$, and the pion decay constant (red-dot-dashed curve) $f_\pi(T)$.

On the other hand, Fig. 5.4 shows the temperature evolution of the pseudoscalar and scalar BS amplitudes. From this figure, one notes that due to the fact of the chiral symmetry restoration at high temperatures, we have $E_\sigma(T) \simeq E_\pi(T)$. In the Random phase approximation (RPA), these dimensionless quantities can be associated to the quark-meson couplings $g_{qq\pi}$ and $g_{qq\sigma}$ because Goldberger-Treiman relation. For example, in the usual NJL model one obtains in the chiral limit the

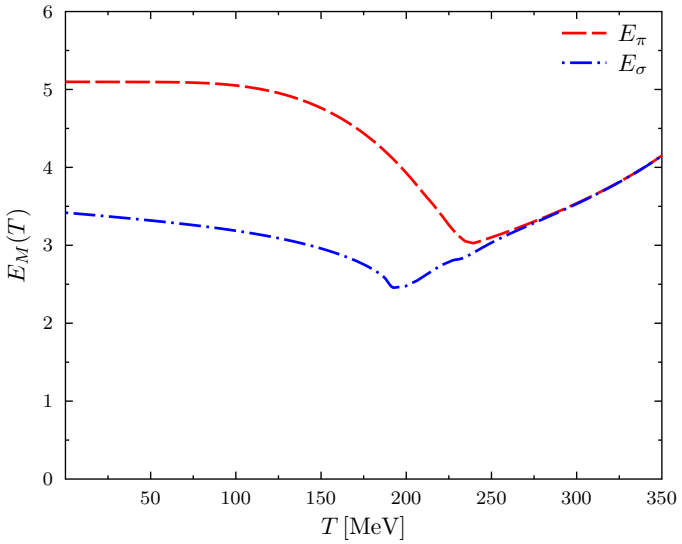

Figure 5.4: Temperature dependence of $E_\pi(T)$ (red-dashed curve) and $E_\sigma(T)$ (blue–dashed-doted curve).

well known result [23]

$$g_{qq\pi}\, f_\pi^0 = M \ . \tag{5.48}$$

Therefore, by comparing the with Goldberger-Treiman relation Eq. (4.58), we conclude that $E_\pi = g_{qq\pi}$. The temperature dependence of these quark-meson couplings have been used for example in recent studies of properties of exotic hadrons like the hadron molecule $\Delta\bar{D}^*$ that can be produced and realistically measured in high-energy heavy-ion collisions [56] and also the transport coefficients η and ζ [153].

In Fig. (5.5) we report the results for the temperature dependence of the kaon mass (top panel) and as well as the pseudovector component of the kaon BSA, $F_K(T)$ and the kaon decay constant $f_K(T)$ (bottom panel). Also, at the top panel of the figure we have include the result for the pion and for $2M_u$ and $M_u + M_s$.

The first observation from figure is the fact that at low temperature the masses of mesons are lower than the masses of their constituents. In this case, the BS kernels for the pion and kaon are real, but crossing the pion and kaon lines with $m_\pi = 2M_u$ and $m_K = M_u + M_s$, the BS kernels acquire an imaginary part. Therefore, when the last situation happens, the meson masses are no longer a discrete solution of the BSE, which implies a transition from the discrete to the continuum that is known as Mott transition. For this transition, there is associated a temperature when the

meson masses becomes equal to the mass of its constituents, and it is known as Mott temperature, T_M. At the top panel of Fig. (5.5), the green dots indicate the points when the transition happens, and one can see that Mott temperatures for π and K mesons are approximately equal, and around $T_M^{\pi,K} \approx 230$ MeV. Above this temperature the meson is not a bound-state anymore, it is some kind of correlation of confined quark and antiquark, which when the temperature increases sufficiently probably will deconfine. Similarly to the pion, above the Mott temperature the kaon mass increases with the temperature, and we observe from the bottom panel

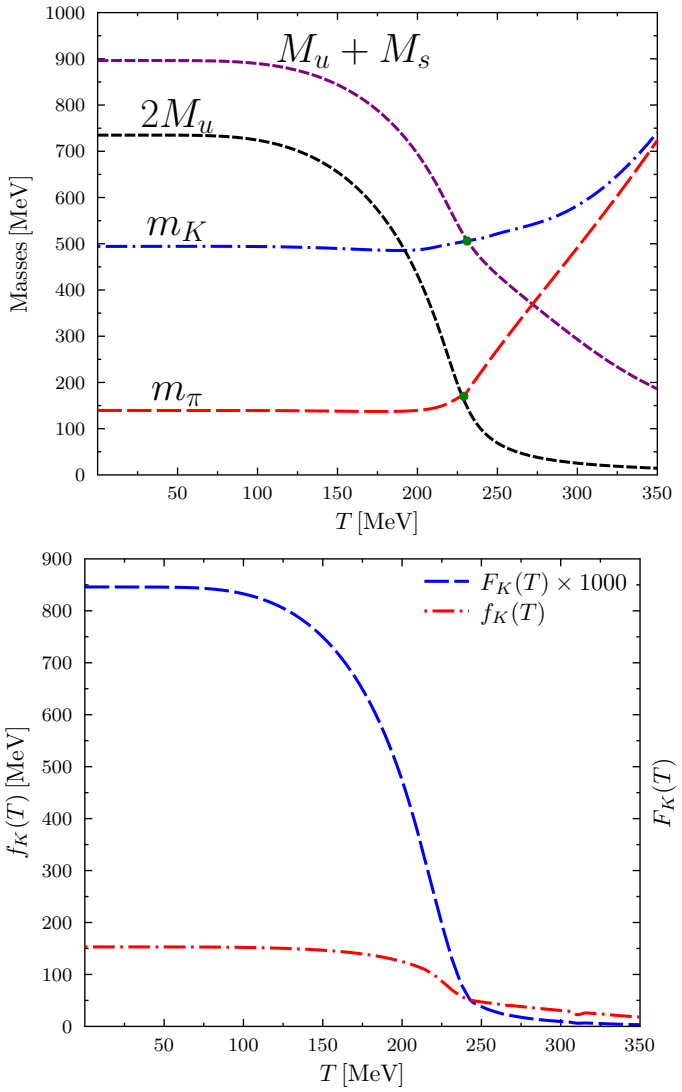

Figure 5.5: Top panel: Temperature dependence of the pion (red-dashed line) and kaon (dot-dashed line) masses as well as the curves $2M_u$ (black-dashed curve) and $M_u + M_s$ (purple-dashed curve). Bottom panel: Temperature evolution of $F_K(T)$ and $f_K(T)$.

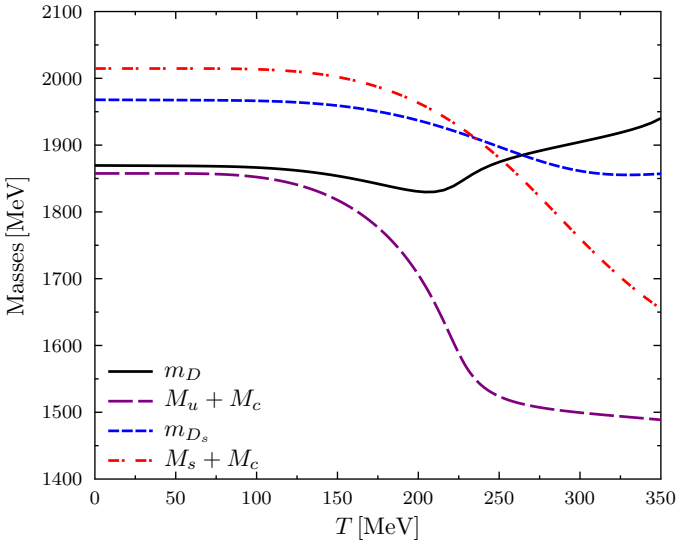

Figure 5.6: Temperature dependence of the D (black-solid line) and D_s (blue–dashed line) masses and as well as the curves $M_u + M_c$ (purple-dashed curve) and $M_s + M_c$ (red-dashed-doted curve).

of figure that the pseudovector component of the kaon BSA, $F_K(T)$, and the kaon decay constant, f_K, tend to disappear at high temperatures.

Finally, in Fig. 5.6 we depict the results for the temperature dependence of D and D_s meson masses and as well as the trajectories of $M_u + M_s$ and $M_s + M_s$. From the figure, we note that for the case of D-meson, at low temperature its mass is a little larger than the masses of their constituents, while for the case of the mass of D_s we have $M_s + M_s > m_{D_s}$. In addition, one observes that m_{D_s} decreases in the interval $120 < T < 230$ MeV, but above this, it increases with the temperature. On the other hand, for the case of D_s-meson, we note that its mass decreases in the interval $120 < T < 280$ MeV, but above this, the mass tends to be constant. For the case of D-meson the result is in quantitative agreement with early calculations using the NJL model [49,154], which report that above the pseudocritical temperature m_D increases.

5.5 Summary

We have used the Matsubara formalism to introduce the temperature dependence into the gap and BS equations using the contact interaction approximation. Here, we focused mainly on the case of pseudoscalar meson. For each pseudoscalar BS

kernels, we have separated the purely divergent contributions from thermal effects. Due to the fact that the thermal contributions into the BS kernels are finite and do not need regularization, we have associated the problem of symmetry violations with the vacuum contributions which are divergent and have to be regularized. To handled with this, we have used the results obtained in chapter. 4, where we have implemented a regularization method which is based on a subtraction scheme that allows us avoid standard steps in the evaluation of divergent integrals that lead to symmetry violation. Finally, with symmetry preserving BS kernels we have computed the temperature dependence for the π, K, D and D_s meson masses and some other meson properties like as decay constants and quark-meson couplings.

Chapter 6

Transport Coefficients of Quark-matter

The goal of this chapter is to investigate the temperature dependence of the shear and bulk viscosities and their ratios to the entropy density. In the next section, we will introduce a formalism for computing these transport coefficients in terms of the quark thermal width, $\Gamma_q^{\rm tw}$, which is deducted from the quark self-energy diagram in the framework of real-time thermal field theory. For the evaluation of the quark thermal width, we will use the results obtained in the previous chapter for the temperature dependence of the quark, pion and sigma masses and as well as its meson Bethe-Salpeter amplitudes.

6.1 Formalism

In the Kubo formalism [155,156], the shear and bulk viscosities are defined in the Lehmann spectral representation of the two-point correlation functions of operators involving the components of the energy-momentum tensor $T_{\mu\nu}$ [157]:

$$\left(\begin{array}{c} \eta \\ \\ \xi \end{array} \right) = \lim_{q_0,|\mathbf{q}|\to 0^+} \frac{1}{q^0} \left(\begin{array}{c} \frac{1}{20}\rho_\eta(q^0,\mathbf{q}) \\ \\ \frac{1}{2}\rho_\zeta(q^0,\mathbf{q}) \end{array} \right) \tag{6.1}$$

with the spectral functions $\rho_\eta(q)$ and $\rho_\zeta(q)$ given by

$$\rho_\eta(q) = \int d^4x\, e^{iq\cdot x}\, \langle [\pi^{ij}(x), \pi^{ij}(0)] \rangle_\beta, \tag{6.2}$$

$$\rho_\zeta(q) = \int d^4x\, e^{iq\cdot x}\, \langle [\mathcal{P}(x), \mathcal{P}(0)] \rangle_\beta, \tag{6.3}$$

where

$$\pi^{ij}(x) = T^{ij}(x) - \frac{1}{3}\delta^{ij} T^k_k, \tag{6.4}$$

$$\mathcal{P}(x) = -\frac{1}{3} T^i_i(x) - v_s^2\, T^{00}(x)\ . \tag{6.5}$$

In the above equations, π^{ij} is the space component of the viscous-stress tensor, $\pi^{\mu\nu}$, v_s^2 is the sound velocity and $\langle\hat{O}\rangle_\beta$ for any operator $\hat{O}$ denotes the equilibrium ensemble average,

$$\langle\hat{O}\rangle_\beta = \mathrm{Tr}\frac{e^{-\beta H}\hat{O}}{\mathcal{Z}} \ , \ \text{with} \ \mathcal{Z} = \mathrm{Tr}\, e^{-\beta H} \ . \tag{6.6}$$

We note here that the second term in the expression for $\mathcal{P}(x)$ is necessary to account for energy conservation in a quasi-particle description of the medium, an approximation we use in the present work; a clear discussion on this issue can be found in Ref. [67].

The $\pi^{\mu\nu}$ comes from the dissipative part of the total-energy momentum tensor, $T^{\mu\nu}$. According to relativistic dissipative hydrodynamics, $T^{\mu\nu}$ can be decomposed into ideal part $T_I^{\mu\nu}$ and a dissipative part $T_D^{\mu\nu}$ [158,159],

$$T^{\mu\nu} = T_I^{\mu\nu} + T_D^{\mu\nu} \ , \tag{6.7}$$

with

$$T_I^{\mu\nu} = \epsilon\, u^\mu u^\nu - P\Delta^{\mu\nu} \ , \ \text{and} \ \ T_D^{\mu\nu} = K^\mu u^\nu + K^\nu u^\mu - \pi^{\mu\nu} \ . \tag{6.8}$$

where $\Delta^{\mu\nu} = g_{\mu\nu} - u^\mu u^\nu$ and ϵ, P, K^μ, u^μ are the respectively energy density, pressure density, heat current and four velocity of the matter. Then, by applying appropriate projection operators one obtains

$$\begin{aligned} \epsilon &= u^\mu u^\nu T_{\mu\nu} \ , \\ P &= -\frac{1}{3}\Delta^{\mu\nu}T_{\mu\nu} \ , \\ K^\rho &= \Delta^{\rho\mu}u^\nu T_{\mu\nu} \ , \\ \pi^{\rho\sigma} &= t^{\rho\sigma}_{\mu\nu}\, T^{\mu\nu} \ , \end{aligned} \tag{6.9}$$

where $t^{\rho\sigma}_{\mu\nu} = \Delta^{\rho\sigma}\Delta_{\mu\nu} - \Delta^\rho_\mu\Delta^\sigma_\nu/3$. We use the effective QCD Lagrangian to obtain the above correlation functions, namely

$$\mathcal{L}^{\mathrm{eff}}_{\mathrm{QCD}} = \bar{\psi}_f(i\gamma^\mu\partial_\mu - M_f)\psi_f \ . \tag{6.10}$$

The energy-momentum tensor is given in terms of the Lagrangian density by

$$T^{\mu\nu} = -g^{\mu\nu}\mathcal{L}^{\mathrm{eff}}_{\mathrm{QCD}} + \frac{\partial\mathcal{L}^{\mathrm{free}}}{\partial(\partial_\mu\psi)}\partial^\nu\psi = g^{\mu\nu}\mathcal{L}^{\mathrm{eff}}_{\mathrm{QCD}} + i\bar{\psi}\gamma^\mu\partial^\nu\psi. \tag{6.11}$$

The model will be treated in the quasi-particle approximation or, equivalently, in the leading-order approximation in the $1/N_c$ expansion, where $N_c = 3$ is the number of colors, which is also equivalent to the traditional Hartree approximation of many-body theory. In this approximation, the thermal spectral functions can be expressed in terms of the quark propagator. We use the formalism of real-time thermal field theory (RTF) to obtain the correlation functions. In RTF, the two point function of any field-theoretic operator has a 2×2 matrix structure reflecting the time ordering with respect to a contour in the complex plane [146]. The relevant matrix can be diagonalized in terms of a single analytic function, which determines completely the dynamics of the corresponding two-point function. In particular, the retarded correlation functions needed for the evaluation of $\rho_\eta(q)$ and $\rho_\zeta(q)$ can be written in terms of the 11 component of the corresponding two-point functions — see Ref. [153] for details. For example, ignoring for the moment quark-meson fluctuations, $\rho_\eta(q)$ can be written as

$$\rho_\eta(q) = 2 \tanh\left(\frac{\beta q_0}{2}\right) \mathrm{Im}\,\Pi_{11}(q), \tag{6.12}$$

with

$$\Pi_{11}(q) = i N_c N_f \int \frac{d^4k}{(2\pi)^4} N(q,k) D_{11}(k) D_{11}(q+k), \tag{6.13}$$

where $D_{11}(q)$ is the scalar part of the 11 component quark-propagator matrix (in the zero width case):

$$D_{11}(k) = \frac{-1}{k_0^2 - E^2(\mathbf{k}) + i\epsilon} - 2\pi i E(\mathbf{k})\, f(E(\mathbf{k}))\delta(k_0^2 - E^2(\mathbf{k}))\ , \tag{6.14}$$

with $E(\mathbf{k}) = \sqrt{\mathbf{k}^2 + M^2}$, and

$$\begin{aligned} N(q,k) &= t^{\rho\sigma}_{\mu\nu} \mathrm{Tr}\left[\gamma^\mu (q+k)^\nu (\not{q} + \not{k} + M)\gamma_\rho k_\sigma (\not{k} + M)\right] \\ &= \frac{32}{3} k_0 (k_0 + q_0)\mathbf{k}\cdot(\mathbf{k}+\mathbf{q}) - 4\left[\mathbf{k}\cdot(\mathbf{k}+\mathbf{q}) + \frac{1}{3}\mathbf{k}^2(\mathbf{k}+\mathbf{q})^2\right]. \end{aligned} \tag{6.15}$$

Figure. 6.1 shows this quark-quark loop diagram, which can be considered as a schematic representation of shear viscosity coefficient at the zero frequency and momentum limit. We recall that M is the temperature dependent quark mass which is obtained by the solution of the gap equation given by Eq. (5.24), and that is depicted at the top panel of Figure. (5.1).

To proceed with the evaluation of the viscosities, we include the dissipative processes due to quark-meson fluctuations. The fluctuations introduce an imaginary

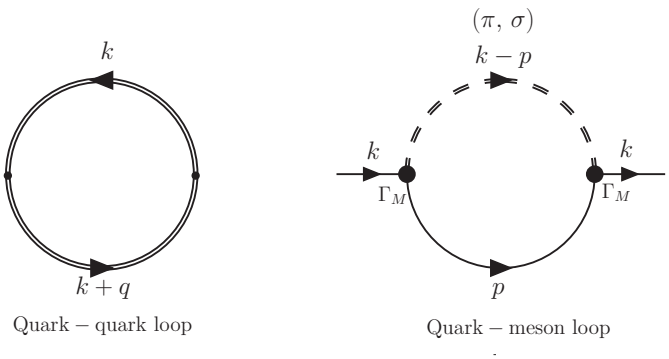

Figure 6.1: The left diagram represents a schematic one-loop diagram of the quark correlator, which can be obtained from the two-point function of the viscous-stress tensor for the quark constituents. The double lines for the quark propagators indicate that they have some finite thermal width which can be derived from the quark self-energy diagrams (right diagram) for quark-meson loops (for π, σ meson).

part in the quark self energy giving a thermal width $\Gamma_q^{\rm tw}$ to the quarks; as it stands, with no finite imaginary part in the quark propagator, Eq. (6.13) leads to divergent viscosities. Adding an on-shell, momentum-dependent thermal width $\Gamma_q^{\rm tw}(q)$ in the quark propagator, one obtains [153] for the shear viscosity the expression

$$\eta(T) = \frac{4N_cN_f}{15T}\int\frac{d^3q}{(2\pi)^3}\,\frac{\mathbf{q}^4\,f(E(\mathbf{q}))\,[1-f(E(\mathbf{q}))]}{E^2(\mathbf{q})\,\Gamma_q^{\rm tw}(\mathbf{q})}. \tag{6.16}$$

This expression for η is identical to the one obtained from the standard relaxation time approximation [160,161]. For bulk viscosity, from Eq. (6.3) we obtain:

$$\begin{aligned}\zeta(T) &= \frac{4N_cN_f}{T}\int\frac{d^3q}{(2\pi)^3}\,\frac{f(E(\mathbf{k}))\,[1-f(E(\mathbf{q}))]}{E^2(\mathbf{q})\,\Gamma_q^{\rm tw}(\mathbf{q})} \\ &\times \left[\left(\frac{1}{3}-v_s^2\right)\mathbf{q}^2 - v_s^2\left(M^2 - MT\frac{dM}{dT}\right)\right]^2 ,\end{aligned} \tag{6.17}$$

which is also identical to the one obtained in Ref. [160] which uses the relaxation time approximation. Note that, at the bottom panel of Figure. (5.1), we have depicted $-dM/dT$, which is needed as an input to evaluate the bulk viscosity. In addition, we have to evaluate the quark thermal width $\Gamma_q^{\rm tw}(\mathbf{q})$, and we do that from the quark-meson loop contributions to the quark self-energy, pictorially represented on the left side in Figure 6.1. For the evaluation of $\Gamma_q^{\rm tw}(\mathbf{q})$ we need the temperature dependence of the meson masses and the meson BS amplitudes, Γ_π and Γ_σ. In the previous chapter, we have obtained the temperature evolution of these quantities,

and for simplicity we will neglect the pseudovector component of the pion BSA because it vanishes at hight temperatures.

Given the meson masses and meson BS amplitudes, the quark thermal width is obtained from the imaginary part of the loop diagrams shown on the right side of Figure. 6.1. The off-shell quark self-energy contains four branch cuts on the energy axis, but on-shell only the Landau cut contributes [153] and the result can be written as

$$\begin{aligned}\Gamma_q^{\rm tw} &= \sum_{M=\pi,\sigma} \Gamma_{q(qM)} \\ &= \left[\int \frac{d^3p}{(2\pi)^3}\,\delta(k^0+E(\mathbf{p})-\omega(\mathbf{u}))\,\frac{f(E(\mathbf{p}))+g(\omega(\mathbf{u}))}{4E(\mathbf{p})\omega(\mathbf{u})}\right. \\ &\times \left. L_{q(qM)}(k^0,\mathbf{k};p^0=-E(\mathbf{p}),\mathbf{p})\right]_{k^0=E(\mathbf{k})}, \end{aligned} \tag{6.18}$$

where $u = k - p$, and $g(\omega(\mathbf{k}))$ being the Bose-Einstein distribution given by

$$g(\omega(\mathbf{k})) = \frac{1}{e^{\beta\omega(\mathbf{k})}-1}, \tag{6.19}$$

with $\omega(\mathbf{u}) = \sqrt{\mathbf{u}^2+m_M^2}$, and

$$L_{q(q\pi)}(k,p) = \frac{12E_\pi^2}{M}\left(M^2-k\cdot p\right), \tag{6.20}$$

$$L_{q(q\sigma)}(k,p) = \frac{4E_\sigma^2}{M}\left(M^2+k\cdot p\right). \tag{6.21}$$

Note that use of an on-shell quark thermal width is consistent with the quasi-particle approximation we are using to describe the system.

The last input needed is the sound velocity v_s, which is required for the evaluation of the bulk viscosity in Eq. (6.17). It can be obtained from the pressure P and energy density ϵ as:

$$v_s^2 = \left(\frac{\partial P}{\partial \epsilon}\right)_s = \frac{s}{c_V}, \tag{6.22}$$

where s is the entropy density and c_V the specific heat at constant volume:

$$s = \frac{\epsilon+P}{T}, \tag{6.23}$$

$$c_V = T\left(\frac{\partial s}{\partial T}\right)_V = \frac{\partial \epsilon}{\partial T}\,. \tag{6.24}$$

The pressure P and energy density ϵ are given in the quasi-particle approximation to the contact interaction model as

$$P(T) = 4N_cN_f \int \frac{d^3q}{(2\pi)^3} \frac{\mathbf{q}^2}{3E(\mathbf{q})} f(E(\mathbf{q})) \ , \tag{6.25}$$

$$\epsilon(T) = 4N_cN_f \int \frac{d^3q}{(2\pi)^3} E(\mathbf{q}) f(E(\mathbf{q})) \ . \tag{6.26}$$

We note that the use of the quasi-particle approximation for the thermodynamic quantities is consistent with the large N_c counting [162]. Inclusion of meson loops contributions requires care with respect to thermodynamic consistency.

6.2 Numerical Results

We start our numerical discussion from on-shell quark thermal width $\Gamma_q^{\rm tw}(\mathbf{k}, T)$, which we present at the top panel of Figure. (6.2) for a specific value of the momentum, $\mathbf{k} = 0.5$ GeV. At the bottom panel of figure we depict the temperature dependence of the quark thermal width for three different values of momentum: $\mathbf{k} = 1000$MeV, $\mathbf{k} = 500$MeV, and $\mathbf{k} = 0$. From this figure, one notes that the peak position and strength of the temperature dependence of $\Gamma_q^{\rm tw}$ is strongly momentum dependent, a feature that reflects the absorption and emission processes of the quark interacting with mesonic modes; recall that $\Gamma_{qqM}^{\rm tw}$ physically means the on-shell probability of forward and inverse scattering between a quark q and the mesonic modes M [163]. In forward scattering, q may be transformed to a thermalized M by absorbing a thermalized anti-quark $\bar{q}$, while in the inverse process, an off-equilibrated q may be regenerated via $M \to q\bar{q}$ dissociation. We should note as well that $\Gamma_q^{\rm tw}$ decreases and ultimately goes to zero for large temperatures; the temperature, for which it tends to be numerically zero, depends of course on $\mathbf{k}$ and is determined by the temperature-dependent quark and meson masses and couplings. The implication of $\Gamma_q^{\rm tw}$ decreasing with T for large T has the implication that $\eta(T)$ and $\zeta(T)$ will increase with T, and again, the value of T where it starts to increase and the rate of increase depend on the parameters of the model.

Before using the full temperature- and momentum-dependent $\Gamma_q^{\rm tw}(k, T)$ in Eqs. (6.16) and (6.17), we have calculated the temperature dependence of η and ζ for different values of constant collisional time $\tau_q = 1/\Gamma_q^{\rm tw}$. Although the temperature and momentum dependence of Γ_q will modify somewhat the results for the viscosi-

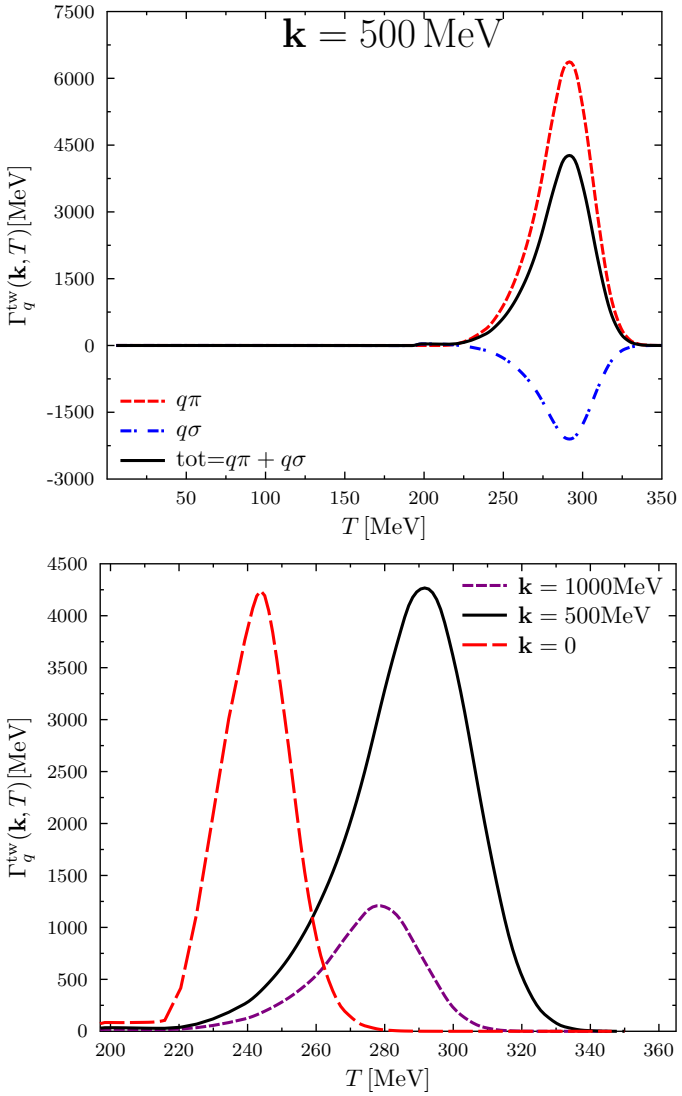

Figure 6.2: Top panel: Temperature dependence of $\Gamma_q^{\mathrm{tw}}(\mathbf{k},T)$ for $k = 0.5$ GeV (black--solid line)and the individual contribution from $\pi-$ (red-dashed line) and $\sigma-$quark loops (blue-dashed-dot line). Bottom panel: Temperature dependence of the quark thermal width for three different values of momentum: $\mathbf{k} = 1000$MeV, $\mathbf{k} = 500$MeV, and $\mathbf{k} = 0$.

ties, the calculation with a constant Γ_q will bring insight regarding the integrands in Eqs. (6.16) and (6.17) when Γ_q can be taken out of the integrals. In Fig. 6.3 we show the corresponding results for η and η/s, for different values of τ_q. While η is a monotonically increasing function of T, the ratio η/s exhibits two different rates of increase in two different temperature domains, which are associated with two different phases. In Fig. 6.4 we show the temperature evolution of the pressure and the energy density (top panel) given by Eq. (6.25) and Eq. (6.26) respectively, and

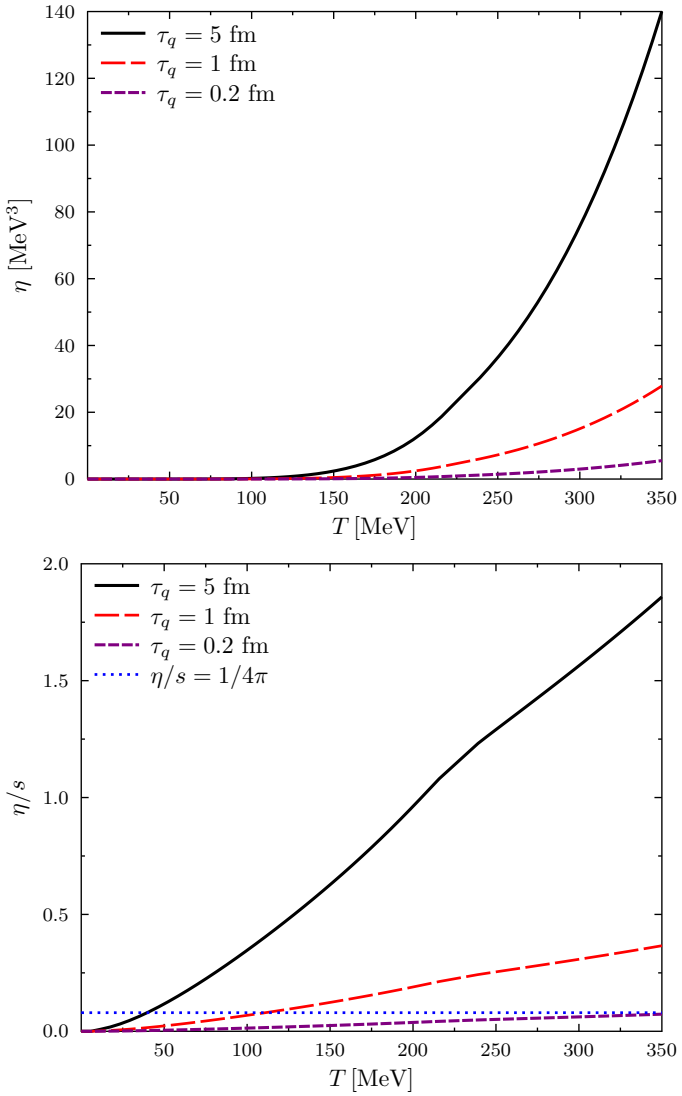

Figure 6.3: Temperature dependence of $\eta(T)$ (top panel) and η/s (bottom panel) for different values of constant collisional time: $\tau_q = 5$ fm (black-solid line), 1 fm (red-dashed line), and 0.2 fm (purple-small-dashed line). The straight horizontal blue dotted line indicates the KSS bound, $\eta/s = 1/4\pi$ [74].

as well as the temperature dependence of $dP(T)/dT$ and $d\epsilon(T)/dT$ (bottom panel). These quantities are needed for the evaluation of the entropy density, s, and the specific heat, c_V. From Fig. (6.4) one notes that the pressure, the energy density and their respective temperature derivatives increase with the temperature. Now, the observed change in the rate of increase of η/s with the temperature can be understood from the temperature dependence of s, normalized by the Stephan-Boltzmann

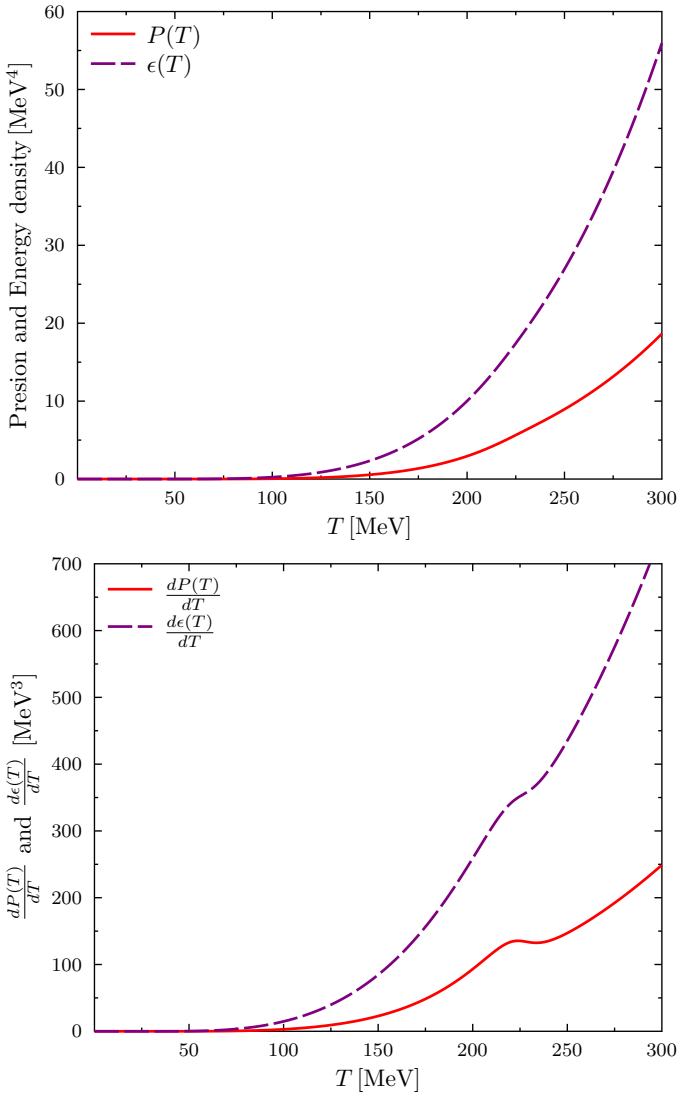

Figure 6.4: Top panel: Temperature dependence of the pressure and density energy. Bottom panel: Temperature dependence of $dP(T)/dT$ and $d\epsilon(T)/dT$.

(SB) limiting value *:

$$s_{\rm SB}(T) = 4N_c N_f \left(\frac{7}{2}\right)\left(\frac{\pi^2}{90}\right) T^3. \tag{6.27}$$

One observes at the top panel of Fig. 6.5 that the rate of increment in $s/s_{\rm SB}$ mainly changes around the interval $T \approx 215-225$ MeV; above this temperature, the entropy density of quark matter becomes almost identical with the SB limiting value, which is denoted by straight horizontal blue dotted line in the figure. It is important to

*When the temperature increases sufficiently, the thermodynamic quantities (pressure, entropy and energy density) should asymptotically exhibit the same characteristics as those assigned to a relativistic gas of non-interacting massless particles at the Stefan-Boltzmann limit.

note that we are taking into account the contributions of the quarks only in the expression for $s_{\rm SB}$; including gluon degrees of freedom will increase s_{SB} by a factor roughly equal to 1.75 (for $N_f = 2$). Being proportional to the slope of s, the specific heat c_V is magnifying the transition by exhibiting a smooth hump structure around $T \approx 215 - 225$ MeV as shown by the red-dashed line at the top panel of Fig. 6.5. Such a behavior of c_V has been obtained also in other recent calculations employing the NJL model, as for example. in Refs. [164,165,166]. Note, however, that the maximum of c_V is still well below the corresponding SB limit in QCD which, of course, includes gluon degrees of freedom and is thereby 1.75 larger than the pure-quark SB limit. This is a welcome feature as lattice QCD simulations [75] show no indication that the specific heat exceeds the QCD SB limit at any temperature. For calculating the bulk viscosity, we have obtained v_s^2 using Eq. (6.22); its temperature dependence is shown at the bottom panel of Fig. 6.5.

Assuming the system is not very far from equilibrium, all thermodynamical quantities are obtained for non-interacting system of quark matter, although a finite (not zero) probability of quark-meson interaction has to be considered for getting a non-divergent values of transport coefficients.

Fig. 6.6 shows results for the temperature dependence of ζ and ζ/s, for different constant values of τ_q. We compare these results with those reported in Fig. 7 of Ref. [167], where the authors have employed a SU(2) NJL model and found a double-peaked structure in the temperature dependence of the bulk viscosity, ζ. From the top panel of Fig. 6.6, clearly that double-peaked structure does not appears for ζ, and we report only one pick around $T \approx 217$ MeV. The different between both results come principally from the the different results of the squared speed of sound v_s^2.

Finally, we present results for the viscosities and viscosity to entropy density ratios with the full momentum dependence of the quark thermal width $\Gamma_q^{\rm tw}(\mathbf{k})$. It is important to reiterate that our results have physical significance only within a limited range of temperatures, approximately in the interval $217 < T < 0.285$ MeV. The lower limit is due to the fact that in the contact interaction model, when using the on-shell thermal width, finite viscosities are obtained for temperatures larger than $T > 217$ MeV because $\Gamma_q^{\rm tw}(k)$ is nonzero only above this value of temperature. As discussed earlier, the off-shell quark self-energy contains four branch cuts on the

energy axis, but on-shell only the Landau cut contributes. The upper limit is not a precise limit, but it is related to the lack of asymptotic freedom in the contact interaction model; it is known that the large temperature behavior of viscosities in QCD, particularly of bulk viscosity, is very different from the one derived from a non-gauge, contact-interaction model [67]. Given this proviso, we discuss next our results for the temperature dependence of η and η/s, and ζ and ζ/s; they are presented respectively in Figs. 6.7 and 6.8.

First of all, one notices from this figures that the use of the full tempera-

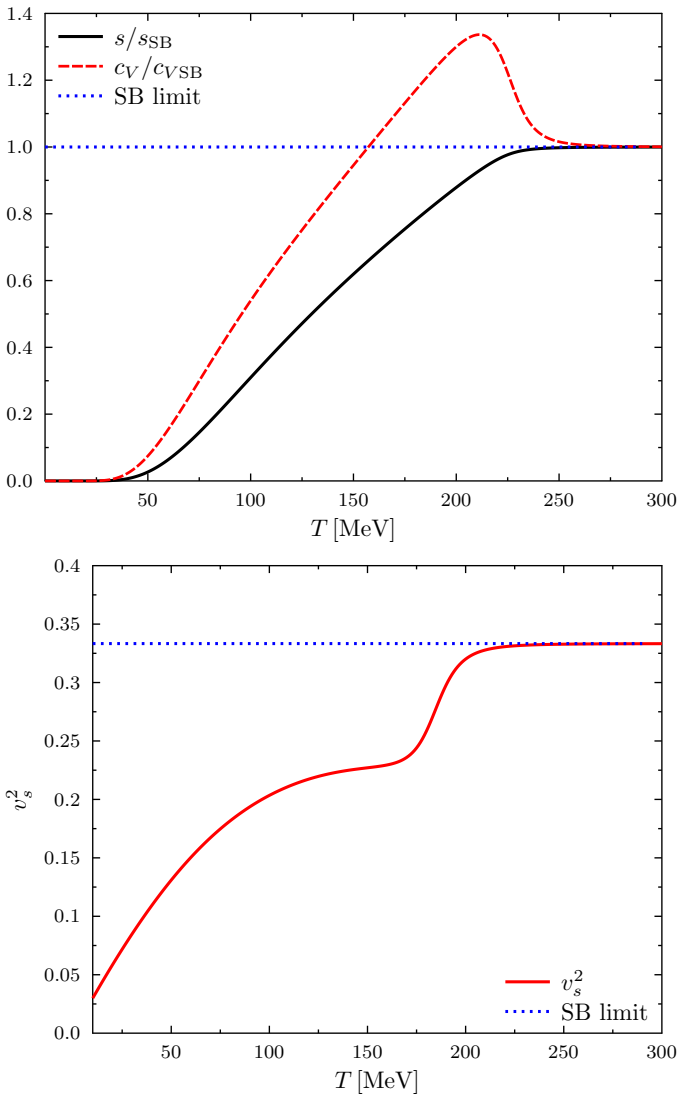

Figure 6.5: Top Panel: The temperature dependence of entropy density, normalized by Stephan-Boltzmann (SB) limiting value $s_{\rm SB}$, given by Eq. (6.27). Bottom panel: The squared speed of sound v_s^2 as a function of the temperature. Straight horizontal dotted lines stand for the corresponding SB limits.

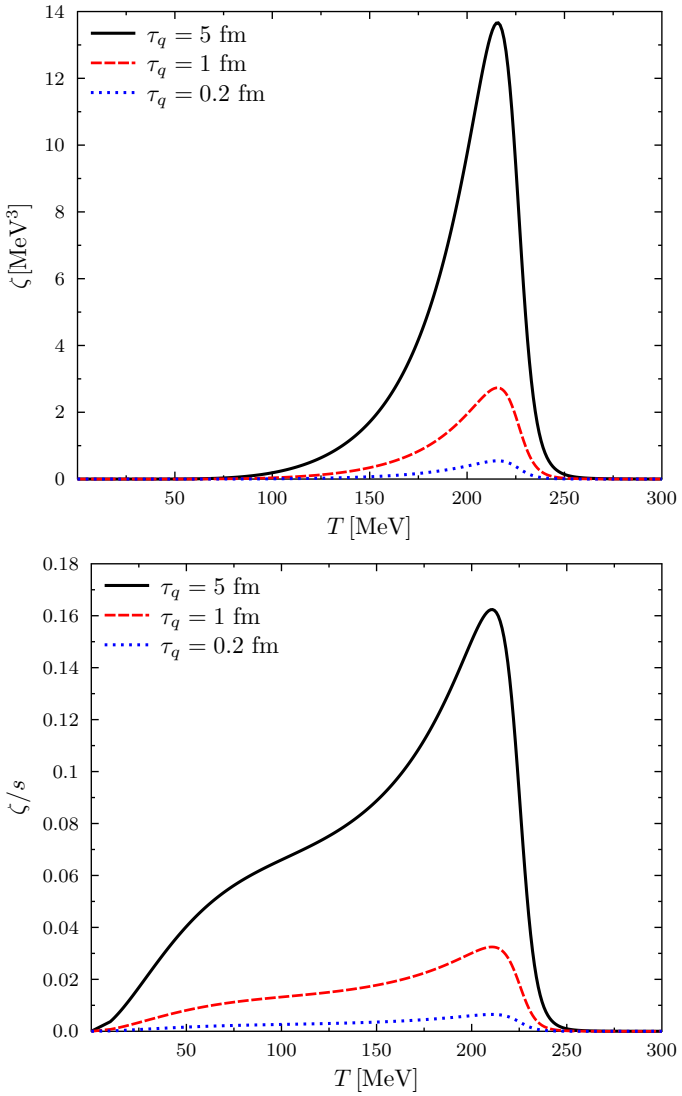

Figure 6.6: Temperature dependence of $\zeta(T)$ (top panel) and ζ/s (bottom panel) for different values of constant collisional time: $\tau_q = 5$ fm (black-solid line), 1 fm (red-dashed line), and 0.2 fm (blue-small-dashed line).

ture dependence of $\Gamma_q^{\rm tw}(k)$ restricts the domain of temperatures where finite viscosities are obtained. Our numerical values of η and η/s within the temperature range $217 < T < 240$ MeV, are quite close to some earlier estimates in Refs. [160,164,78,168,169,170]. We notes that our result for η/s has a minimum very close to the conjectured AdS/CFT lower bound, $\eta/s = 1/4\pi$ [74]. Similarly, the results reported in Fig. (6.8) can be comparable with some earlier results of Refs. [160,164,171,172]. In addition, the figures show that the viscosities have a rapid increase with temperature for $T \geq 280$ MeV. This is due to the fact that for high temperatures, the contributions from quark-meson fluctuations to $\Gamma_q^{\rm tw}(k)$

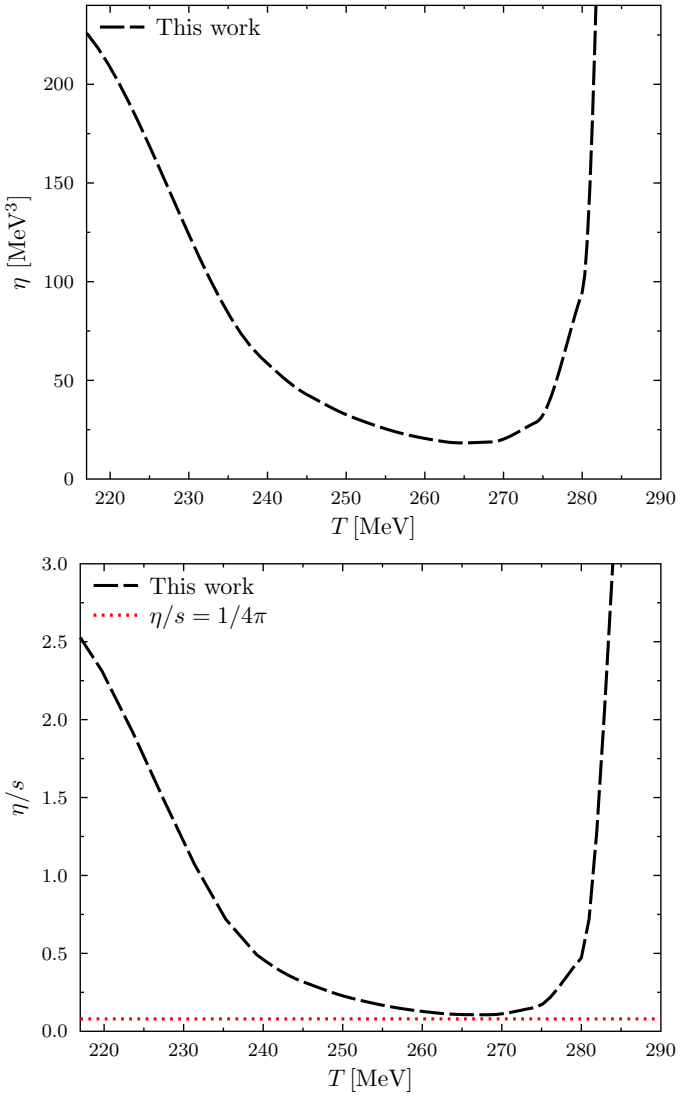

Figure 6.7: Temperature dependence of $\eta(T)$ (top panel) and η/s (bottom panel) using the full momentum dependence of the quark thermal with $\Gamma_q^{\rm tw}(\mathbf{k})$.

decrease rapidly for large T, as shown in the top panel of Fig. 6.2. At higher temperatures, quark-quark and quark-gluon scatterings will become more important than quark-meson scattering. To include such processes, one would probably need a model that incorporates asymptotic freedom, as already mentioned in the previous paragraph.

6.3 Summary

we have calculated the temperature dependence of shear η and bulk ζ viscosities of quark matter due to quark-meson fluctuations. The quark thermal width originating

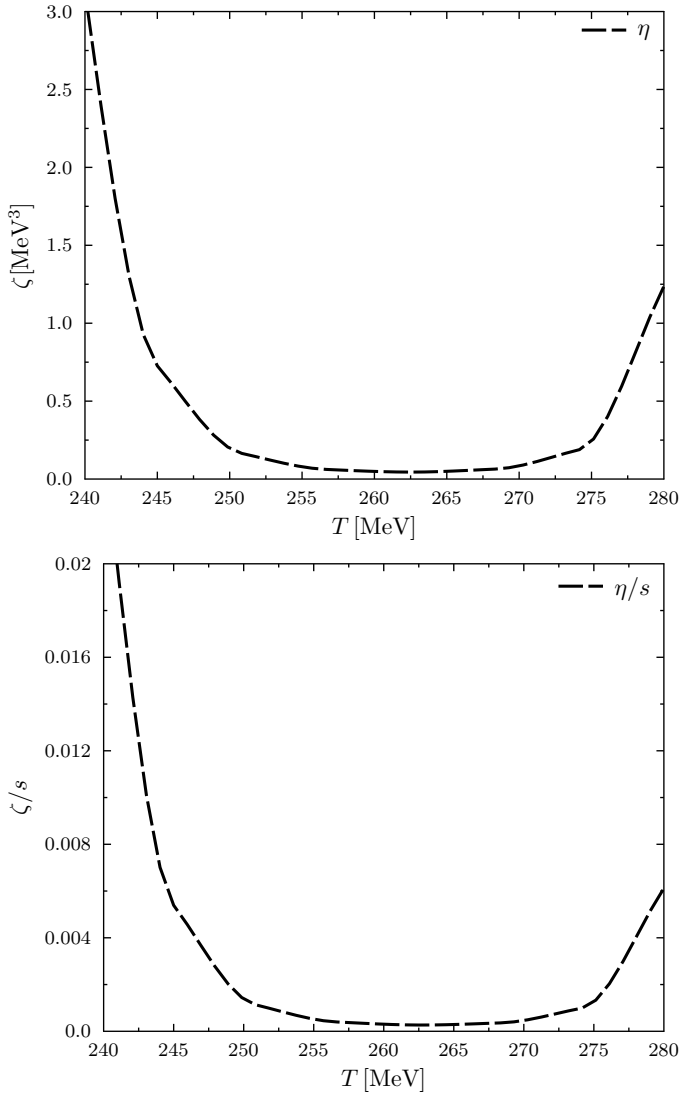

Figure 6.8: Temperature dependence of ζ (top panel) and ζ/s (bottom panel) using the full momentum dependence of the quark thermal with $\Gamma_q^{\rm tw}(\mathbf{k})$.

from quantum fluctuations of quark-π and quark-σ loops at finite temperature is calculated with the formalism of real-time thermal field theory. For theses calculations we have used our second results for the pion and sigma mesons, which means that we have used the temperature-dependent constituent-quark and meson masses, and quark-meson couplings which were obtained from the Dyson-Schwinger and Bethe-salpeter equations with the contact interaction approximation. Our results for the ratios η/s and ζ/s, where s is the entropy density (also determined in the contact interaction model in the quasi-particle approximation), are in fair agreement with results of the literature obtained from different models and techniques. In particu-

lar, our result for η/s has a minimum very close to the conjectured AdS/CFT lower bound, $\eta/s = 1/4\pi$.

Chapter 7

Conclusions

In this thesis we examined the CI model introduced in Ref. [125] within the perspective of a regularization scheme that allows to separate symmetry-violating parts in BS amplitudes in a choice independent of the momentum partition between the quark and antiquark in the bound state. In doing so, spacetime-translation symmetry and the WGT identities reflecting global symmetries of the model are preserved by the regularization. Symmetry-offending parts of the amplitudes, the integrals $A_{\mu\nu}$, $B_{\mu\nu}$, $C_{\mu\nu}$ and $D_{\mu\nu}$, can be neatly separated. In general, a cutoff regularization scheme leads to nonzero values for the symmetry-violating integrals, while dimensional regularization leads to the vanishing of the symmetry-offending integrals. In a nonrenormalizable model, like the contact-interaction model discussed here, the vanishing of $A_{\mu\nu}$, $B_{\mu\nu}$ and $C_{\mu\nu}$ must be imposed in an *ad hoc* manner and te imposition becomes an integral part of the model.

In order to check the subtraction scheme we have studied properties of the heavy-light D, D_s, D^* and D_s mesons, for which symmetry violating terms in a CI model have catastrophic consequences, as well as of light mesons π, K, ρ and K^*. We have shown that using the subtraction scheme we can obtain values for the masses of all of these mesons that agree well with experiment. In addition, we can obtain the correct trend of the weak decay constants of the pseudoscalar mesons, $f_\pi < f_K < f_D < f_{D_s}$, and their individual values are also in good agreement with experiment and lattice QCD simulations. The values of the decay constants of the ρ and D^* agree very well with experiment and lattice QCD simulations, respectively; but the model predicts the wrong orderings $f_\rho < f_K$ and $f_{D^*} < f_{D_s^*}$. These difficulties in the vector sector might not be related to intrinsic deficiencies of a contact interaction, as similar deficiencies have been observed in RL calculations using the DS-BS equations

employing sophisticated finite-range interaction kernels.

Due to the successful application of the subtraction scheme at zero temperature, in chapter. 4, we have considered an extension of the model for the case of pseudoscalar and scalar mesons at nonzero temperature via Matsubara formalism. For both case, in the gap equation and BS kernels, the purely vacuum contributions are separated from thermal effects in such a way that we are left with ultraviolet divergent momentum integrals that depend on vacuum quantities only. Again, the results for properties of the light pseudoscalar mesons π, K and the scalar meson σ, can be comparable with results obtained by other authors. Specifically, the fact that the masses of pion and sigma mesons increase linearly and becomes degenerate above the pseudocritical temperature, $T_{\rm ps} \approx 220$ MeV. In addition, the decay constant and pseudovector component of the BSA for the pion and kaon tend to vanish above this pseudocritical temperature. For the case of the masses of the heavy-light mesons, we found that above $T_{\rm ps}$, m_D increases, while m_{D_s} decreases and remains constant at high temperatures.

Also in this thesis, we have studied the temperature dependence of the quark-matter shear η and bulk ζ viscosities and their ratios to the entropy density s. The focus of interest was on the contributions from $q\pi$ and $q\sigma$ fluctuations to the on-shell quark thermal width $\Gamma_q^{\rm tw}$, a crucial ingredient in the calculation of viscosities. We calculated $\Gamma_q^{\rm tw}$ from the imaginary part of the quark self-energy arising from $q\pi$ and $q\sigma$ loops using temperature-dependent quark and meson masses and quark-meson couplings. We have investigated in detail the Landau-cut structure of the quark self-energy using real-time thermal field-theory. The entropy density and the speed of sound, which is needed to calculate ζ, were also obtained in the contact interaction model within the quasi-particle approximation.

We found that the temperature dependence of the masses and quark-meson couplings non-trivially influences the Landau-cut structure of the quark self-energy. The quark thermal width, calculated from the on-shell quark self-energy, becomes non-zero and non-negligible within a range of temperature and momentum where the quark pole is situated well inside the Landau-cut. When using a temperature- and momentum-independent quark thermal width $\Gamma_q^{\rm tw}$, a monotonically increasing shear viscosity as a function of temperature was obtained.

On the other hand, when the full temperature and momentum-dependent ther-

mal width is used, finite viscosities are obtained only for temperatures larger than $T = 217$ MeV. In addition, for high temperatures, due to rapidly increasing mesonic masses and decreasing of the constituent quark mass, the probability for quark-meson fluctuations become negligible and the viscosities increase considerable and other processes not related to quark-meson processes take place. Between the two extremes, our results for the η/s and ζ/s are in fair agreement with results from the literature, although marked differences can be observed. In particular, our result for η/s has a minimum very close to the conjectured AdS/CFT lower bound, $\eta/s = 1/4\pi$.

As a possible future application of the subtraction scheme we mention the study of strong couplings of charmed hadrons with light hadrons, in particular the couplings of $D-$mesons to nucleons. Such couplings are relevant in studies of the $D-$nucleon interaction at low energies [173,174,175,176], $D-$mesic nuclei [177,178,179], J/ψ binding to nuclei [180,54,55], among others. There is no experimental information about the $D-$nucleon interaction, most of the knowledge on this interaction comes from calculations using hadronic Lagrangians motivated by SU(4) extensions of light-flavor chiral Lagrangians. Since the symmetry is badly broken by the widely different values of the quark masses, it is important to check the validity of SU(4) symmetry in the couplings not only in vacuum [181,137,182,138,183,184], but at finite temperature and density as well. Another future application is to study charm meson diffusion in mesonic matter. Here it is necessary to compute for example the temperature dependence of masses of D^+ (D^-) mesons and also the light mesons π, K and ηs. With these inputs, one is able to compute the drag and diffusion of D^+ meson in hadronic medium. In addition, the subtraction scheme can be applicable to study baryons via Faddeev equation within the contact interaction model at finite temperature and density.

Appendix A

Notation and Conventions

In this appendix we present the notations and conventions used in this thesis. We will started with Minkowski space conventions and later we shall show how to go from this to the Euclidean space.

A.1 Minkowski Space Conventions

In Minkowski space the space coordinates are denoted by

$$x^\mu = (x^0, x^1, x^2, x^3) \equiv (t, x, y, z) = (t, \boldsymbol{x}) \ , \tag{A.1}$$

this is a contravariant four-verctor. Now the covariant four-vector is obtained by changing the sign of the spatial components of the contravariant vector, namely

$$x_\mu = (x_0, x_1, x_2, x_3) \equiv (t, -x, -y, -z) = (t, -\boldsymbol{x}) \ , \tag{A.2}$$

which we can rewrite in form

$$x_\mu = g_{\mu\nu} x^\nu \ , \tag{A.3}$$

where we have introduced the metric tensor $g_{\mu\nu}$, which is defined as

$$g_{\mu\nu} = \begin{pmatrix} 1 & 0 & 0 & 0 \\ 0 & -1 & 0 & 0 \\ 0 & 0 & -1 & 0 \\ 0 & 0 & 0 & -1 \end{pmatrix} \ . \tag{A.4}$$

Now we define the product of two four-vector a and b as

$$a \cdot b = g_{\mu\nu} a^\mu b^\nu = a_\mu b^\mu \ . \tag{A.5}$$

The Poincar-invariant length of any vector is

$$x^2 = x \cdot x = t^2 - \boldsymbol{x}^2 \ . \tag{A.6}$$

Similarly the momentum four-vector is defined as

$$p^\mu = (p^0, p^1, p^2, p^3) \equiv (E, p_x, p_y, p_z) = (E, \boldsymbol{p}) \ , \tag{A.7}$$

and

$$(p, q) = E_p E_q - \boldsymbol{p} \cdot \boldsymbol{q} \ , \tag{A.8}$$

$$(x, p) = t\, E - \boldsymbol{x} \cdot \boldsymbol{p} \ . \tag{A.9}$$

The momentum operator is defined as

$$p^\mu := i\frac{\partial}{\partial x_\mu} = \left(i\frac{\partial}{\partial t}, -i\boldsymbol{\nabla}\right) := i\nabla^\mu \ , \tag{A.10}$$

which as a contravariant four-vector, namely

$$p_\mu p^\mu := -\partial^2 = -\frac{\partial}{\partial x_\mu}\frac{\partial}{\partial x^\mu} \ . \tag{A.11}$$

Now in our conventions, we defined the Fourier transform as

$$f(x, y) = \int \frac{d^4p}{(2\pi)^4}\, e^{-ip\cdot(x-y)} f(p) \ . \tag{A.12}$$

A.2 Dirac Matrices

On the other hand, we introduce now the Dirac matrices, which are indispensable to describe particles with spin.

The Dirac matrices are defined by the Clifford Algebra

$$\{\gamma^\mu, \gamma^\nu\} = 2\mathbf{1}_{4\times4} g^{\mu\nu} \ , \tag{A.13}$$

where $\mathbf{1}_{4\times4}$ is the 4×4 identity matrix. The common ×4 representation of Dirac matrices is

$$\boldsymbol{\gamma} = \begin{pmatrix} 0 & \boldsymbol{\tau} \\ -\boldsymbol{\tau} & 0 \end{pmatrix}, \ \gamma^0 = \begin{pmatrix} \mathbf{1}_{2\times2} & 0 \\ 0 & -\mathbf{1}_{2\times2} \end{pmatrix}, \tag{A.14}$$

where $\mathbf{1}_{2\times2}$ is the 2×2 identity matrix and $\boldsymbol{\tau} = (\tau^1, \tau^2, \tau^3)$ are the Pauli matrices, defind as

$$\tau^0 = \begin{pmatrix} 1 & 0 \\ 0 & 1 \end{pmatrix}, \ \tau^1 = \begin{pmatrix} 0 & 1 \\ 1 & 0 \end{pmatrix}, \ \tau^2 = \begin{pmatrix} 0 & -i \\ i & 0 \end{pmatrix}, \ \tau^3 = \begin{pmatrix} 1 & 0 \\ 0 & -1 \end{pmatrix} \ , \tag{A.15}$$

One can see easily that the gamma matrices have the properties

$$\gamma_0^\dagger = \gamma_0 \ , \qquad \boldsymbol{\gamma}^\dagger = -\boldsymbol{\gamma} \ . \tag{A.16}$$

Now we introduce

$$\gamma^5 = \gamma_5 = i\,\gamma^1\,\gamma^2\,\gamma^3\,\gamma^4 = \frac{i}{4!}\epsilon_{\mu\nu\rho\sigma}\gamma^\mu\gamma^\nu\gamma^\rho\gamma^\sigma \ , \tag{A.17}$$

where $\epsilon_{\mu\nu\rho\sigma}$ is the completely antisymmetric Levi-Civita tensor in four dimensions. In the Pauli-Dirac representation, γ_5 is given by

$$\gamma_5 = \begin{pmatrix} 0 & 1 \\ 1 & 0 \end{pmatrix} \ . \tag{A.18}$$

Some of its properties are

$$\{\gamma_5, \gamma^\mu\} = 0 \ , \qquad \gamma_5^\dagger = \gamma_5 \ , \tag{A.19}$$

$$[\gamma_5, \sigma^{\mu\nu}] = 0 \ , \ \text{ where } \ \sigma^{\mu\nu} = \frac{i}{2}[\gamma^\mu, \gamma^\nu] \ . \tag{A.20}$$

The following identities are important in evaluating the cross-sections for decay and scattering processes

$$\mathrm{Tr}[\gamma_5] = 0 \ , \ \ \mathrm{Tr}[\mathbf{1}] = 4 \ , \ \ \mathrm{Tr}[\not{a}\not{b}] = 4(a\cdot b) \ , \tag{A.21}$$

$$\mathrm{Tr}[\not{a}_1\not{a}_2\not{a}_3\not{a}_4] = 4[(a_1\cdot a_2)(a_3\cdot a_4) - (a_1\cdot a_3)(a_2\cdot a_4) + (a_1\cdot a_4)(a_2\cdot a_3)], \tag{A.22}$$

$$\mathrm{Tr}[\not{a}_1 \cdots \not{a}_n] = 0 \ , \quad \text{for n odd} \ , \tag{A.23}$$

$$\mathrm{Tr}[\gamma_5\not{a}\not{b}] = 0 \tag{A.24}$$

$$\mathrm{Tr}[\gamma_5\not{a}\not{b}] = 0 \tag{A.25}$$

$$\mathrm{Tr}[\gamma_5\not{a}_1\not{a}_2\not{a}_3\not{a}_4] = 4i\epsilon_{\mu\nu\rho\sigma}\gamma^\mu\gamma^\nu\gamma^\rho\gamma^\sigma \ , \tag{A.26}$$

$$\gamma_\mu\not{a}\gamma^\mu = -2\not{a} \ , \tag{A.27}$$

$$\gamma_\mu\not{a}\not{b}\gamma^\mu = 4(a\cdot b) \ , \tag{A.28}$$

$$\gamma_\mu\not{a}\not{b}\not{c}\gamma^\mu = -2\not{c}\not{a}\not{b} \ , \tag{A.29}$$

where we have used the "slash" notation, $\not{a} = \gamma^\mu a_\mu$.

A.3 Euclidean Space Conventions

In Euclidean space we define the Fourier transform as

$$f(x,y) = \int \frac{d^4p}{(2\pi)^4}\, e^{ip\cdot(x-y)} f(p) \ . \tag{A.30}$$

Now in order to go from Minkowski space to Euclidean space we consider the free fermion field. The action for free Dirac fields is

$$S_0^{\psi} = \int d^4x\, \bar{\psi}(x)(i\not{\partial} - m + i\eta)\psi(x) \tag{A.31}$$

$$= \int_{-\infty}^{\infty} dt \int d^3x\, \bar{\psi}(x)(i\not{\partial} - m + i\eta)\psi(x)\ . \tag{A.32}$$

First we make a change of variables and introduce a Euclidean time: $t \to -it^E$ (Wick rotation). In order to apply this we must first see its effect on $i\not{\partial}$ and $\not{A}$, namely

$$\begin{aligned} i\not{\partial} = ig_{\mu\nu}\gamma^\mu\partial^\nu = i\gamma^0\frac{\partial}{\partial t} + i\gamma^i\frac{\partial}{\partial x^i} &\xrightarrow{M\to E} i\gamma^0\frac{\partial}{\partial(-it^E)} + i\gamma^i\frac{\partial}{\partial x^i} \\ &= -\gamma^0\frac{\partial}{\partial(t^E)} - (-i\gamma^i)\frac{\partial}{\partial x^i} \\ &= -\gamma_\mu^E\partial^E\ , \end{aligned} \tag{A.33}$$

$$\not{A} = g_{\mu\nu}\gamma^\mu A^\nu = \gamma^0 A^0 - \gamma^i A^i \xrightarrow{M\to E} -i\gamma^E\cdot A^E \tag{A.34}$$

where we can define the Euclidean Dirac matrices as

$$\gamma_4^E = \gamma^0\ ; \quad \gamma_i^E = -i\gamma^i\ , \quad i = 1,2,3. \tag{A.35}$$

These matrices are hermitian and satisfy the algebra

$$\{\gamma_\mu, \gamma_\nu\} = 2\,\delta_{\mu\nu}\ , \tag{A.36}$$

where $\delta_{\mu\nu}$ is the Kronecker delta. For four-vectors A, B we define

$$A\cdot B\ =\ \delta_{\mu\nu}\,A_\mu\,B_\nu = \sum_{i=1}^{4} A_i\,B_i\ , \tag{A.37}$$

we have also

$$\gamma_5 = -\,\gamma_1\,\gamma_2\,\gamma_3\,\gamma_4\ ; \tag{A.38}$$

$$\mathrm{tr}[\gamma_5\,\gamma_\mu\,\gamma_\nu\,\gamma_\rho\,\gamma_\sigma] = -\,4\,\epsilon_{\mu\nu\rho\sigma}\ . \tag{A.39}$$

In Eucliden space the Dirac matrices have the form

$$\boldsymbol{\gamma} = \begin{pmatrix} 0 & -i\vec{\tau} \\ i\vec{\tau} & 0 \end{pmatrix},\ \gamma_4 = \begin{pmatrix} \boldsymbol{\tau}^0 & 0 \\ 0 & -\boldsymbol{\tau}^0 \end{pmatrix}\ . \tag{A.40}$$

Appendix B

Deriving Dyson-Schwinger Equations

There are various ways to derive DSEs for a given quantum field theory. One of these and preferred is based on the simple fact that path integral of functional derivative vanish given appropriate boundary conditions. In order to explain the basic idea of that trick we will consider for simplicity the quantum field theory of the real scalar field.

B.1 DSE for the scalar field theory

let us consider the generating functional $Z[J]$ (analogous to the partition function in statistical mechanic) which generates all n-point correlation functions of the real scalar field which is given by:

$$Z[J] = \int \mathcal{D}\Phi \, e^{-S[\Phi]+J\cdot\Phi} \ , \quad S[\Phi] = \int d^4x \left[\frac{1}{2}(\partial\Phi)^2 + \frac{m^2}{2}\Phi^2 + V(\Phi)\right] \ , \qquad \text{(B.1)}$$

being J an external source, $S[\Phi]$ the Euclidean scalar action where $V(\Phi)$ contains terms like ($\lambda_3\Phi^3$, $\lambda_4\Phi^4, \cdots$), and $J\cdot\Phi$ denotes

$$J\cdot\Phi \ = \ \int d^4x J(x)\Phi(x) \ . \qquad \text{(B.2)}$$

Correlation functions or Euclidean Green functions of the scalar field Φ are obtained as a functional derivatives of $Z[J]$ with respect to J, where it is set to zero at the end:

$$\begin{aligned} G^{(N)}(x_1,...,x_n) &= \langle\Phi(x_1)\cdots\Phi(x_n)\rangle \\ &= \frac{1}{Z}\int \mathcal{D}\Phi \, \Phi(x_1)\cdots\Phi(x_n)\, e^{-S[\Phi]} \\ &= \left.\frac{\delta^n Z[J]}{\delta J(x_1)\cdots\delta J(x_n)}\right|_{J=0} . \end{aligned} \qquad \text{(B.3)}$$

Now, for ordinary integrals, we have that

$$\int_{-\infty}^{\infty} dx \frac{df(x)}{dx} = f(\infty) - f(-\infty) = 0 \ , \tag{B.4}$$

so long as $f(\infty) = f(-\infty)$, which includes $f(\pm\infty) = 0$. Let consider for example the integral $I(a)$ given by

$$I(a) = \int dx \, e^{ax} \ . \tag{B.5}$$

Then, one has that:

$$\begin{aligned} \int dx \, f(x) e^{ax} &= \int dx \, f\left(\frac{d}{da}\right) e^{ax} \\ &= f\left(\frac{d}{da}\right) \int dx \, e^{ax} \\ &= f\left(\frac{d}{da}\right) I(a) \ . \end{aligned} \tag{B.6}$$

Making the generalization to path integrals, the equivalent to Eq. (B.4) is

$$\int \mathcal{D}\Phi \frac{\delta}{\delta\Phi(x)} e^{-S[\Phi]+J\cdot\Phi} = 0 \ ,$$

or writing explicitly, one has

$$\int \mathcal{D}\Phi \left[-\frac{\delta S}{\delta\Phi(x)} + J(x)\right] e^{-S[\Phi]+J\cdot\Phi} = 0 \ . \tag{B.7}$$

We see that the equivalent of Eq. (B.6) is, then:

$$\left[-\frac{\delta S[\Phi]}{\delta\Phi(x)}\left(\frac{\delta}{\delta J(x)}\right) + J(x)\right] Z[J] = 0 \ . \tag{B.8}$$

The last equation is a compact form of equations of motion for Euclidean Green functions, which are called the Dyson-Schwinger equations: an infinite set of relations between correlation functions obtained by expanding in powers of the source $J(x)$ and setting $J(x) = 0$ at the end. In practice, we are usually more interested in the connected Green functions and the one-particle-irreducible (1PI) Green functions (connected and amputated vertex functions). In fact, we can also define a generating functional $W[J]$, which generates connected correlation functions:

$$Z[J] = e^{W[J]} \ , \tag{B.9}$$

this is very analogous to the free energy in statistical mechanic. Then, the connected n-point correlation function can be calculated via

$$\begin{aligned}\langle\Phi(x_1)\cdots\Phi(x_n)\rangle_{\rm c} &= \frac{1}{Z}\int \mathcal{D}\Phi\,\Phi(x_1)\cdots\Phi(x_n)\,e^{-S[\Phi]} \\ &= \left.\frac{\delta^n \ln Z[J]}{\delta J(x_1)\cdots\delta J(x_n)}\right|_{J=0} \\ &= \left.\frac{\delta^n W[J]}{\delta J(x_1)\cdots\delta J(x_n)}\right|_{J=0} . \end{aligned} \tag{B.10}$$

Combining Eq. (B.8) with Eq. (B.9) and also using the relation $e^{-X}f(\partial)e^{X} = f(\partial + \partial X)$, we can write:

$$\frac{\delta S[\Phi]}{\delta\Phi(x)}\left[\frac{\delta W[J]}{\delta J(x)} + \frac{\delta}{\partial J(x)}\right] - J(x) = 0 \ . \tag{B.11}$$

This is a compact form of the DSEs for connected correlation functions.

On the other hand, 1PI or proper vertices are obtained via derivatives of the effective action $\Gamma[\tilde{\Phi}]$, which is related to $W[J]$ via a Legendre transformation*:

$$\Gamma[\tilde{\Phi}] = \tilde{\Phi}\cdot J - W[J] \ , \tag{B.12}$$

where $\tilde{\Phi}$ is the conjugate variable to the clasical external source $J(x)$ defined by imposing Eq. (B.12) to be stationary with respect to functional derivations of $J(x)$ at $\tilde{\Phi}$ fixed:

$$\tilde{\Phi}(x) = \frac{\delta W[J]}{\delta J(x)} \ . \tag{B.13}$$

which writing explicitly, one has

$$\begin{aligned}\tilde{\Phi}(x) &= \tilde{\Phi}(x;J) \\ &= \frac{1}{Z[J]}\frac{\delta Z(J)}{\delta J(x)} \\ &= \frac{1}{Z[J]}\int \mathcal{D}\Phi\,\Phi(x)\,e^{-S[\Phi]+J.\Phi} \\ &= \langle\Phi(x)\rangle_J \ . \end{aligned} \tag{B.14}$$

Thus, $\Gamma[\tilde{\Phi}]$ depends on the averaged field $\tilde{\Phi}$, which is the vacuum expectation value of Φ in the presence of the source J, which vanish in the physical limit $J = 0$†.

*In analogy with statistical mechanic, Γ and W are thermodynamic potentials. With Φ being the extensive variable and J the intensive variable.

†With minimal modification, the case of spontaneous symmetry breaking can also handled with this formalism [107].

Note that the functional derivative of the effective action Eq. (B.12) with respect to $\tilde{\Phi}$ leads to

$$\begin{aligned}\frac{\delta\Gamma[\tilde{\Phi}]}{\delta\tilde{\Phi}(x)} &= J(x) + \int d^4x' \left[\tilde{\Phi}(x') - \frac{W(J)}{\delta J(x')}\right] \frac{\delta J(x')}{\delta\tilde{\Phi}(x)} \\ &= J(x) \ , \end{aligned} \tag{B.15}$$

where we have used Eq .(B.13).

From Eq. (B.11) and using the definition of $\Gamma[\tilde{\Phi}]$ we can derive equations for the proper vertices, explicitly this is

$$\begin{aligned} J(x) &= e^{-\tilde{\Phi}\cdot J+\Gamma[\tilde{\Phi}]} \frac{\partial S[\Phi]}{\partial\Phi(x)} \left[\frac{\delta}{\delta J(x)}\right] e^{\tilde{\Phi}\cdot J-\Gamma[\tilde{\Phi}]} \\ &= \frac{\partial S[\Phi]}{\partial\Phi(x)}\left[\tilde{\Phi}(x) + \int d^4x' \frac{\delta\tilde{\Phi}(x')}{\delta J(x)} J(x') - \int d^4x' \frac{\delta\Gamma[\tilde{\Phi}]}{\delta\tilde{\Phi}(x')} \frac{\delta\tilde{\Phi}(x')}{\delta J(x)}\right. \\ &- \left. \int d^4x' \frac{\delta\tilde{\Phi}(x')}{\delta J(x)} \frac{\delta}{\delta\Phi(x')}\right] \\ &= \frac{\partial S[\Phi]}{\partial\Phi}\left[\tilde{\Phi} - \frac{\delta\tilde{\Phi}}{\delta J}\cdot\frac{\delta}{\delta\tilde{\Phi}}\right] \ , \end{aligned} \tag{B.16}$$

where we have used Eq. (B.15). Now, from Eq. (B.15) and Eq. (B.13) , we have

$$\frac{\delta J(x)}{\delta\tilde{\Phi}(x')} = \frac{\delta^2\Gamma[\tilde{\Phi}]}{\delta\tilde{\Phi}(x')\delta\tilde{\Phi}(x)} \ , \quad \frac{\delta\tilde{\Phi}(x)}{\delta J(x')} = \frac{\delta^2 W[J]}{\delta J(x')\delta J(x)} \ , \tag{B.17}$$

and

$$\begin{aligned}\delta^4(x-x') &= \int d^4z \frac{\delta\tilde{\Phi}(x)}{\delta J(z)} \frac{\delta J(z)}{\delta\tilde{\Phi}(x')} \\ &= \int d^4z \frac{\delta^2 W[J]}{\delta J(z)\delta J(x)} \frac{\delta^2\Gamma[\tilde{\Phi}]}{\delta\tilde{\Phi}(z)\delta\tilde{\Phi}(x)} \ . \end{aligned} \tag{B.18}$$

This implies that

$$\frac{\delta^2 W[J]}{\delta J(x)\delta J(y)} = \left[\frac{\delta^2\Gamma[\tilde{\Phi}]}{\delta\tilde{\Phi}(x)\delta\tilde{\Phi}(y)}\right]^{-1} \ . \tag{B.19}$$

From Eq. (B.10) we conclude that

$$\Delta_J^{-1}(x-y) = \frac{\delta^2\Gamma[\tilde{\Phi}]}{\delta\tilde{\Phi}(x)\delta\tilde{\Phi}(y)} \ . \tag{B.20}$$

Therefore, DSEs for the proper Green's vertices can be derived from

$$\frac{\delta\Gamma[\tilde{\Phi}]}{\delta\tilde{\Phi}} - \frac{\delta S[\Phi]}{\delta\Phi}\left[\tilde{\Phi} - \left(\frac{\delta^2\Gamma[\tilde{\Phi}]}{\delta\tilde{\Phi}\delta\tilde{\Phi}}\right)^{-1}\frac{\delta}{\delta\tilde{\Phi}}\right] = 0 \ . \tag{B.21}$$

In summary, equations (B.8), (B.11) and (B.21) provide a means to derive DSEs for n-point correlation functions by taking n-th derivatives with respect to external sources J or conjugate fields $\tilde{\Phi}$ of the appropriate generating functional, and setting all sources or conjugate fields to zero afterwards.

B.2 DSE for $\lambda\Phi^4$ theory

In order to illustrate the application of these equations, let's consider the simplest scalar field theory, $\lambda\Phi^4$. Then, the functional derivative of the classical action $S[\Phi]$ defined in Eq. (B.1) is given by

$$\frac{\delta S[\Phi]}{\delta\Phi(x)} = \left(\partial^2 + m^2\right)\Phi(x) + \frac{\lambda}{3!}\Phi^3(x) \ , \tag{B.22}$$

With this, Eq .(B.8) can be rewritten as

$$\left[\left(\partial^2 + m^2\right)\frac{\delta}{\delta J(x)} + \frac{\lambda}{3!}\left(\frac{\delta}{\delta J(x)}\right)^3\right] Z[J] = J(x)Z[J] \ . \tag{B.23}$$

Using (B.9) in the last equation, we arrive to:

$$\begin{aligned}\frac{\delta\Gamma[\tilde{\Phi}]}{\delta\tilde{\Phi}(x)} &= (\partial^2 + m^2)\tilde{\Phi}(x) + \frac{\lambda}{3!}\Bigg[\tilde{\Phi}^3(x) + 3\tilde{\Phi}(x)\Delta_J(x-x) \\ &+ \frac{\delta}{\delta J(x)}\left(\frac{\delta^2\Gamma[\tilde{\Phi}]}{\delta\tilde{\Phi}(x)\delta\tilde{\Phi}(x)}\right)^{-1}\Bigg].\end{aligned} \tag{B.24}$$

where we have used equations (B.13), (B.20). The next step is evaluate the last term in Eq. (B.24) as follows:

$$\begin{aligned}\frac{\delta}{\delta J(x)}\left(\frac{\delta^2\Gamma[\tilde{\Phi}]}{\delta\tilde{\Phi}(x)\delta\tilde{\Phi}(x)}\right)^{-1} &= \int d^4z\,\frac{\delta\tilde{\Phi}(z)}{\delta J(x)}\frac{\delta}{\delta\tilde{\Phi}(z)}\left(\frac{\delta^2\Gamma[\tilde{\Phi}]}{\delta\tilde{\Phi}(x)\delta\tilde{\Phi}(x)}\right)^{-1} \\ &= \int d^4z\,d^4z'\,d^4z"\,\frac{\delta\Phi(z)}{\delta J(x)}\left(\frac{\delta^2\Gamma[\tilde{\Phi}]}{\delta\tilde{\Phi}(x)\delta\tilde{\Phi}(z)}\right)^{-1} \\ &\times \left(\frac{\delta^3\Gamma[\tilde{\Phi}]}{\delta\tilde{\Phi}(z')\delta\tilde{\Phi}(z)\delta\tilde{\Phi}(z")}\right)\left(\frac{\delta^2\Gamma[\tilde{\Phi}]}{\delta\tilde{\Phi}(x)\delta\tilde{\Phi}(z")}\right)^{-1} \\ &= \int d^4z\,d^4z'\,d^4z"\,\Delta_J(x-z)\Delta_J(x-z') \\ &\times \Gamma_J(z',z,z")\Delta_J(x-z") \ ,\end{aligned} \tag{B.25}$$

where we have used the following relation for finite dimensional matrices

$$\frac{dA(x)^-1}{dx} = A(x)^{-1}\frac{dA(x)}{dx}A(x)^{-1} \ , \tag{B.26}$$

and also we have defined $\Gamma_J(z', z, z")$ as

$$\Gamma_J(z', z, z") = \frac{\delta^3\Gamma[\tilde{\Phi}]}{\delta\tilde{\Phi}(z')\delta\tilde{\Phi}(z)\delta\tilde{\Phi}(z")} \ . \tag{B.27}$$

Applying another functional derivative with respect $\tilde{\Phi}$ into Eq. (B.24), we get

$$\begin{aligned}\frac{\delta^2\Gamma[\tilde{\Phi}]}{\delta\tilde{\Phi}(x)\delta\tilde{\Phi}(y)} &= (\partial^2 + m^2)\delta^4(x-y) + \frac{\lambda}{3!}\Big[3\delta^4(x-y)\tilde{\Phi}^2(x) + 3\delta^4(x-y)\Delta_J(x-x) \\ &+ 3\tilde{\Phi}(x)\frac{\delta\Delta_J(x-x)}{\delta\tilde{\Phi}(y)} + \frac{\delta}{\delta\tilde{\Phi}(y)}\int d^4z\, d^4z'\, d^4z"\, \Delta_J(x-z)\Delta_J(x-z') \\ &\times \Gamma_J(z', z, z")\Delta_J(x-z")\Big] \ . \end{aligned} \tag{B.28}$$

Now, setting $\tilde{\Phi} = 0$ and also knowing that there is no three-point vertex in Φ^4 theory, we arrive to:

$$\begin{aligned}\Delta^{-1}(x-y) &= \Delta_0^{-1}(x-y) + \frac{\lambda}{3!}\Big[3\delta^4(x-y)\Delta(x-x) \\ &+ \int d^4z\, d^4z'\, d^4z"\, \Delta(x-z)\Delta(x-z') \\ &\times \Gamma_4(y, z', z, z")\Delta(x-z")\Big] \ , \end{aligned} \tag{B.29}$$

being $\Gamma_4(y, z', z, z")$ the four-point vertex defined by

$$\Gamma_4(y, z', z, z") = \frac{\delta^4\Gamma[\tilde{\Phi}]}{\delta\tilde{\Phi}(y)\delta\tilde{\Phi}(z')\delta\tilde{\Phi}(z)\delta\tilde{\Phi}(z")}\bigg|_{\tilde{\Phi}=0} \ . \tag{B.30}$$

Equation (B.29), is the DSE for Φ^4 theory and states that the inverse of the dressed propagator is the sum of the inverse free propagator plus quantum loop corrections. This equation is exact and depends on the four-point vertex defined by Eq. (B.30) which itself satisfies its own DSE. The diagrammatic representation of Eq. (B.29) is displayed if Fig.B.1.

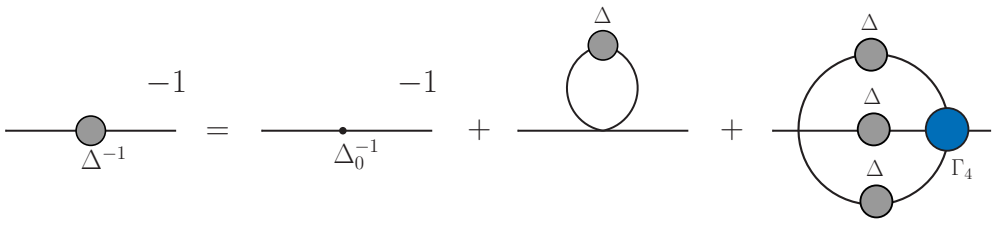

Figure B.1: Diagrammatic representation of the Dyson-Schwinger equation for $\lambda\Phi^4$ theory Eq. (B.29); filled circles indicate fully dressed objects.

Appendix C

Structure of Meson Bethe-Sapeter amplitudes

In this appendix we will explain how to construct the meson BSAs. We will consider the case of the scalar, pseudoscalar and vector mesons.

C.1 Scalar and pseudoscalar BSAs

One notes that the basic ingredients to construct a covariant structure of the BSAs are the three four-vectors:

$$\gamma_\mu,\ k_\mu,\ \ P_\mu. \tag{C.1}$$

Now, we characterize each meson by one set of quantum number $J^{\mathcal{P}C}$ (being J the total angular momentum, $\mathcal{P}$ the parity and C charge parity). We start with the scalar meson which has $J = 0$, positive parity and positive charge conjugation, namely $J^{\mathcal{P}C} = 0^{++}$.

Then, we need to find all possible and linearly independent Dirac structures (Dirac covariants) obtainable from the vector given by Eq. (C.1). For $J = 0$ the BSA can be written as a sum over Dirac covariants T_i multiplied by Lorentz-invariant functions F_i in the form

$$\Gamma(k;P) = \sum_{i=1}^{N_J} T_i(\gamma;k,P)F_i(k^2, k\cdot P, P^2) \tag{C.2}$$

being $N_J = 4$ for $J = 0$ and $N_J = 8$ for all other values of J. Then, we will build an orthogonal basis in Dirac space. The first basis element is $\mathbb{1}$ because k^2, P^2, $\gamma_\mu\gamma^\mu$ and $k\cdot P$ are proportional to $\mathbb{1}$.

The next step is see orthogonality, which means that we need a scalar product that in this case is defined as

$$\mathrm{Tr}[T_i\cdot T_j] = 0\ , \quad \text{for } i \neq j\ . \tag{C.3}$$

For our four-vectors we have also $\gamma\cdot k$ and $\gamma\cdot P$ and we can see that them are orthogonal to $\mathbb{1}$, namely

$$\mathrm{Tr}[\mathbb{1}\cdot(\gamma\cdot k)] = \mathrm{Tr}[\mathbb{1}\cdot(\gamma\cdot P)] = 0 \ . \tag{C.4}$$

On the other hand, on has

$$\mathrm{Tr}[(\gamma\cdot k)\cdot(\gamma\cdot P)] = 4(k\cdot P)\mathbb{1} \ , \tag{C.5}$$

which means that they are not orthogonal to each other. However, these two terms can be made orthogonal by the small modification of one of them, namely

$$\gamma\cdot k \to \gamma\cdot k - \gamma\cdot P\frac{k\cdot P}{P^2} \ , \tag{C.6}$$

where the last term in the right-hand side is a transversal projection with respect to the total momentum P. Therefore one has

$$\mathrm{Tr}\left[\left(\gamma\cdot k - \gamma\cdot P\frac{k\cdot P}{P^2}\right)\cdot\gamma\cdot P\right] = 0 \ . \tag{C.7}$$

The next possibility is $\gamma\cdot k\gamma\cdot P$ and one finds that the construction $[\gamma\cdot k, \gamma\cdot P]$ is orthogonal to the three elements that we already have, namely

$$\begin{aligned}
\mathrm{Tr}\left\{\mathbb{1}\cdot[\gamma\cdot k, \gamma\cdot P]\right\} &= 0 \ , \\
\mathrm{Tr}\left\{\left(\gamma\cdot k - \gamma\cdot P\frac{k\cdot P}{P^2}\right)\cdot[\gamma\cdot k, \gamma\cdot P]\right\} &= 0 \ , \\
\mathrm{Tr}\left\{\gamma\cdot P\cdot[\gamma\cdot k, \gamma\cdot P]\right\} &= 0 \ .
\end{aligned} \tag{C.8}$$

It is not possible to find any additional linearly independent covariants, since any products of $[\gamma\cdot k, \gamma\cdot P]$ with $\gamma\cdot k$ or $\gamma\cdot P$ or itself can be reduced to already known covariants via the Clifford algebra, $\{\gamma_\mu, \gamma_\nu\} = 2\delta_{\mu\nu}$. Hence, the basis in Dirac space for a scalar meson with $J^P = 0^+$ can be given by

$$T_1 = \mathbb{1} \ , \quad T_2 = i\gamma\cdot P \ , \quad T_3 = i\gamma\cdot k \ , \quad T_4 = [\gamma\cdot k, \gamma\cdot P] \ . \tag{C.9}$$

We note that a pseudoscalar meson set of covariants can be constructed from here by multiplication of each covariant by γ_5, since this object has negative parity, so the result is

$$T_1 = i\gamma_5 \ , \quad T_2 = \gamma_5\gamma\cdot P \ , \quad T_3 = \gamma_5\gamma\cdot k \ , \quad T_4 = i\gamma_5[\gamma\cdot k, \gamma\cdot P] \ . \tag{C.10}$$

Now let us to consider the charge parity of each of the covariants for the scalar and pseudoscalar cases. It is easily to note that $\mathbb{1}$ and $\gamma\cdot k$ have positive charge parity, but $\gamma\cdot P$ has negative charge parity. We can see that the covariant $[\gamma\cdot k, \gamma\cdot P]$ has positive charge parity, namely

$$\begin{aligned}(C[\gamma\cdot k,\gamma\cdot P]C^{-1})^T &= (C\gamma\cdot k\gamma\cdot PC^{-1})^T - (C\gamma\cdot P\gamma\cdot kC^{-1})^T \\ &= (C\gamma\cdot kC^{-1}C\gamma\cdot PC^{-1})^T - (C\gamma\cdot PC^{-1}C\gamma\cdot kC^{-1})^T \\ &= -\gamma\cdot P\gamma\cdot k + \gamma\cdot k\gamma\cdot P = [\gamma\cdot k,\gamma\cdot P]\ . \end{aligned} \tag{C.11}$$

Then, we can write the BSA for a scalar meson with positive charge parity, $J^{PC} = 0^{++}$ as

$$\begin{aligned}\Gamma_{\rm S}(k;P) &= \mathbb{1}F_1(k^2,k\cdot P,P^2) + i\gamma\cdot PF_2(k^2,k\cdot P,P^2) \\ &+ i\gamma\cdot k\,F_3(k^2,k\cdot P,P^2) + \sigma_{\mu\nu}k_\mu P_\nu F_4(k^2,k\cdot P,P^2)\ . \end{aligned} \tag{C.12}$$

Here we have charge parities of T_1, T_2, T_3 and T_4 being $+$, $-$, $+$ and $+$ and $+$, $-$, $+$ and $+$ for the Lorentz-invariant functions F_1, F_2, F_3 and F_4. Now, for the pseudoscalar covariants one can similarly find that:

$$\begin{aligned}(C\gamma_5\gamma\cdot PC^{-1})^T &= (C\gamma_5C^{-1}C\gamma\cdot PC^{-1})^T = -\gamma\cdot P\gamma_5 = \gamma_5\gamma\cdot P\ , \\ (C\gamma_5\gamma\cdot kC^{-1})^T &= (C\gamma_5C^{-1}C\gamma\cdot kC^{-1})^T = \gamma\cdot k\gamma_5 = -\gamma_5\gamma\cdot k\ , \\ (C\gamma_5[\gamma\cdot k,\gamma\cdot P]C^{-1})^T &= \gamma_5[\gamma\cdot k,\gamma\cdot P]\ . \end{aligned} \tag{C.13}$$

Thus, in order to have a pseudoscalar meson with $J^{\mathcal{P}C} = 0^{-+}$, one needs charge parities $+$, $+$, $-$ and $+$ as well for F_1, F_2, F_3 and F_4. Then, the BSA for the pseudoscalar meson can be written as

$$\begin{aligned}\Gamma_{\rm PS}(k;P) &= \gamma_5\big[iF_1(k^2,k\cdot P,P^2) + \gamma\cdot PF_2(k^2,k\cdot P,P^2) \\ &+ \gamma\cdot k\,F_3(k^2,k\cdot P,P^2) + \sigma_{\mu\nu}k_\mu P_\nu F_4(k^2,k\cdot P,P^2)\big]\ . \end{aligned} \tag{C.14}$$

C.2 Vector BSA

For the case of vector mesons there are 12 independent Dirac covariants, but since a vector BSA is transverse the number of allowed covariants reduces to 8, so that

the general form of this amplitude is

$$\Gamma_\mu(k;P) = \sum_{i=1}^{8} T_\mu^i(\gamma;k,P) F_i(k^2, k\cdot P, P^2) \ , \tag{C.15}$$

where

$$\begin{aligned}
T_\mu^1 &= \gamma_\mu^T \ , \qquad T_\mu^2 = k_\mu^T \gamma\cdot k \ , \\
T_\mu^3 &= k_\mu^T \, \gamma\cdot P \ , \quad T_\mu^4 = \gamma_\mu^T [\gamma\cdot k, \gamma\cdot P] - k_\mu^T \gamma\cdot P \ , \\
T_\mu^5 &= k_\mu^T \mathbb{1} \ , \qquad T_\mu^6 = i \left[\gamma_\mu^T, \gamma\cdot k\right] \ , \\
T_\mu^7 &= i\gamma_\mu^T \gamma\cdot P \ , \quad T_\mu^8 = i\gamma_\mu^T [\gamma\cdot k, \gamma\cdot P] \ .
\end{aligned} \tag{C.16}$$

where T_μ^3 and T_μ^6 have positive parity and the others negative. If we wants a vector meson with $J^{\mathcal{P}C} = 1^{--}$, F_3 and F_6 must be odd functions of $k\cdot P$, and the others even. The construction of the axial vector ($J^{\mathcal{P}C} = 1^{+-}$) BSA follows in the same way to the case of the pseudoscalar, just by multiplication of each covariants given in Eq. (C.16) by γ_5.

Appendix D

Bethe-Salpeter Kernels

Here we present some details of the derivation of the subtracted kernels for pseudoscalar and vector channels.

D.1 Pseudoscalar kernels

We start with the kernels $K_{\rm PS}^{EE}$ given by Eq. (4.14), which as we have seen in the chapter 4 can be written as:

$$\begin{aligned}\mathcal{K}_{\rm PS}^{EE}(P) &= 16\int_q^\Lambda \frac{q_+\cdot q_- + M_l M_h}{(q_+^2+M_l^2)(q_-^2+M_h^2)} \\ &= 8\int_q^\Lambda \left\{ \frac{1}{q_+^2+M_l^2} + \frac{1}{q_-^2+M_h^2} - \frac{P^2+(\Delta M_{hl})^2}{(q_+^2+M_l^2)(q_+^2+M_h^2)} \right\}, \end{aligned} \quad \text{(D.1)}$$

where $\Delta M_{lh} = M_l - M_h$. The next step is evaluate the following Feynman integrals

$$I_1^l = \int_q^\Lambda \frac{1}{q_+^2+M_l^2}\ , \quad \text{(D.2)}$$

$$I_2^{lh} = \int_q^\Lambda \frac{1}{(q_+^2+M_l^2)(q_+^2+M_l^2)}\ , \quad \text{(D.3)}$$

By using thrice the identity of Eq. (4.22), Eq. (D.2) can be rewritten as

$$\begin{aligned} I_1^l &= I_{\rm quad}(M^2) - (M_l^2-M^2)I_{\log}(M^2) + \eta_\pm^2\, P_\mu P_\nu A_{\mu\nu}(M^2) \\ &+ \int_q \frac{(k_1^2+M_l^2-M^2)^2}{(q^2+M^2)^3} - \int_q \frac{(2k_1\cdot q + k_1^2+M_l^2-M^2)^3}{(q^2+M^2)^3(q_+^2+M_l^2)}\ , \end{aligned} \quad \text{(D.4)}$$

with

$$A_{\mu\nu}(M^2) = \int_q^\Lambda \frac{4q_\mu q_\nu - (q^2+M^2)\delta_{\mu\nu}}{(q^2+M^2)^3}\ . \quad \text{(D.5)}$$

We can see that the two last integrals in Eq. (D.4) are finite. Therefore, after solving these finite integrals we arrive to

$$\begin{aligned} I_1^l &= I_{\rm quad}(M^2) - (M_l^2 - M^2) I_{\log}(M^2) \\ &- \frac{1}{(4\pi)^2}\left[M_l^2 - M^2 - M_l^2 \ln\left(\frac{M_l^2}{M^2}\right)\right] + \eta_\pm^2\, P_\mu P_\nu A_{\mu\nu}(M^2)\ . \end{aligned} \tag{D.6}$$

The result for the integral I_1^h is the same just change $l \to h$. For the integral given by Eq. (D.3) we use Eq. (4.22) once for each denominator, to obtain

$$\begin{aligned} I_2^{lh} &= I_{\log}(M^2) - \int_q \frac{(2k_1\cdot q + k_1^2 + M_l^2 - M^2)}{(q^2+M^2)^2(q_+^2+M_l^2)} \\ &- \int_q \frac{(2k_2\cdot q + k_2^2 + M_h^2 - M^2)}{(q^2+M^2)^2(q_+^2+M_h^2)} \\ &- \int_q \frac{(2k_1\cdot q + k_1^2 + M_l^2 - M^2)(2k_2\cdot q + k_2^2 + M_h^2 - M^2)}{(q^2+M^2)^2(q_+^2+M_l^2)(q_+^2+M_h^2)}\ . \end{aligned} \tag{D.7}$$

The three last integrals are finite and after evaluating them using the standard techniques we obtain

$$I_2^{lh} = I_{\log}(M^2) - Z_0(M_l^2, M_h^2, P^2; M^2)\ . \tag{D.8}$$

where $Z_0(M_l^2, M_h^2, P^2; M^2)$ is the finite integral defined by Eq. (4.27). Then, the kernel $K_{\rm PS}^{EE}$ can be written as

$$\begin{aligned} \mathcal{K}_{\rm PS}^{EE}(P) &= 8\Big\{-\left[P^2 + (\Delta M_{hl})^2\right]\left[I_{\log}(M^2) - Z_0(M_l^2, M_h^2, P^2; M^2)\right] \\ &+ I_{\rm quad}(M_l^2) + I_{\rm quad}(M_h^2) + \left(\eta_+^2 + \eta_-^2\right) A_{\mu\nu}(M^2) P_\mu P_\nu\Big\}. \end{aligned} \tag{D.9}$$

After evaluating the trace in Eq. (4.15) the kernel $K_{\rm PS}^{EF}$ can be rewritten as

$$\begin{aligned} \mathcal{K}_{\rm PS}^{EF}(P) &= \frac{8}{M_{lh}}\int_q^\Lambda \frac{[M_h(P\cdot q_+) - M_l(P\cdot q_-)]}{(q_+^2+M_l^2)(q_-^2+M_h^2)} \\ &= \frac{8}{M_{lh}}\left\{[M_h(P\cdot k_1) - M_l(P\cdot k_2)] I_2^{lh} - (M_l - M_h) I_{2\mu}^{lh}\right\}\ , \end{aligned} \tag{D.10}$$

where we have defined $I_{2\mu}^{lh}$ as

$$I_{2\mu}^{lh} = \int_q^\Lambda \frac{q_\mu}{(q_+^2+M_l^2)(q_+^2+M_l^2)}\ . \tag{D.11}$$

For this integral we use Eq. (4.22) twice for each denominator. By doing so we

obtain

$$\begin{aligned} I^{lh}_{2\mu} &= -\frac{1}{2}(k_1+k_2)_\alpha A_{\alpha\mu}(M^2) - \frac{1}{2}(k_1+k_2)_\mu I_{\log}(M^2) \\ &+ \int_q \frac{(2k_2\cdot q + k_2^2 + M_h^2 - M^2)^2 q_\mu}{(q^2+M^2)^3(q_+^2+M_h^2)} + \int_q \frac{(2k_2\cdot q + k_2^2 + M_h^2 - M^2)^2 q_\mu}{(q^2+M^2)^3(q_+^2+M_h^2)} \\ &+ \int_q \frac{(2k_1\cdot q + k_1^2 + M_l^2 - M^2)(2k_2\cdot q + k_2^2 + M_h^2 - M^2) q_\mu}{(q^2+M^2)^2(q_+^2+M_l^2)(q_+^2+M_h^2)} \ . \end{aligned} \tag{D.12}$$

Again after evaluating the finite integrals we obtain

$$\begin{aligned} I^{lh}_{2\mu} &= -\frac{1}{2}(k_1+k_2)_\alpha A_{\alpha\mu}(M^2) - \frac{1}{2}(k_1+k_2)_\mu I_{\log}(M^2) \\ &+ P_\mu Z_1(M_l^2, M_h^2, P^2; M^2) + k_{2\mu} Z_0(M_h^2, M_l^2, P^2; M^2) \ , \end{aligned} \tag{D.13}$$

where $Z_1(M_l^2, M_h^2, P^2; M^2)$ is another finite integral that can be related [46] to Z_0 as

$$\begin{aligned} Z_1(M_l^2, M_h^2, P^2; M^2) &= \frac{1}{(4\pi)^2}\int_0^1 dz\, z \ln\left[\frac{H(z)}{M^2}\right] \\ &= \frac{1}{2P^2}\Bigg\{ M_h^2\left[1 - \ln\left(\frac{M_h^2}{M^2}\right)\right] - M_l^2\left[1 - \ln\left(\frac{M_l^2}{M^2}\right)\right] \\ &+ (P^2 + M_h^2 - M_l^2) Z_0(M_l^2, M_h^2, P^2; M^2)\Bigg\}. \end{aligned} \tag{D.14}$$

Putting Eq. (D.8) and Eq. (D.13) into Eq. (D.10) and after performing same algebraic manipulation we obtain

$$\begin{aligned} \mathcal{K}^{EF}_{\rm PS}(P) &= = \frac{8P^2}{M_{lh}}\Bigg\{ \frac{M_h + M_l}{2} I_{\log}(M^2) \\ &+ (M_l - M_h) Z_1(M_l^2, M_h^2, P^2; M^2) - M_l Z_0(M_l^2, M_h^2, P^2; M^2)\Bigg\} \\ &+ \frac{4A_{\mu\nu}(M^2)}{M_{lh}}(M_l - M_h) P_\mu P_\nu (\eta_+ - \eta_-) \ . \end{aligned} \tag{D.15}$$

Now, by using the trace properties we can see that the kernel $K^{FE}_{\rm PS}$ can be written as

$$K^{FE}_{\rm PS}(P) = \frac{2M_{lh}^2}{P^2} K^{EF}_{\rm PS}(P) \ . \tag{D.16}$$

Finally the evaluation of the trace in Eq. (4.17) leads to

$$\begin{aligned} K^{FF}_{\rm PS}(P) &= -\frac{16}{P^2}\int_q^\Lambda \frac{(P\cdot q_+)(P\cdot q_-)}{(q_+^2 + M_l^2)(q_+^2 + M_l^2)} \\ &+ 4\int_q^\Lambda \left\{ \frac{1}{q_+^2 + M_l^2} + \frac{1}{q_-^2 + M_h^2} - \frac{P^2 + (M_l + M_h)^2}{(q_+^2 + M_l^2)(q_+^2 + M_h^2)} \right\} . \end{aligned} \tag{D.17}$$

The result of the first term is

$$
\begin{aligned}
-\frac{16}{P^2}\int_q^\Lambda \frac{(P\cdot q_+)(P\cdot q_-)}{(q_+^2+M_l^2)(q_+^2+M_l^2)} &= 8(P^2+M_h^2-M_l^2)[Z_0(M_l^2,M_h^2,P^2;M^2) \\
&- Z_1(M_l^2,M_h^2,P^2;M^2)] + 8\Bigg[I_{\rm quad}(M_l) \\
&- \left(\frac{P^2+M_h^2-M_l^2}{2}\right) I_{\log}(M_l)\Bigg] \\
&+ \frac{8}{P^2}\,P_\mu P_\nu D_{\mu\nu}(M^2)\ , \qquad \text{(D.18)}
\end{aligned}
$$

where $D_{\mu\nu}(M^2)$ is given by

$$
\begin{aligned}
D_{\mu\nu}(M^2) &= B_{\mu\nu}(M^2) - \frac{(\eta_+-\eta_-)^2 P_\mu P_\alpha}{2} A_{\alpha\nu}(M^2) - \frac{(\eta_+-\eta_-)^2 P_\nu P_\beta}{2} A_{\beta\mu}(M^2) \\
&- \frac{[P^2(\eta_+^2-\eta_-^2)+M_h^2-M_l^2]}{2} A_{\mu\nu}(M^2) + \frac{(\eta_+^2+\eta_-^2-\eta_+\eta_-)P_\alpha P_\beta}{3} \\
&\times \Big[C_{\alpha\beta\mu\nu}(M^2) + \delta_{\alpha\beta}A_{\mu\nu}(M_h^2) + \delta_{\alpha\mu}A_{\beta\nu}(M^2) + \delta_{\alpha\nu}A_{\mu\beta}(M^2)\Big]\ . \qquad \text{(D.19)}
\end{aligned}
$$

The second term in Eq. (D.17) have the same integrals that appear in the kernel $K_{\rm PS}^{EE}(P)$. Then, putting all together in Eq. (D.17) we obtain after some manipulation that the kernel $K_{\rm PS}^{FF}(P)$ can be written as

$$
\begin{aligned}
\mathcal{K}_{\rm PS}^{FF}(P) &= 8\frac{(M_l^2-M_h^2)}{2P^2}\left[I_{\rm quad}(M_h^2) - I_{\rm quad}(M_l^2)\right] \\
&- \frac{8(M_l+M_h)^2[P^2+(\Delta M_{hl})^2]}{2P^2}\Big[I_{\log}(M^2) - Z_0(M_l^2,M_h^2,P^2;M^2)\Big] \\
&+ \frac{8}{P^2}\,P_\mu P_\nu \bar{D}_{\mu\nu}(M^2), \qquad \text{(D.20)}
\end{aligned}
$$

where

$$
\bar{D}_{\mu\nu}(M^2) = D_{\mu\nu}(M^2) - 2P_\alpha P_\beta[\eta_+^2 A_{\alpha\beta}(M^2) + \eta_-^2 A_{\alpha\beta}(M^2)] \qquad \text{(D.21)}
$$

For the normalization of the BS amplitudes $E_{\rm PS}^{lh}$ and $F_{\rm PS}^{lh}$, stated by Eq. (4.50) we get

$$
\begin{aligned}
1 &= -\frac{3}{2}\Bigg\{\left(E_{\rm PS}^{lh}\right)^2 \frac{\partial \mathcal{K}_{\rm PS}^{EE}}{\partial P^2} \\
&+ 2E_{\rm PS}^{lh}F_{\rm PS}^{lh}\left[-\frac{1}{2P^2}\mathcal{K}_{\rm PS}^{EF} + \frac{\partial \mathcal{K}_{\rm PS}^{EF}}{\partial P^2}\right] + \frac{\left(F_{\rm PS}^{lh}\right)^2 P^2}{2M_{lh}^2}\frac{\partial \mathcal{K}_{\rm PS}^{FF}}{\partial P^2}\Bigg\}\Bigg|_{P^2=-m_{\rm PS}^2}\ , \qquad \text{(D.22)}
\end{aligned}
$$

with the derivatives of the kernels given by the following expressions:

$$\begin{aligned}\frac{\partial \mathcal{K}_{\rm PS}^{EE}}{\partial P^2} &= -8\left[I_{\log}(M^2) - Z_0(M_l^2, M_h^2, P^2; M^2)\right] \\ &- 8[P^2 + (\Delta M_{hl})^2]Y_1(M_l^2, M_h^2, P^2; M^2) \qquad \text{(D.23)}\\ \frac{\partial \mathcal{K}_{\rm PS}^{EF}}{\partial P^2} &= \frac{\mathcal{K}_{\rm PS}^{EF}}{P^2} + \frac{8P^2}{M_{lh}}\big[(M_l - M_h)Y_2(M_l^2, M_h^2, P^2; M^2) \\ &- M_l Y_1(M_l^2, M_h^2, P^2; M^2)\big], \qquad \text{(D.24)}\\ \frac{\partial \mathcal{K}_{\rm PS}^{FF}}{\partial P^2} &= -\frac{\mathcal{K}_{\rm PS}^{FF}}{P^2} - 8\frac{(M_l + M_h)^2}{2P^2}\Big\{\left[I_{\log}(M^2) - Z_0(M_l^2, M_h^2, P^2; M^2)\right] \\ &+ [P^2 + (\Delta M_{hl})^2]Y_1(M_l^2, M_h^2, P^2; M^2)\Big\}, \qquad \text{(D.25)}\end{aligned}$$

where we have defined

$$\begin{aligned}Y_1(M_l^2, M_h^2, P^2; M^2) &= \frac{1}{(4\pi)^2}\int_0^1 dz z(1-z)\left[e^{-H(z)\tau_{\rm ir}^2} - 1\right], \qquad \text{(D.26)}\\ Y_2(M_l^2, M_h^2, P^2; M^2) &= \frac{1}{P2}Z_1(M_l^2, M_h^2, P^2; M^2) + \frac{1}{2P^2}\Big[Z_0(M_l^2, M_h^2, P^2; M^2) \\ &+ (P^2 + M_h^2 - M_l^2)Y_1(M_l^2, M_h^2, P^2; M^2)\Big], \qquad \text{(D.27)}\end{aligned}$$

From the eigenvalue equation, one obtains

$$E_{\rm PS}^{lh}(P) = \frac{\mathcal{K}_{\rm PS}^{EF}}{\left(\frac{3m_G^2}{4\pi\alpha_{\rm IR}} - \mathcal{K}_{\rm PS}^{EE}\right)}F_{\rm PS}^{lh}(P). \qquad \text{(D.28)}$$

Combining this with Eq. (D.22), the individual amplitudes $E_{\rm PS}^{lh}(P)$ and $F_{\rm PS}^{lh}(P)$ are determined.

D.2 Vector kernel

After performing the necessary number of subtractions in the integrand of Eq. (4.21), one obtains again finite integrals and divergent integrals that are independent of $\eta_\pm$ and symmetry violating terms:

$$\begin{aligned}\mathcal{K}_{\rm V}^{EE}(P) &= \frac{4}{3}\Big\{-[P^2 + (\Delta M_{lh})^2 - 4M_l M_h]\left[I_{\log}(M^2) - Z_0(M_l^2, M_h^2, P^2, M^2)\right] \\ &+ 2(P^2 + M_h^2 - M_l^2)\Big[Z_0(M_l^2, M_h^2, P^2; M^2) - Z_1(M_l^2, M_h^2, P^2; M^2)\Big] \\ &+ 3\,I_{\rm quad}(M_l) + I_{\rm quad}(M_h) - (P^2 + M_h^2 - M_l^2)I_{\log}(M_l^2) \\ &+ \left(\eta_+^2 + \eta_-^2\right)A_{\mu\nu}(M^2)P_\mu P_\nu + \frac{1}{2}\frac{P_\mu P_\nu D_{\mu\nu}(M^2)}{P^2}\Big\}, \qquad \text{(D.29)}\end{aligned}$$

where the term $D_{\mu\nu}(M^2)$ is defined in Eq. (D.19). The vector meson decay constant is given by

$$f_{\rm V} = \frac{N_c}{2} E_V^{lh}(P) \mathcal{K}_{\rm V}^{EE}(P) \Big|_{P^2=-m_V^2} . \tag{D.30}$$

where the BS amplitude is normalized as in the case of pseudoscalar mesons and is is fixed as

$$\frac{1}{(E_V^{lh})^2} = N_c \frac{\partial \mathcal{K}_{\rm V}^{EE}(P)}{\partial P^2} \Big|_{P^2=-m_V^2} . \tag{D.31}$$

Appendix E

Evaluating Matsubara Sums

In general, calculations in the Matsubara or imaginary time formalism, requires that we have to evaluate infinite sums over Matsubara frequencies. In this appendix, we will illustrate a method for evaluating these frequency sums through the computation of propagators, as also the results for the sums which are needed in this thesis.

E.1 Bosonic propagator

Let us use the frequency sum over a scalar or Matsubara bosonic propagator

$$S_B = \frac{1}{\beta}\sum_{n=-\infty}^{\infty}\Delta_B(i\omega_n,\mathbf{k}), \tag{E.1}$$

where

$$\begin{aligned}\Delta_B(i\omega_n,\mathbf{k}) &= \frac{1}{\omega_n^2+\mathbf{k}^2+m^2}\\ &= \frac{1}{\omega_n^2+E^2(\mathbf{k})}\ ,\end{aligned} \tag{E.2}$$

begin $\omega_n \equiv 2n\pi/\beta$, with $n\in\mathbb{Z}$, and we have defined $E(\mathbf{k})=\sqrt{\mathbf{k}^2+m^2}$. The trick here is to use a contour integral in the complex energy plane and taking advantage of the residue theorem. In order to do that, we think of k_0 as a fourth of a Minkowski four vector k. Then, we can write Eq. (E.1) as a contour integral

$$\begin{aligned}S_B &= \oint_{\mathcal{C}}\frac{dk_0}{2\pi i}\frac{1}{[E^2(\mathbf{k})-k_0^2]}\frac{1}{e^{\beta k_0}-1}\ ,\\ &= \oint_{\mathcal{C}}\frac{dk_0}{2\pi i}\,\Delta_B(k_0,\mathbf{k})g(k_0)\end{aligned} \tag{E.3}$$

where the contour $\mathcal{C}$ is as shown on the left panel in Figure. E.1. In the last equation, $g(k_0)=1/(e^{\beta k_0}-1)$ is the Bose-Einstein distribution. We can note that $\Delta_B(k_0,\mathbf{k})$

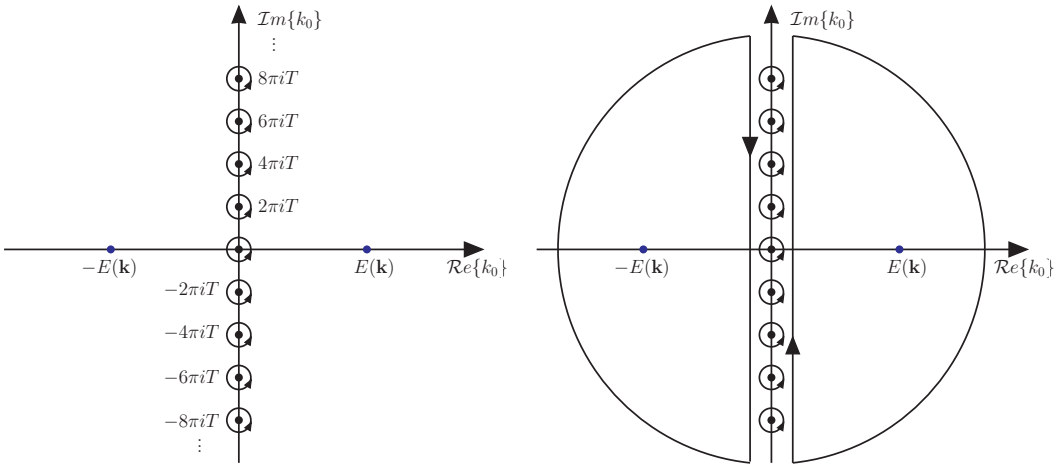

Figure E.1: Left panel: Integration contour for equation (E.3). Right panel: Contour deformation for the evaluation of equation (E.3).

has isolated poles at $k_0 = \pm E(\mathbf{k})$, with residues $\mp E(\mathbf{k})$. On the other hand, the function $g(k_0)$ with poles at $k_0 = 2n\pi iT$. Then, we may deform the contour $\mathcal{C}$ (infinitely many circles surrounding the poles) as is shown on the right panel in Figure. E.1 and obtain

$$\begin{aligned} S_B &= \frac{1}{2\pi i}\int_{i\infty-\epsilon}^{-i\infty-\epsilon} dk_0\, \Delta_B(k_0,\mathbf{k}) g(k_0)\ . \\ &+ \frac{1}{2\pi i}\int_{-i\infty+\epsilon}^{i\infty+\epsilon} dk_0\, \Delta_B(k_0,\mathbf{k}) g(k_0)\ . \end{aligned} \tag{E.4}$$

Then, after performing the change of variable $k_0 \to -k_0$ in the first term, we obtain

$$S_B = \frac{1}{2\pi i}\int_{-i\infty+\epsilon}^{i\infty+\epsilon} dk_0\, \Delta_B(k_0,\mathbf{k})\left[1+2g(k_0)\right]\ , \tag{E.5}$$

where we also have used the fact that $g(E)+g(-E)=-1$. We now use the residue theorem and we can close the contour in the positive half-plane at infinity and pick up the pole at $k_0 = E(\mathbf{k})$

$$S_B = \frac{1}{2E(\mathbf{k})}[1+2g(E(\mathbf{k}))]\ . \tag{E.6}$$

Let consider now a generic case, where we have to evaluate the following Matsubara sum

$$S = \frac{1}{\beta}\sum_{n=-\infty}^{\infty} G(i\omega_n,\mathbf{k})\ . \tag{E.7}$$

Again, we may express the last equation as a contour integral

$$S = \oint_{\mathcal{C}} \frac{dk_0}{2\pi i} G(k_0, \mathbf{k}) g(k_0) \ , \tag{E.8}$$

which its results after following the same steps as in the previous example we obtain

$$\begin{aligned} S_B &= \frac{1}{2\pi i} \int_{-i\infty+\epsilon}^{i\infty+\epsilon} dk_0 \, \frac{1}{2} \left[G(k_0, \mathbf{k}) + G(-k_0, \mathbf{k}) \right] \\ &+ \frac{1}{2\pi i} \int_{-i\infty+\epsilon}^{i\infty+\epsilon} dk_0 \, \left[G(k_0, \mathbf{k}) + G(-k_0, \mathbf{k}) \right] g(k_0) \ . \end{aligned} \tag{E.9}$$

Thus, for the case of $G(k_0, \mathbf{k}) = \Delta_B(k_0, \mathbf{k})$, we recovered the result given by Eq. (E.6). We note from Eq. (E.9) that for the case of $G(i\omega_n, \mathbf{k}) = i\omega_n/(\omega_n^2 + E^2(\mathbf{k}))$, one has

$$\frac{1}{\beta} \sum_{n=-\infty}^{\infty} \frac{i\omega_n}{\omega_n^2 + E^2(\mathbf{k})} = 0 \ , \tag{E.10}$$

because in this case we have $G(-k_0, \mathbf{k}) = -G_B(k_0, \mathbf{k})$.

E.2 Fermionic propagator

For the Fermionic case we will use the same ideas like as in the bosonic case. For example, we are interested in evaluate the following Matsubara sum

$$S_F = \frac{1}{\beta} \sum_{n=-\infty}^{\infty} F(i\omega_n, \mathbf{k}) \ , \tag{E.11}$$

with $\omega_n = (2n+1)\pi/\beta$, and

$$F(i\omega_n, \mathbf{k}) = \frac{1}{\omega_n^2 + E^2(\mathbf{k})} \ . \tag{E.12}$$

The sum given by Eq. (E.11) can be expressed as a contour integral

$$S_F = \oint_{\mathcal{C}} \frac{dk_0}{2\pi i} F(k_0, \mathbf{k}) f(k_0) \ , \tag{E.13}$$

where $f(k_0) = 1/(1 + e^{\beta k_0})$, is the Fermi-Dirac distribution, which has poles with unit residues at the values $k_0 = (2n+1)\pi i T$. Then, After closing the integration contour in the positive half-plane, one obtains

$$\begin{aligned} S_F &= \frac{1}{2\pi i} \int_{-i\infty+\epsilon}^{i\infty+\epsilon} dk_0 F(k_0, \mathbf{k}) \left[1 - 2f(k_0) \right] \\ &= \frac{1}{2E(\mathbf{k})} \left[1 - 2f(E(\mathbf{k})) \right] \ , \end{aligned} \tag{E.14}$$

where in the intermediate steps we have used the fact that $f(-E)+f(E)=1$. Now, for the case of $F(i\omega_n,\mathbf{k})=i\omega_n/(\omega_n^2+E^2(\mathbf{k}))$, we have

$$\begin{aligned}
\frac{1}{\beta}\sum_{n=-\infty}^{\infty}\frac{i\omega_n}{\omega_n^2+E^2(\mathbf{k})} &= \oint_C \frac{dk_0}{2\pi i}\frac{k_0}{[E^2(\mathbf{k})-k_0^2]}f(k_0) \\
&= \frac{1}{2\pi i}\int_{-i\infty+\epsilon}^{i\infty+\epsilon} dk_0 F(k_0,\mathbf{k})[f(-k_0)+f(k_0)] \\
&= \frac{1}{2\pi i}\int_{-i\infty+\epsilon}^{i\infty+\epsilon} dk_0 F(k_0,\mathbf{k}) \\
&= \mathrm{Res}\left[F(k_0,\mathbf{k})\right]\Big|_{k_0=-E(\mathbf{k})} + \mathrm{Res}\left[F(k_0,\mathbf{k})\right]\Big|_{k_0=E(\mathbf{k})} \\
&= 0\ . \qquad \text{(E.15)}
\end{aligned}$$

Appendix F

Bethe-Salpeter Kernels at Finite Temperature

In this appendix we present the details of the separation of the purely divergent part from the thermal effects into the BS kernels. We will consider the case of the pseudoscalar mesons.

F.1 Pseudoscalar BS kernels

Again, after replacing Eq. (5.26) into Eq. (5.25) we can rewrite it in the matrix form

$$\begin{bmatrix} E^{lh}_{\rm PS}(\mathbf{P},\nu_n) \\ F^{lh}_{\rm PS}(\mathbf{P},\nu_n) \end{bmatrix} = \frac{1}{3m^l_{\rm G}m^h_{\rm G}} \begin{bmatrix} \mathcal{K}^{EE}_{\rm PS}(\mathbf{P},\nu_n) & \mathcal{K}^{EF}_{\rm PS}(\mathbf{P},\nu_n) \\ \mathcal{K}^{FE}_{\rm PS}(\mathbf{P},\nu_n) & \mathcal{K}^{FF}_{\rm PS}(\mathbf{P},\nu_n) \end{bmatrix} \begin{bmatrix} E^{lh}_{\rm PS}(\mathbf{P},\nu_n) \\ F^{lh}_{\rm PS}(\mathbf{P},\nu_n) \end{bmatrix}, \quad \text{(F.1)}$$

where the pseudoscalar kernel's matrix elements are given by,

$$\mathcal{K}^{EE}_{\rm PS}(\mathbf{P},\nu_n) = -\frac{1}{\beta}\sum_{m=-\infty}^{\infty}\int_{\mathbf{q}} \mathrm{Tr}\left[\gamma_5\gamma_\mu S_l(\omega_+,\mathbf{q}_+)\gamma_5 S_h(\omega_-,\mathbf{q}_-)\gamma_\mu\right], \quad \text{(F.2)}$$

$$\mathcal{K}^{EF}_{\rm PS}(\mathbf{P},\nu_n) = \frac{i}{2M_{lh}}\frac{1}{\beta}\sum_{m=-\infty}^{\infty}\int_{\mathbf{q}} \mathrm{Tr}\left[\gamma_5\gamma_\mu\, S_l(\omega_+,\mathbf{q}_+)\gamma_5\gamma\cdot P S_h\omega_-,\mathbf{q}_-)\gamma_\mu\right], \quad \text{(F.3)}$$

$$\mathcal{K}^{FE}_{\rm PS}(\mathbf{P},\nu_n) = \frac{2iM_{lh}}{P^2}\frac{1}{\beta}\sum_{m=-\infty}^{\infty}\int_{\mathbf{q}} \mathrm{Tr}\left[\gamma_5\gamma\cdot P\gamma_\mu S_l(\omega_+,\mathbf{q}_+)\gamma_5 S_h(\omega_-,\mathbf{q}_-)\,\gamma_\mu\right], \quad \text{(F.4)}$$

$$\mathcal{K}^{FF}_{\rm PS}(\mathbf{P},\nu_n) = \frac{1}{P^2}\frac{1}{\beta}\sum_{m=-\infty}^{\infty}\int_{\mathbf{q}} \mathrm{Tr}\left[\gamma_5\gamma\cdot P\gamma_\mu S_l(\omega_+,\mathbf{q}_+)\gamma_5\gamma\cdot P S_h(\omega_-,\mathbf{q}_-)\gamma_\mu\right]. \quad \text{(F.5)}$$

We start with the evaluation of the kernel given by Eq. (F.2), which after taking the trace over Dirac matrices one obtains

$$\begin{aligned}\mathcal{K}^{EE}_{\rm PS}(\mathbf{P},\nu_n) &= \frac{16}{\beta}\sum_{m=-\infty}^{\infty}\int_{\mathbf{q}}\frac{\omega_+\omega_- + \mathbf{q}_+\mathbf{q}_- + M_lM_h}{[\omega_+^2+E_l^2(\mathbf{q}_+)][\omega_-^2+E_h^2(\mathbf{q}_-)]}, \\ &= -\frac{8}{\beta}\sum_{m=-\infty}^{\infty}\int_{\mathbf{q}}\left\{\frac{1}{\omega_+^2+E_l^2(\mathbf{q}_+)}+\frac{1}{\omega_-^2+E_l^2(\mathbf{q}_-)}\right. \\ &- \left.\frac{\left[\mathbf{P}^2+\nu_n^2+(\Delta M_{hl})^2\right]}{[\omega_+^2+E_l^2(\mathbf{q}_+)][\omega_-^2+E_h^2(\mathbf{q}_-)]}\right\}. \end{aligned} \quad \text{(F.6)}$$

For this kernel we have to evaluate the following sums over Matsubara frequencies

$$S_{\pm} = \frac{1}{\beta}\sum_{m=-\infty}^{\infty}\frac{1}{\omega_{\pm}^2+E_{l,h}^2(\mathbf{q}_{\pm})}\,, \tag{F.7}$$

$$S_{+-} = \frac{1}{\beta}\sum_{m=-\infty}^{\infty}\frac{1}{[\omega_{+}^2+E_{l}^2(\mathbf{q}_{+})][\omega_{-}^2+E_{h}^2(\mathbf{q}_{-})]}\,. \tag{F.8}$$

In a similar way as the Matsubara sum that appears in Eq. (5.20), we can write Eq. (F.7) as

$$S_{\pm} = \frac{1}{\beta}\sum_{m=-\infty}^{\infty}\frac{1}{2E_{l,h}(\mathbf{q}_{\pm}))}\left[\frac{1}{i\omega_{\pm}+E_{l,h}(\mathbf{q}_{\pm})}-\frac{1}{i\omega_{\pm}-E_{l,h}(\mathbf{q}_{\pm})}\right]\,. \tag{F.9}$$

In order to evaluate the Matsubara sum using the relation given by Eq. (5.21), first we note that due the fact that $\omega_{\pm}=\omega_m\pm\chi_{\pm}\nu_n=2(m\pm\chi_{\pm}n+1)\pi/\beta$, with $\chi_{\pm}\in\mathbb{Z}$, there is always the possibility to make the change o variable $m\to m'=m\pm\chi_{\pm}n$. In doing so, and after using Eq. (5.21) the result for the sum $S_{\pm}$ is

$$S_{\pm}=\frac{1}{2E_{l,h}(\mathbf{q}_{\pm})}\left[1-2f(E_{l,h}(\mathbf{q}_{\pm}))\right]\,. \tag{F.10}$$

For the case of Eq. (F.8) we write it in the form

$$\begin{aligned} S_{+-} &= \frac{1}{\beta}\sum_{m=-\infty}^{\infty}\frac{1}{4E_l(\mathbf{q}_+)E_h(\mathbf{q}_-)}\left[\frac{1}{i\omega_+ + E_l(\mathbf{q}_+)}-\frac{1}{i\omega_+ - E_l(\mathbf{q}_+)}\right] \\ &\times \left[\frac{1}{i\omega_- + E_h(\mathbf{q}_-)}-\frac{1}{i\omega_- - E_h(\mathbf{q}_-)}\right], \end{aligned} \tag{F.11}$$

which after some algebraic manipulation can be rewritten as

$$S_{+-} = \frac{1}{4E_l(\mathbf{q}_+)E_h(\mathbf{q}_-)}\left[S_{hl}^{++}+S_{hl}^{--}-S_{hl}^{-+}-S_{hl}^{+-}\right], \tag{F.12}$$

where

$$S_{hl}^{++}=\frac{1}{[i\nu_n+E_l(\mathbf{q}_+)-E_h(\mathbf{q}_-)]}\frac{1}{\beta}\sum_{m=-\infty}^{\infty}\left[\frac{1}{i\omega_-+E_h(\mathbf{q}_-)}-\frac{1}{i\omega_++E_l(\mathbf{q}_+)}\right], \tag{F.13}$$

$$S_{hl}^{--}=\frac{1}{[i\nu_n-E_l(\mathbf{q}_+)+E_h(\mathbf{q}_-)]}\frac{1}{\beta}\sum_{m=-\infty}^{\infty}\left[\frac{1}{i\omega_--E_h(\mathbf{q}_-)}-\frac{1}{i\omega_+-E_l(\mathbf{q}_+)}\right], \tag{F.14}$$

$$S_{hl}^{-+}=\frac{1}{[i\nu_n+E_l(\mathbf{q}_+)+E_h(\mathbf{q}_-)]}\frac{1}{\beta}\sum_{m=-\infty}^{\infty}\left[\frac{1}{i\omega_--E_h(\mathbf{q}_-)}-\frac{1}{i\omega_++E_l(\mathbf{q}_+)}\right], \tag{F.15}$$

$$S_{hl}^{+-} = \frac{1}{[i\nu_n - E_l(\mathbf{q}_+) - E_h(\mathbf{q}_-)]}\frac{1}{\beta}\sum_{m=-\infty}^{\infty}\left[\frac{1}{i\omega_- + E_h(\mathbf{q}_-)} - \frac{1}{i\omega_+ - E_l(\mathbf{q}_+)}\right]. \quad \text{(F.16)}$$

Then, after using Eq. (5.21) and performing some manipulations one obtains

$$\begin{aligned} S_{+-} &= \frac{1}{2E_l(\mathbf{q}_+)E_h(\mathbf{q}_-)}\frac{E_l(\mathbf{q}_+)+E_h(\mathbf{q}_-)}{[[E_l(\mathbf{q}_+)+E_h(\mathbf{q}_-)]^2-(i\nu_n)^2]} \\ &+ \frac{f(E_l(\mathbf{q}_+))}{2E_l(\mathbf{q}_+)\,[[i\nu_n+E_l(\mathbf{q}_+)]^2-E_h^2(\mathbf{q}_-)]} \\ &+ \frac{f(E_l(\mathbf{q}_+))}{2E_l(\mathbf{q}_+)\,[[i\nu_n-E_l(\mathbf{q}_+)]^2-E_h^2(\mathbf{q}_-)]} \\ &+ \frac{f(E_h(\mathbf{q}_-))}{2E_h(\mathbf{q}_-)\,[[i\nu_n+E_h(\mathbf{q}_-)]^2-E_l^2(\mathbf{q}_+)]} \\ &+ \frac{f(E_h(\mathbf{q}_-))}{2E_h(\mathbf{q}_-)\,[[i\nu_n-E_h(\mathbf{q}_-)]^2-E_l^2(\mathbf{q}_+)]}. \end{aligned} \quad \text{(F.17)}$$

Now, putting all together Eq. (F.10) and Eq. (F.17) into Eq. (F.6), the kernel $\mathcal{K}_{\rm PS}^{EE}(\mathbf{P},\nu_n)$ can be written as

$$\mathcal{K}_{\rm PS}^{EE}(\mathbf{P},\nu_n) = \mathcal{K}_{\rm PS}^{EE}(\mathbf{P},\nu_n)|_{\rm div} + \mathcal{K}_{\rm PS}^{EE}(\mathbf{P},\nu_n)|_{\rm fin}\ , \quad \text{(F.18)}$$

where $\mathcal{K}_{\rm PS}^{EE}(\mathbf{P},\nu_n)|_{\rm div}$ and $\mathcal{K}_{\rm PS}^{EE}(\mathbf{P},\nu_n)|_{\rm fin}$ are given by

$$\begin{aligned} \mathcal{K}_{\rm PS}^{EE}(\mathbf{P},\nu_n)|_{\rm div} &= 8\int_{\mathbf{q}}\left\{\frac{1}{2E_l(\mathbf{q}_+)}+\frac{1}{2E_h(\mathbf{q}_-)}\right. \\ &- \left.\frac{\left[\mathbf{P}^2+\nu_n^2+(\Delta M_{hl})^2\right]}{2E_l(\mathbf{q}_+)E_h(\mathbf{q}_-)}\frac{[E_l(\mathbf{q}_+)+E_h(\mathbf{q}_-)]}{[[E_l(\mathbf{q}_+)+E_h(\mathbf{q}_-)]^2-(i\nu_n)^2]}\right\}, \end{aligned} \quad \text{(F.19)}$$

$$\begin{aligned} \mathcal{K}_{\rm PS}^{EE}(\mathbf{P},\nu_n)|_{\rm fin} &= -8\int_{\mathbf{q}}\left\{\frac{f(E_l(\mathbf{q}_+))}{2E_l(\mathbf{q}_+)}+\frac{f(E_h(\mathbf{q}_-))}{2E_h(\mathbf{q}_-)}+\frac{\left[\mathbf{P}^2+\nu_n^2+(\Delta M_{hl})^2\right]}{4E_l(\mathbf{q}_+)E_h(\mathbf{q}_-)}\right. \\ &\times \left[\frac{2E_h(\mathbf{q}_-)f(E_l(\mathbf{q}_+))}{[i\nu_n+E_l(\mathbf{q}_+)]^2-E_h^2(\mathbf{q}_-)}+\frac{2E_h(\mathbf{q}_-)f(E_l(\mathbf{q}_+))}{[i\nu_n-E_l(\mathbf{q}_+)]^2-E_h^2(\mathbf{q}_-)}\right. \\ &+ \left.\left.\frac{2E_l(\mathbf{q}_+)f(E_h(\mathbf{q}_-))}{[i\nu_n+E_h(\mathbf{q}_-)]^2-E_l^2(\mathbf{q}_+)}+\frac{2E_l(\mathbf{q}_+)f(E_h(\mathbf{q}_-))}{[i\nu_n-E_h(\mathbf{q}_-)]^2-E_l^2(\mathbf{q}_+)}\right]\right\}. \end{aligned} \quad \text{(F.20)}$$

One notes that when $T=0$ in Eq. (F.18) the second term vanishes and Eq. (F.19) is exactly the purely divergent vacuum contribution Eq. (4.23) after integrating in q_4 in the complex plane. Of course, at $T\neq 0$ the first the term in Eq. (F.18) is temperature dependent. In order to check that Eq. (F.19) correspond to Eq. (4.23) after integrating in the temporal variable, let us consider the Minkowski space version of

the integrals in Eq. (4.23), namely

$$\begin{aligned} I_1^{\pm} &= i\int \frac{d^4q}{(2\pi)^4}\frac{1}{q_{\pm}^2 - M_{l,h}^2 + i\epsilon} \ , \\ I_2^{+-} &= i\int \frac{d^4q}{(2\pi)^4}\frac{1}{(q_{+}^2 - M_{l}^2 + i\epsilon)(q_{-}^2 - M_{h}^2 + i\epsilon)} \ . \end{aligned} \tag{F.21}$$

For example, from the first integral one has

$$I_1^{+} = i\int \frac{d^3q}{(2\pi)^3}\int_{-\infty}^{\infty}\frac{dq_0}{(2\pi)}F(q^0) \ , \tag{F.22}$$

where we have defined $F(q^0)$ as

$$F(q^0) = \frac{1}{[q_+^0 - (E_l(\mathbf{q}_+) - i\epsilon)]\,[q_+^0 + (E_l(\mathbf{q}_+) - i\epsilon)]}. \tag{F.23}$$

being $q_+^0 = q^0 + k_{01}$. The integral has two simple poles located at $q_0 = -k_{01} \pm E_l(\mathbf{q}_+) \mp i\epsilon$. By using the residue theorem, and closing the integration contour upward as is depicted in Figure. F.1, and picking up the residue of the pole in the upper half-plane we obtain

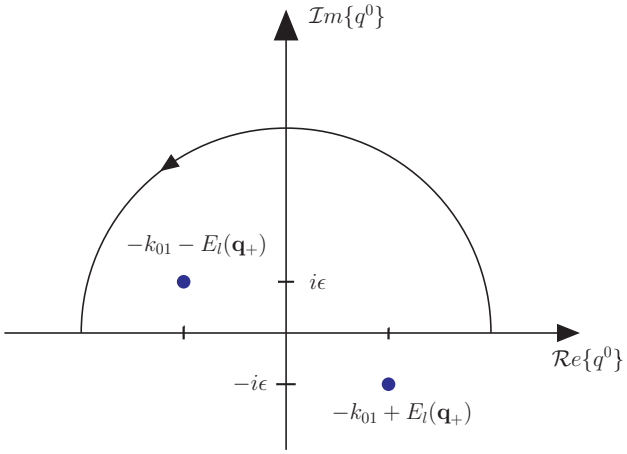

Figure F.1: The integration contour in the complex q^0 for the evaluation of the integral I_1^+.

$$\begin{aligned} I_1^{+} &= \frac{i}{2\pi}\int \frac{d^3q}{(2\pi)^3}\,2\pi i\,\mathrm{Res}\left[F(q_0), q_0 = -k_{01} - E_l)\right] \ , \\ &= \int \frac{d^3q}{(2\pi)^3}\frac{1}{2E_l(\mathbf{q}_+)} \ . \end{aligned} \tag{F.24}$$

For the case of I_1^- we obtain a similar result. On the other hand, the integral I_2^{+-} has four simple poles located at $q_0 = -k_{01} \pm E_l(\mathbf{q}_+) \mp i\epsilon$ and $q_0 = -k_{02} \pm E_h(\mathbf{q}_-) \mp i\epsilon$, see Figure. F.2. Again, after closing the integration contour upward and picking up the residue of the poles one obtains

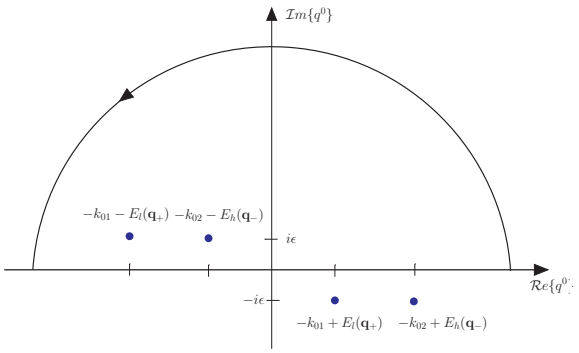

Figure F.2: The integration contour in the complex q^0 for the evaluation of the integral I_2^+.

$$
\begin{aligned}
I_2^{+-} &= \int \frac{d^3q}{(2\pi)^3} \frac{1}{4E_l(\mathbf{q}_+)E_h(\mathbf{q}_-)} \left[\frac{1}{-P^0 + E_l(\mathbf{q}_+) + E_h(\mathbf{q}_-)} \right. \\
&+ \left. \frac{1}{P^0 + E_l(\mathbf{q}_+) + E_h(\mathbf{q}_-)} \right] \\
&= \int \frac{d^3q}{(2\pi)^3} \frac{1}{2E_l(\mathbf{q}_+)E_h(\mathbf{q}_-)} \frac{E_l(\mathbf{q}_+) + E_h(\mathbf{q}_-)}{[[E_l(\mathbf{q}_+) + E_h(\mathbf{q}_-)]^2 - (P^0)^2]} \,. \qquad \text{(F.25)}
\end{aligned}
$$

where we have defined $P^0 = k_{01} - k_{02}$. With this results we have verified that Eq. (F.19) is exactly Eq. (4.23) after integrating in the time variable. Therefore, we can write Eq. (F.19) as

$$
\begin{aligned}
\mathcal{K}_{\rm PS}^{EE}(\mathbf{P}, -i\omega)|_{\rm div} &= 8\Big\{ I_{\rm quad}(M_l^2) + I_{\rm quad}(M_h^2) - \left[\mathbf{P}^2 + \omega^2 + (\Delta M_{hl})^2\right] \\
&\times \left[I_{\log}(M_0^2) - Z_0(M_l^2, M_h^2, \left(\mathbf{P}^2 + \omega^2\right); M_0^2) \right] \\
&+ \left(\eta_+^2 + \eta_-^2\right) A_{\mu\nu}(M_0^2) P_\mu P_\nu \Big\}, \qquad \text{(F.26)}
\end{aligned}
$$

where we have also taken the analytic continuation $i\nu_n \to \omega + \eta$. In the last equation, $I_{\rm quad}(M_{l,h}^2)$ is given by Eq. (4.31), with $M = M_0$, being M_0 the vacuum subtracted mass.

Now, let us continue with the second kernel given by Eq. (F.3), which after

evaluating the Dirac trace on obtains

$$\mathcal{K}^{EF}_{\rm PS}(\mathbf{P},\nu_n) = \frac{8}{M_{lh}}\frac{1}{\beta}\sum_{m=-\infty}^{\infty}\int_{\mathbf{q}}\frac{\nu_n(M_h\omega_+ - M_l\omega_-) + M_h(\mathbf{P}\cdot\mathbf{q}_+) - M_l(\mathbf{P}\cdot\mathbf{q}_-)}{[\omega_+^2 + E_l^2(\mathbf{q}_+)][\omega_-^2 + E_h^2(\mathbf{q}_-)]}. \quad \text{(F.27)}$$

From the last equation only we have to evaluate the following Matsubara sum

$$\begin{aligned} S^{\omega_\pm}_{+-} &= \frac{1}{\beta}\sum_{m=-\infty}^{\infty}\frac{\omega_\pm}{[\omega_+^2 + E_l^2(\mathbf{q}_+)][\omega_-^2 + E_h^2(\mathbf{q}_-)]} \\ &= \frac{1}{\beta}\sum_{m=-\infty}^{\infty}\frac{1}{4E_l(\mathbf{q}_+)E_h(\mathbf{q}_-)}\left[\frac{\omega_\pm}{i\omega_+ + E_l(\mathbf{q}_+)} - \frac{\omega_\pm}{i\omega_+ - E_l(\mathbf{q}_+)}\right] \\ &\times \left[\frac{\omega_\pm}{i\omega_- + E_h(\mathbf{q}_-)} - \frac{\omega_\pm}{i\omega_- - E_h(\mathbf{q}_-)}\right], \end{aligned} \quad \text{(F.28)}$$

which can be done in the same way as in Eq. (F.11). Then, after using the following identities

$$\frac{\omega_\pm}{i\omega_- + E_h(\mathbf{q}_-)} - \frac{\omega_\pm}{i\omega_+ + E_l(\mathbf{q}_+)} = \frac{i\nu_n \mp E_{h,l}(\mathbf{q}_\mp)}{i\omega_- + E_h(\mathbf{q}_-)} \pm \frac{E_{l,h}(\mathbf{q}_\pm)}{i\omega_+ + E_l(\mathbf{q}_+)}, \quad \text{(F.29)}$$

$$\frac{\omega_\pm}{i\omega_- - E_h(\mathbf{q}_-)} - \frac{\omega_\pm}{i\omega_+ - E_l(\mathbf{q}_+)} = \frac{i\nu_n \pm E_{h,l}(\mathbf{q}_\mp)}{i\omega_- - E_h(\mathbf{q}_-)} \mp \frac{E_{l,h}(\mathbf{q}_\pm)}{i\omega_+ - E_l(\mathbf{q}_+)}, \quad \text{(F.30)}$$

$$\frac{\omega_\pm}{i\omega_- - E_h(\mathbf{q}_-)} - \frac{\omega_\pm}{i\omega_+ + E_l(\mathbf{q}_+)} = \frac{i\nu_n + E_{h,l}(\mathbf{q}_\mp)}{i\omega_- - E_h(\mathbf{q}_-)} + \frac{E_{l,h}(\mathbf{q}_\pm)}{i\omega_+ + E_l(\mathbf{q}_+)}, \quad \text{(F.31)}$$

$$\frac{\omega_\pm}{i\omega_- + E_h(\mathbf{q}_-)} - \frac{\omega_\pm}{i\omega_+ - E_l(\mathbf{q}_+)} = \frac{i\nu_n - E_{h,l}(\mathbf{q}_\mp)}{i\omega_- + E_h(\mathbf{q}_-)} - \frac{E_{l,h}(\mathbf{q}_\pm)}{i\omega_+ - E_l(\mathbf{q}_+)}, \quad \text{(F.32)}$$

and in addition, after evaluating the Matsubara sums, we obtain after some algebraic manipulation, the Eq. (F.28) can be written as

$$\begin{aligned} S^{\omega_\pm}_{+-} &= \pm\frac{i(i\nu_n)}{2E_{h,l}(\mathbf{q}_\mp)[(i\nu_n)^2 - [E_l(\mathbf{q}_+) + E_h(\mathbf{q}_-)]^2]} \\ &- i\Bigg\{ \pm \frac{[i\nu_n \mp E_{h,l}(\mathbf{q}_\mp)]f(E_{h,l}(\mathbf{q}_\mp))}{2E_{h,l}(\mathbf{q}_\mp)[[i\nu_n \mp E_{h,l}(\mathbf{q}_\mp)]^2 - E^2_{l,h}(\mathbf{q}_\pm)]} \\ &\pm \frac{[i\nu_n \pm E_{h,l}(\mathbf{q}_\mp)]f(E_{h,l}(\mathbf{q}_\mp))}{2E_{h,l}(\mathbf{q}_\mp)[[i\nu_n \pm E_{h,l}(\mathbf{q}_\mp)]^2 - E^2_{l,h}(\mathbf{q}_\pm)]} \\ &- \frac{E_{l,h}(\mathbf{q}_\pm)f(E_{l,h}(\mathbf{q}_\pm))}{2E_{l,h}(\mathbf{q}_\pm)[[i\nu_n \pm E_{l,h}(\mathbf{q}_\pm)]^2 - E^2_{h,l}(\mathbf{q}_\mp)]} \\ &+ \frac{E_{l,h}(\mathbf{q}_\pm)f(E_{l,h}(\mathbf{q}_\pm))}{2E_{l,h}(\mathbf{q}_\pm)[[i\nu_n \mp E_{l,h}(\mathbf{q}_\pm)]^2 - E^2_{h,l}(\mathbf{q}_\mp)]}\Bigg\}. \end{aligned} \quad \text{(F.33)}$$

Thus, after putting all together, which means that using the results given by Eq. (F.17) and Eq. (F.33) into Eq. (F.27), one obtains

$$\mathcal{K}^{EF}_{\rm PS}(\mathbf{P},\nu_n) = \mathcal{K}^{EF}_{\rm PS}(\mathbf{P},\nu_n)|_{\rm div} + \mathcal{K}^{EF}_{\rm PS}(\mathbf{P},\nu_n)|_{\rm fin}, \quad \text{(F.34)}$$

where the purely divergent part of the kernel $\mathcal{K}^{EF}_{\rm PS}(\mathbf{P},\nu_n)$ is

$$\begin{aligned}\mathcal{K}^{EF}_{\rm PS}(\mathbf{P},\nu_n)|_{\rm div} &= \frac{8}{M_{l,h}}\int_{\mathbf{q}}\Bigg\{\frac{(i\nu_n)^2[M_hE_l(\mathbf{q}_+)-M_lE_h(\mathbf{q}_-)]}{2E_l(\mathbf{q}_+)E_h(\mathbf{q}_-)[(i\nu_n)^2-[E_l(\mathbf{q}_+)+E_h(\mathbf{q}_-)]^2]}\\ &- \frac{[M_h(\mathbf{P}\cdot\mathbf{q}_+)-M_l(\mathbf{P}\cdot\mathbf{q}_-)][E_l(\mathbf{q}_+)+E_h(\mathbf{q}_-)]}{2E_l(\mathbf{q}_+)E_h(\mathbf{q}_-)[(i\nu_n)^2-[E_l(\mathbf{q}_+)+E_h(\mathbf{q}_-)]^2]}\Bigg\}\,, \qquad \text{(F.35)}\end{aligned}$$

and the finite thermal part by

$$\begin{aligned}\mathcal{K}^{EF}_{\rm PS}(\mathbf{P},\nu_n)|_{\rm fin} &= \frac{8}{M_{l,h}}\int_{\mathbf{q}}\Bigg\{\frac{[(M_l-M_h)E_h(\mathbf{q}_-)-(i\nu_n)M_h]f(E_h(\mathbf{q}_-))}{2E_h(\mathbf{q}_-)[[i\nu_n+E_h(\mathbf{q}_-)]^2-E_l^2(\mathbf{q}_+)]}\\ &- \frac{[(M_l-M_h)E_h(\mathbf{q}_-)+(i\nu_n)M_h]f(E_h(\mathbf{q}_-))}{2E_h(\mathbf{q}_-)[[i\nu_n-E_h(\mathbf{q}_-)]^2-E_l^2(\mathbf{q}_+)]}\\ &+ \frac{[(M_l-M_h)E_l(\mathbf{q}_+)-(i\nu_n)M_l]f(E_l(\mathbf{q}_+))}{2E_l(\mathbf{q}_+)[[i\nu_n-E_l(\mathbf{q}_+)]^2-E_h^2(\mathbf{q}_-)]}\\ &- \frac{[(M_l-M_h)E_l(\mathbf{q}_+)+(i\nu_n)M_l]f(E_l(\mathbf{q}_+))}{2E_l(\mathbf{q}_+)[[i\nu_n+E_l(\mathbf{q}_+)]^2-E_h^2(\mathbf{q}_-)]}\Bigg\}\\ &+ \frac{8}{M_{l,h}}\int_{\mathbf{q}}\frac{[M_h(\mathbf{P}\cdot\mathbf{q}_+)-M_l(\mathbf{P}\cdot\mathbf{q}_-)]}{4E_l(\mathbf{q}_+)E_h(\mathbf{q}_-)}\\ &\times \Bigg\{\frac{2E_h(\mathbf{q}_-)f(E_l(\mathbf{q}_+))}{[i\nu_n+E_l(\mathbf{q}_+)]^2-E_h^2(\mathbf{q}_-)}+\frac{2E_h(\mathbf{q}_-)f(E_l(\mathbf{q}_+))}{[i\nu_n-E_l(\mathbf{q}_+)]^2-E_h^2(\mathbf{q}_-)}\\ &+ \frac{2E_l(\mathbf{q}_+)f(E_h(\mathbf{q}_-))}{[i\nu_n+E_h(\mathbf{q}_-)]^2-E_l^2(\mathbf{q}_+)}+\frac{2E_l(\mathbf{q}_+)f(E_h(\mathbf{q}_-))}{[i\nu_n-E_h(\mathbf{q}_-)]^2-E_l^2(\mathbf{q}_+)}\Bigg\}. \qquad \text{(F.36)}\end{aligned}$$

The divergent part Eq. (F.35) is exactly Eq. (D.10) after integrating over the time variable in the same way as in the case of the kernel $\mathcal{K}^{EE}_{\rm PS}(\mathbf{P},\nu_n)|_{\rm div}$, which was verified above. Therefore, Eq. (F.35) can be written as

$$\begin{aligned}\mathcal{K}^{EF}_{\rm PS}(\mathbf{P},-i\omega)|_{\rm div} &= \frac{8(\mathbf{P}^2+\omega^2)}{M_{lh}}\Bigg\{(M_l-M_h)Z_1(M_l^2,M_h^2,(\mathbf{P}^2+\omega^2);M_0^2)\\ &- M_lZ_0(M_l^2,M_h^2,(\mathbf{P}^2+\omega^2);M_0^2)+\frac{M_h+M_l}{2}I_{\log}(M_0^2)\Bigg\}\\ &+ \frac{4A_{\mu\nu}(M_0^2)}{M_{lh}}(M_l-M_h)P_\mu P_\nu(\eta_+-\eta_-)\,, \qquad \text{(F.37)}\end{aligned}$$

where we have taken the analytic continuation $i\nu_n\to\omega+\eta$. Finally, for the case of the kernel $\mathcal{K}^{FF}_{\rm PS}(\mathbf{P},-i\omega)$ one has after evaluation of the Dirac trace in Eq. (F.5)

$$\begin{aligned}\mathcal{K}^{FF}_{\rm PS}(\mathbf{P},\nu_n) &= -\frac{16}{P^2}\frac{1}{\beta}\sum_{m=-\infty}^{\infty}\int_{\mathbf{q}}\Bigg\{\frac{\nu_n^2\,\omega_+\omega_-+\nu_n[(\mathbf{P}\cdot\mathbf{q}_+)\omega_-+(\mathbf{P}\cdot\mathbf{q}_-)\omega_+]}{[\omega_+^2+E_l^2(\mathbf{q}_+)][\omega_-^2+E_h^2(\mathbf{q}_-)]}\\ &+ \frac{(\mathbf{P}\cdot\mathbf{q}_+)(\mathbf{P}\cdot\mathbf{q}_-)}{[\omega_+^2+E_l^2(\mathbf{q}_+)][\omega_-^2+E_h^2(\mathbf{q}_-)]}\Bigg\}+\frac{1}{2}\mathcal{K}^{EE}_{\rm S}(\mathbf{P},\nu_n)\,, \qquad \text{(F.38)}\end{aligned}$$

where $\mathcal{K}_{\rm S}^{EE}(\mathbf{P},-i\omega)$ is the scalar BS kernel defined as

$$\mathcal{K}_{\rm S}^{EE}(\mathbf{P},\nu_n)=\frac{1}{\beta}\sum_{m=-\infty}^{\infty}\int_{\mathbf{q}}{\rm Tr}[\mathbb{1}S_l(q_+,\omega_+)\mathbb{1}S_h(q_+,\omega_+)]\ . \tag{F.39}$$

It is not difficult to convince that the scalar kernel can be written as

$$\mathcal{K}_{\rm S}^{EE}(\mathbf{P},-i\omega)=\mathcal{K}_{\rm S}^{EE}(\mathbf{P},-i\omega)|_{\rm div}+\mathcal{K}_{\rm S}^{EE}(\mathbf{P},-i\omega)|_{\rm fin}\ , \tag{F.40}$$

where the divergent part is given by

$$\begin{aligned}\mathcal{K}_{\rm S}^{EE}(\mathbf{P},-i\omega)|_{\rm div} &= 8\Big\{I_{\rm quad}(M_l^2)+I_{\rm quad}(M_h^2)-\left[\mathbf{P}^2+\omega^2+(M_l+M_h)^2\right]\\ &\times\ \left[I_{\log}(M_0^2)-Z_0(M_l^2,M_h^2,\left(\mathbf{P}^2+\omega^2\right);M_0^2)\right]\\ &+\ \left(\eta_+^2+\eta_-^2\right)A_{\mu\nu}(M_0^2)P_\mu P_\nu\Big\},\end{aligned} \tag{F.41}$$

and the finite part

$$\begin{aligned}\mathcal{K}_{\rm S}^{EE}(\mathbf{P},-i\omega)|_{\rm fin} &= -8\int_{\mathbf{q}}\left\{\frac{f(E_l(\mathbf{q}_+))}{2E_l(\mathbf{q}_+)}+\frac{f(E_h(\mathbf{q}_-))}{2E_h(\mathbf{q}_-)}+\frac{[\mathbf{P}^2+\omega^2+(M_l+M_h)^2]}{4E_l(\mathbf{q}_+)E_h(\mathbf{q}_-)}\right.\\ &\times\ \left[\frac{2E_h(\mathbf{q}_-)f(E_l(\mathbf{q}_+))}{[\omega+E_l(\mathbf{q}_+)]^2-E_h^2(\mathbf{q}_-)}+\frac{2E_h(\mathbf{q}_-)f(E_l(\mathbf{q}_+))}{[\omega-E_l(\mathbf{q}_+)]^2-E_h^2(\mathbf{q}_-)}\right.\\ &+\ \left.\left.\frac{2E_l(\mathbf{q}_+)f(E_h(\mathbf{q}_-))}{[\omega+E_h(\mathbf{q}_-)]^2-E_l^2(\mathbf{q}_+)}+\frac{2E_l(\mathbf{q}_+)f(E_h(\mathbf{q}_-))}{[\omega-E_h(\mathbf{q}_-)]^2-E_l^2(\mathbf{q}_+)}\right]\right\}.\end{aligned} \tag{F.42}$$

In the first term in Eq. (F.38) we only have to evaluate the following Matsubara sum

$$\begin{aligned}S_{+-}^{\omega_+\omega_-} &= \frac{1}{\beta}\sum_{m=-\infty}^{\infty}\frac{\omega_+\omega_-}{[\omega_+^2+E_l^2(\mathbf{q}_+)][\omega_-^2+E_h^2(\mathbf{q}_-)]}\\ &= \frac{1}{\beta}\sum_{m=-\infty}^{\infty}\frac{1}{4E_l(\mathbf{q}_+)E_h(\mathbf{q}_-)}\left[\frac{\omega_+\omega_-}{i\omega_++E_l(\mathbf{q}_+)}-\frac{\omega_+\omega_-}{i\omega_+-E_l(\mathbf{q}_+)}\right]\\ &\times\ \left[\frac{\omega_+\omega_-}{i\omega_-+E_h(\mathbf{q}_-)}-\frac{\omega_+\omega_-}{i\omega_--E_h(\mathbf{q}_-)}\right]\ .\end{aligned} \tag{F.43}$$

Before evaluating the sums over the Matsubara frequencies, we will consider the following identities

$$\begin{aligned}\frac{\omega_+\omega_-}{i\omega_-+E_h(\mathbf{q}_-)}-\frac{\omega_+\omega_-}{i\omega_++E_l(\mathbf{q}_+)} &= i\nu_n+E_l(\mathbf{q}_+)-E_h(\mathbf{q}_-)\\ &-\ \frac{E_h(\mathbf{q}_-)[i\nu_n-E_h(\mathbf{q}_-)]}{i\omega_-+E_h(\mathbf{q}_-)}\\ &-\ \frac{E_l(\mathbf{q}_+)[i\nu_n+E_l(\mathbf{q}_+)]}{i\omega_++E_l(\mathbf{q}_+)}\ ,\end{aligned} \tag{F.44}$$

$$\begin{aligned}\frac{\omega_+\omega_-}{i\omega_- - E_h(\mathbf{q}_-)} - \frac{\omega_+\omega_-}{i\omega_+ - E_l(\mathbf{q}_+)} &= i\nu_n - E_l(\mathbf{q}_+) + E_h(\mathbf{q}_-) \\ &+ \frac{E_h(\mathbf{q}_-)[i\nu_n + E_h(\mathbf{q}_-)]}{i\omega_- - E_h(\mathbf{q}_-)} \\ &+ \frac{E_l(\mathbf{q}_+)[i\nu_n - E_l(\mathbf{q}_+)]}{i\omega_+ - E_l(\mathbf{q}_+)} \,, \end{aligned} \tag{F.45}$$

$$\begin{aligned}\frac{\omega_+\omega_-}{i\omega_- - E_h(\mathbf{q}_-)} - \frac{\omega_+\omega_-}{i\omega_+ + E_l(\mathbf{q}_+)} &= i\nu_n + E_l(\mathbf{q}_+) + E_h(\mathbf{q}_-) \\ &+ \frac{E_h(\mathbf{q}_-)[i\nu_n + E_h(\mathbf{q}_-)]}{i\omega_- - E_h(\mathbf{q}_-)} \\ &- \frac{E_l(\mathbf{q}_+)[i\nu_n + E_l(\mathbf{q}_+)]}{i\omega_+ + E_l(\mathbf{q}_+)} \,, \end{aligned} \tag{F.46}$$

$$\begin{aligned}\frac{\omega_+\omega_-}{i\omega_- + E_h(\mathbf{q}_-)} - \frac{\omega_+\omega_-}{i\omega_+ - E_l(\mathbf{q}_+)} &= i\nu_n - E_l(\mathbf{q}_+) - E_h(\mathbf{q}_-) \\ &- \frac{E_h(\mathbf{q}_-)[i\nu_n - E_h(\mathbf{q}_-)]}{i\omega_- + E_h(\mathbf{q}_-)} \\ &+ \frac{E_l(\mathbf{q}_+)[i\nu_n - E_l(\mathbf{q}_+)]}{i\omega_+ - E_l(\mathbf{q}_+)} \,. \end{aligned} \tag{F.47}$$

Then, after using these identities and evaluating the Matsubara sums, we obtain after some algebraic manipulations the following result

$$\begin{aligned} S_{+-}^{\omega_+\omega_-} &= -\frac{1}{2[(i\nu_n)^2 - [E_l(\mathbf{q}_+) + E_h(\mathbf{q}_-)]^2]} \\ &- \frac{[i\nu_n - E_h(\mathbf{q}_-)]f(E_l(\mathbf{q}_+))}{[i\nu_n + E_l(\mathbf{q}_+)]^2 - E_h^2(\mathbf{q}_-)} + \frac{[i\nu_n + E_h(\mathbf{q}_-)]f(E_l(\mathbf{q}_+))}{[i\nu_n - E_l(\mathbf{q}_+)]^2 - E_h^2(\mathbf{q}_-)} \\ &+ \frac{[i\nu_n + E_l(\mathbf{q}_+)]f(E_h(\mathbf{q}_-))}{[i\nu_n + E_h(\mathbf{q}_-)]^2 - E_l^2(\mathbf{q}_+)} - \frac{[i\nu_n - E_l(\mathbf{q}_+)]f(E_h(\mathbf{q}_-))}{[i\nu_n - E_h(\mathbf{q}_-)]^2 - E_l^2(\mathbf{q}_+)} \,. \end{aligned} \tag{F.48}$$

Therefore, using Eq. (F.17), Eq. (F.33) and Eq. (F.48) into Eq. (F.38), we obtain that

$$\mathcal{K}_{\rm PS}^{FF}(\mathbf{P}, \nu_n) = \mathcal{K}_{\rm PS}^{FF}(\mathbf{P}, \nu_n)|_{\rm div} + \mathcal{K}_{\rm PS}^{FF}(\mathbf{P}, \nu_n)|_{\rm fin} \tag{F.49}$$

with the divergent part $\mathcal{K}^{FF}_{\rm PS}(\mathbf{P},\nu_n)|_{\rm div}$ given by

$$\begin{aligned}\mathcal{K}^{FF}_{\rm PS}(\mathbf{P},\nu_n)|_{\rm div} &= -\frac{16}{P^2}\int_{\mathbf{q}}\Bigg\{\frac{(i\nu_n)^2}{2[(i\nu_n)^2-[E_l(\mathbf{q}_+)+E_h(\mathbf{q}_-)]^2]}\\ &+ \frac{(i\nu_n)^2[E_l(\mathbf{q}_+)(\mathbf{P}\cdot\mathbf{q}_-)-E_h(\mathbf{q}_-)(\mathbf{P}\cdot\mathbf{q}_+)]}{2E_l(\mathbf{q}_+)E_h(\mathbf{q}_-)[(i\nu_n)^2-[E_l(\mathbf{q}_+)+E_h(\mathbf{q}_-)]^2]}\\ &- \frac{(\mathbf{P}\cdot\mathbf{q}_-)(\mathbf{P}\cdot\mathbf{q}_+)[E_l(\mathbf{q}_+)+E_h(\mathbf{q}_-)]}{2E_l(\mathbf{q}_+)E_h(\mathbf{q}_-)[(i\nu_n)^2-[E_l(\mathbf{q}_+)+E_h(\mathbf{q}_-)]^2]}\Bigg\}\\ &+ \frac{1}{2}\mathcal{K}^{EE}_{\rm S}(\mathbf{P},\nu_n)|_{\rm div}\ ,\end{aligned} \tag{F.50}$$

and for the case of the finite part $\mathcal{K}^{FF}_{\rm PS}(\mathbf{P},\nu_n)|_{\rm fin}$ we will not give the explicit expression because it contain a lot terms more than in Eq. (F.36). The last equation is exactly Eq. (D.17) after integrating in the time variable. Therefore, we have

$$\begin{aligned}\mathcal{K}^{FF}_{\rm PS}(\mathbf{P},-i\omega)|_{\rm div} &= 8\frac{(M_l^2-M_h^2)}{2(\mathbf{P}^2+\omega^2)}\left[I_{\rm quad}(M_h^2)-I_{\rm quad}(M_l^2)\right]\\ &- \frac{8(M_l+M_h)^2[\mathbf{P}^2+\omega^2+(\Delta M_{hl})^2]}{2(\mathbf{P}^2+\omega^2)}\\ &\times \left[I_{\log}(M_0^2)-Z_0(M_l^2,M_h^2,(\mathbf{P}^2+\omega^2);M_0^2)\right]\\ &+ \frac{8}{(\mathbf{P}^2+\omega^2)}P_\mu P_\nu\bar{D}_{\mu\nu}(M_0^2).\end{aligned} \tag{F.51}$$

Again, similar to the case of $T=0$, to obtain the temperature dependence of the pseudoscalar meson masses and BS amplitudes, we have to solve the eigenvalue problem defined by Eq. (F.1), but evaluated at the rest frame of the meson, $\mathbf{P}=0$, and taking $\omega = m_{\rm PS}$.

To summary, we will present the results for the temperature dependence BS kernels obtained above with the rest frame configuration. Then, the divergent and finite contributions of the kernel $\mathcal{K}^{EE}_{\rm PS}(\mathbf{0},-i\omega)$ are

$$\begin{aligned}\mathcal{K}^{EE}_{\rm PS}(\mathbf{0},-i\omega)|_{\rm div} &= 8\Big\{I_{\rm quad}(M_l^2)+I_{\rm quad}(M_h^2)-\left[\omega^2+(\Delta M_{hl})^2\right]\\ &\times \left[I_{\log}(M_0^2)-Z_0(M_l^2,M_h^2,\omega^2;M_0^2)\right]\\ &+ \left(\eta_+^2+\eta_-^2\right)A_{\mu\nu}(M_0^2)P_\mu P_\nu\Big\},\end{aligned} \tag{F.52}$$

with $P=(0,-i\omega)$, and the finite part of the kernel is given by

$$\begin{aligned}
\mathcal{K}^{EE}_{\rm PS}(\mathbf{0},-i\omega)|_{\rm fin} &= -8\int_{\mathbf{q}}\Bigg\{\frac{f(E_l(\mathbf{q}))}{2E_l(\mathbf{q})}+\frac{f(E_h(\mathbf{q}))}{2E_h(\mathbf{q})}+\frac{\left[\omega^2+(\Delta M_{hl})^2\right]}{4E_l(\mathbf{q})E_h(\mathbf{q})}\\
&\times\ \Bigg[\frac{2E_h(\mathbf{q})f(E_l(\mathbf{q}))}{[\omega+E_l(\mathbf{q})]^2-E_h^2(\mathbf{q})}+\frac{2E_h(\mathbf{q})f(E_l(\mathbf{q}))}{[\omega-E_l(\mathbf{q})]^2-E_h^2(\mathbf{q})}\\
&+\ \frac{2E_l(\mathbf{q})f(E_h(\mathbf{q}))}{[\omega+E_h(\mathbf{q})]^2-E_l^2(\mathbf{q})}+\frac{2E_l(\mathbf{q})f(E_h(\mathbf{q}))}{[\omega-E_h(\mathbf{q})]^2-E_l^2(\mathbf{q})}\Bigg]\Bigg\}. \qquad \text{(F.53)}
\end{aligned}$$

Now, the divergent and finite parts of the kernel $\mathcal{K}^{EF}_{\rm PS}(\mathbf{0},-i\omega)$ are given respectively by

$$\begin{aligned}
\mathcal{K}^{EF}_{\rm PS}(\mathbf{0},-i\omega)|_{\rm div} &= \frac{8\omega^2}{M_{lh}}\Bigg\{(M_l-M_h)Z_1(M_l^2,M_h^2,\omega^2;M_0^2)\\
&-\ M_lZ_0(M_l^2,M_h^2,\omega^2;M_0^2)+\frac{M_h+M_l}{2}I_{\log}(M_0^2)\Bigg\}\\
&+\ \frac{4A_{\mu\nu}(M_0^2)}{M_{lh}}(M_l-M_h)P_\mu P_\nu(\eta_+-\eta_-)\ , \qquad \text{(F.54)}\\
\mathcal{K}^{EF}_{\rm PS}(\mathbf{0},-i\omega)|_{\rm fin} &= \frac{8}{M_{l,h}}\int_{\mathbf{q}}\Bigg\{\frac{[(M_l-M_h)E_h(\mathbf{q})-\omega M_h]f(E_h(\mathbf{q}))}{2E_h(\mathbf{q}_-)[[\omega+E_h(\mathbf{q})]^2-E_l^2(\mathbf{q})]}\\
&-\ \frac{[(M_l-M_h)E_h(\mathbf{q})+\omega M_h]f(E_h(\mathbf{q}))}{2E_h(\mathbf{q})[[\omega-E_h(\mathbf{q})]^2-E_l^2(\mathbf{q})]}\\
&+\ \frac{[(M_l-M_h)E_l(\mathbf{q})-\omega M_l]f(E_l(\mathbf{q}))}{2E_l(\mathbf{q})[[\omega-E_l(\mathbf{q})]^2-E_h^2(\mathbf{q})]}\\
&-\ \frac{[(M_l-M_h)E_l(\mathbf{q})+\omega M_l]f(E_l(\mathbf{q}))}{2E_l(\mathbf{q})[[\omega+E_l(\mathbf{q})]^2-E_h^2(\mathbf{q})]}\Bigg\}, \qquad \text{(F.55)}
\end{aligned}$$

and finally, the divergent and finite parts of the kernel $\mathcal{K}^{FF}_{\rm PS}(\mathbf{0},-i\omega)$ are

$$\begin{aligned}
\mathcal{K}^{FF}_{\rm PS}(\mathbf{0},-i\omega)|_{\rm div} &= 8\frac{(M_l^2-M_h^2)}{2\omega^2}\left[I_{\rm quad}(M_h^2)-I_{\rm quad}(M_l^2)\right]\\
&-\ \frac{8(M_l+M_h)^2[\omega^2+(\Delta M_{hl})^2]}{2\omega^2}\\
&\times\ \Bigg[I_{\log}(M_0^2)-Z_0(M_l^2,M_h^2,\omega^2;M_0^2)\Bigg]\\
&+\ \frac{8}{\omega^2}\,P_\mu P_\nu\bar{D}_{\mu\nu}(M_0^2), \qquad \text{(F.56)}\\
\mathcal{K}^{FF}_{\rm PS}(\mathbf{0},-i\omega)|_{\rm fin} &= 16\int_{\mathbf{q}}\Bigg\{\frac{[\omega+E_l(\mathbf{q})]f(E_l(\mathbf{q}))}{2[[\omega+E_l(\mathbf{q})]^2-E_h^2(\mathbf{q})]}-\frac{[\omega-E_l(\mathbf{q})]f(E_l(\mathbf{q}))}{2[[\omega-E_l(\mathbf{q})]^2-E_h^2(\mathbf{q})]}\\
&+\ \frac{[\omega+E_h(\mathbf{q})]f(E_h(\mathbf{q}))}{2[[\omega+E_h(\mathbf{q})]^2-E_l^2(\mathbf{q})]}-\frac{[\omega-E_h](\mathbf{q})f(E_h(\mathbf{q}))}{2[[\omega-E_h(\mathbf{q})]^2-E_l^2(\mathbf{q})]}\Bigg\}\\
&+\ \frac{1}{2}\mathcal{K}^{EE}_{\rm S}(\mathbf{0},-i\omega)|_{\rm fin}\ . \qquad \text{(F.57)}
\end{aligned}$$

Bibliography

[1] David J. Gross and Frank Wilczek. Ultraviolet Behavior of Nonabelian Gauge Theories. *Phys. Rev. Lett.*, 30:1343–1346, 1973.

[2] H. David Politzer. Reliable Perturbative Results for Strong Interactions? *Phys. Rev. Lett.*, 30:1346–1349, 1973.

[3] Ian C. Clöet and Craig D. Roberts. Explanation and Prediction of Observables using Continuum Strong QCD. *Prog. Part. Nucl. Phys.*, 77:1–69, 2014.

[4] Gernot Eichmann, Helios Sanchis-Alepuz, Richard Williams, Reinhard Alkofer, and Christian S. Fischer. Baryons as relativistic three-quark bound states. *Prog. Part. Nucl. Phys.*, 91:1–100, 2016.

[5] Daniele Binosi, Lei Chang, Joannis Papavassiliou, Si-Xue Qin, and Craig D. Roberts. Symmetry preserving truncations of the gap and Bethe-Salpeter equations. *Phys. Rev.*, D93(9):096010, 2016.

[6] P. Maris and P. C. Tandy. QCD modeling of hadron physics. *Nucl. Phys. Proc. Suppl.*, 161:136–152, 2006.

[7] Trang Nguyen, Nicholas A. Souchlas, and Peter C. Tandy. Soft and Hard scale QCD Dynamics in Mesons. *AIP Conf. Proc.*, 1361:142–151, 2011.

[8] N. Souchlas. A dressed quark propagator representation in the BetheSalpeter description of mesons. *J. Phys.*, G37(11):115001, 2010.

[9] N. Souchlas. Bethe-Salpeter dynamics and the constituent mass concept for heavy quark mesons. *Phys. Rev.*, D81:114019, 2010.

[10] Adnan Bashir, Lei Chang, Ian C. Cloet, Bruno El-Bennich, Yu-Xin Liu, Craig D. Roberts, and Peter C. Tandy. Collective perspective on advances in Dyson-Schwinger Equation QCD. *Commun. Theor. Phys.*, 58:79–134, 2012.

[11] María Gómez-Rocha, Thomas Hilger, and Andreas Krassnigg. First Look at HeavyLight Mesons with a Dressed QuarkGluon Vertex. *Few Body Syst.*, 56(6-9):475–480, 2015.

[12] E. Rojas, B. El-Bennich, and J. P. B. C. de Melo. Exciting flavored bound states. *Phys. Rev.*, D90:074025, 2014.

[13] M. Gómez-Rocha, T. Hilger, and A. Krassnigg. Effects of a dressed quark-gluon vertex in pseudoscalar heavy-light mesons. *Phys. Rev.*, D92(5):054030, 2015.

[14] M. Gómez-Rocha, T. Hilger, and A. Krassnigg. Effects of a dressed quark-gluon vertex in vector heavy-light mesons and theory average of the B_c^* meson mass. *Phys. Rev.*, D93(7):074010, 2016.

[15] T. Hilger and A. Krassnigg. Quasi-exotic open-flavor mesons. 2016.

[16] Thomas Hilger and Andreas Krassnigg. Charming quasi-exotic open-flavor mesons. *EPJ Web Conf.*, 137:01010, 2017.

[17] T. Hilger, M. Gómez-Rocha, A. Krassnigg, and W. Lucha. Aspects of open-flavour mesons in a comprehensive DSBSE study. 2017.

[18] R. A. Briceno et al. Issues and Opportunities in Exotic Hadrons. *Chin. Phys.*, C40(4):042001, 2016.

[19] Gastão Krein. Review of hadrons in medium. *AIP Conf. Proc.*, 1701:020012, 2016.

[20] F. E. Serna, M. A. Brito, and G. Krein. Symmetry-preserving contact interaction model for heavy-light mesons. *AIP Conf. Proc.*, 1701:100018, 2016.

[21] Yoichiro Nambu and G. Jona-Lasinio. Dynamical Model of Elementary Particles Based on an Analogy with Superconductivity. 1. *Phys. Rev.*, 122:345–358, 1961.

[22] U. Vogl and W. Weise. The Nambu and Jona Lasinio model: Its implications for hadrons and nuclei. *Prog. Part. Nucl. Phys.*, 27:195–272, 1991.

[23] S. P. Klevansky. The Nambu-Jona-Lasinio model of quantum chromodynamics. *Rev. Mod. Phys.*, 64:649–708, 1992.

[24] Tetsuo Hatsuda and Teiji Kunihiro. QCD phenomenology based on a chiral effective Lagrangian. *Phys. Rept.*, 247:221–367, 1994.

[25] Johan Bijnens. Chiral Lagrangians and Nambu-Jona-Lasinio - like models. *Phys. Rept.*, 265:369–446, 1996.

[26] G. Krein, Craig D. Roberts, and Anthony G. Williams. On the implications of confinement. *Int. J. Mod. Phys.*, A7:5607–5624, 1992.

[27] Craig D. Roberts and Anthony G. Williams. Dyson-Schwinger equations and their application to hadronic physics. *Prog. Part. Nucl. Phys.*, 33:477–575, 1994.

[28] Christian S. Fischer and Reinhard Alkofer. Nonperturbative propagators, running coupling and dynamical quark mass of Landau gauge QCD. *Phys. Rev.*, D67:094020, 2003.

[29] Dietmar Ebert, Thorsten Feldmann, and Hugo Reinhardt. Extended NJL model for light and heavy mesons without q - anti-q thresholds. *Phys. Lett.*, B388:154–160, 1996.

[30] H. J. Munczek. Dynamical chiral symmetry breaking, Goldstone's theorem and the consistency of the Schwinger-Dyson and Bethe-Salpeter Equations. *Phys. Rev.*, D52:4736–4740, 1995.

[31] A. Bender, Craig D. Roberts, and L. Von Smekal. Goldstone theorem and diquark confinement beyond rainbow ladder approximation. *Phys. Lett.*, B380:7–12, 1996.

[32] H. L. L. Roberts, A. Bashir, L. X. Gutierrez-Guerrero, C. D. Roberts, and D. J. Wilson. pi- and rho-mesons, and their diquark partners, from a contact interaction. *Phys. Rev.*, C83:065206, 2011.

[33] H. L. L. Roberts, C. D. Roberts, A. Bashir, L. X. Gutierrez-Guerrero, and P. C. Tandy. Abelian anomaly and neutral pion production. *Phys. Rev.*, C82:065202, 2010.

[34] Chen Chen, Lei Chang, Craig D. Roberts, Shaolong Wan, and David J. Wilson. Spectrum of hadrons with strangeness. *Few Body Syst.*, 53:293–326, 2012.

[35] D. J. Wilson, I. C. Cloet, L. Chang, and C. D. Roberts. Nucleon and Roper electromagnetic elastic and transition form factors. *Phys. Rev.*, C85:025205, 2012.

[36] Chen Chen, Lei Chang, Craig D. Roberts, Sebastian M. Schmidt, Shaolong Wan, and David J. Wilson. Features and flaws of a contact interaction treatment of the kaon. *Phys. Rev.*, C87:045207, 2013.

[37] Hannes L. L. Roberts, Lei Chang, Ian C. Cloet, and Craig D. Roberts. Masses of ground and excited-state hadrons. *Few Body Syst.*, 51:1–25, 2011.

[38] Kun-lun Wang, Yu-xin Liu, Lei Chang, Craig D. Roberts, and Sebastian M. Schmidt. Baryon and meson screening masses. *Phys. Rev.*, D87(7):074038, 2013.

[39] Jorge Segovia, Chen Chen, Craig D. Roberts, and Shaolong Wan. Insights into the gamma* N -¿ Delta transition. *Phys. Rev.*, C88(3):032201, 2013.

[40] Jorge Segovia, Chen Chen, Ian C. Clot, Craig D. Roberts, Sebastian M. Schmidt, and Shaolong Wan. Elastic and Transition Form Factors of the $\Delta(1232)$. *Few Body Syst.*, 55:1–33, 2014.

[41] Marco A. Bedolla, J. J. Cobos-Martnez, and Adnan Bashir. Charmonia in a contact interaction. *Phys. Rev.*, D92(5):054031, 2015.

[42] Marco A. Bedolla, Khpani Raya, J. J. Cobos-Martnez, and Adnan Bashir. η_c elastic and transition form factors: Contact interaction and algebraic model. *Phys. Rev.*, D93(9):094025, 2016.

[43] O. A. Battistel, G. Dallabona, and G. Krein. A Predictive formulation of the Nambu–Jona-Lasinio model. *Phys. Rev.*, D77:065025, 2008.

[44] O. A. Battistel and G. Dallabona. From scale properties of physical amplitudes to a predictive formulation of the Nambu-Jona-Lasinio model. *Phys. Rev.*, D80:085028, 2009.

[45] R. L. S. Farias, Dyana C. Duarte, Gasto Krein, and Rudnei O. Ramos. Thermodynamics of quark matter with a chiral imbalance. *Phys. Rev.*, D94(7):074011, 2016.

[46] O.A. Battistel. *PhD Thesis: Uma nova Estratégia para Manipulaões e Cálculos Envolvendo Divergências em TQC*. Universidade Federal de Minas Gerais, Brazil 1999.

[47] M. Sampaio, A. P. Baeta Scarpelli, B. Hiller, A. Brizola, M. C. Nemes, and S. Gobira. Comparing implicit, differential, dimensional and BPHZ renormalization. *Phys. Rev.*, D65:125023, 2002.

[48] John C. Collins. *Renormalization*, volume 26 of *Cambridge Monographs on Mathematical Physics*. Cambridge University Press, Cambridge, 1986.

[49] D. Blaschke, P. Costa, and Yu. L. Kalinovsky. D mesons at finite temperature and density in the PNJL model. *Phys. Rev.*, D85:034005, 2012.

[50] Bruno El-Bennich, Gasto Krein, Eduardo Rojas, and Fernando E. Serna. Excited hadrons and the analytical structure of bound-state interaction kernels. *Few Body Syst.*, 57(10):955–963, 2016.

[51] J. Haidenbauer and G. Krein. The Reaction $\bar{p}p \to \bar{\Lambda}_c^- - \Lambda_c^+$ close to threshold. *Phys. Lett.*, B687:314–319, 2010.

[52] J. Haidenbauer and G. Krein. Production of charmed pseudoscalar mesons in antiproton-proton annihilation. *Phys. Rev.*, D89(11):114003, 2014.

[53] J. Haidenbauer and G. Krein. $\Psi(3770)$ Resonance and Its Production in $\overline{p}p$ $D\overline{D}$. *Phys. Rev.*, D91(11):114022, 2015.

[54] G. Krein, A. W. Thomas, and K. Tsushima. J/Ψ mass shift in nuclear matter. *Phys. Lett.*, B697:136–141, 2011.

[55] K. Tsushima, D. H. Lu, G. Krein, and A. W. Thomas. J/Ψ-nuclear bound states. *Phys. Rev.*, C83:065208, 2011.

[56] T.F. Carams, C.E. Fontoura, G. Krein, K. Tsushima, J. Vijande, and A. Valcarce. Hadronic molecules with a $\bar{D}$ meson in a medium. *Phys. Rev.*, D94(3):034009, 2016.

[57] Paul Romatschke and Ulrike Romatschke. Viscosity Information from Relativistic Nuclear Collisions: How Perfect is the Fluid Observed at RHIC? *Phys. Rev. Lett.*, 99:172301, 2007.

[58] Matthew Luzum and Paul Romatschke. Conformal Relativistic Viscous Hydrodynamics: Applications to RHIC results at $\sqrt{(}s_{NN}) = 200$ GeV. *Phys. Rev.*, C78:034915, 2008.

[59] Huichao Song and Ulrich W. Heinz. Suppression of elliptic flow in a minimally viscous quark-gluon plasma. *Phys. Lett.*, B658:279–283, 2008.

[60] Huichao Song and Ulrich W. Heinz. Multiplicity scaling in ideal and viscous hydrodynamics. *Phys. Rev.*, C78:024902, 2008.

[61] Victor Roy, A. K. Chaudhuri, and Bedangadas Mohanty. Comparison of results from a 2+1D relativistic viscous hydrodynamic model to elliptic and hexadecapole flow of charged hadrons measured in Au-Au collisions at $\sqrt{s_{\rm NN}}$ = 200 GeV. *Phys. Rev.*, C86:014902, 2012.

[62] Ulrich Heinz, Chun Shen, and Huichao Song. The viscosity of quark-gluon plasma at RHIC and the LHC. *AIP Conf. Proc.*, 1441:766–770, 2012.

[63] H. Niemi, G. S. Denicol, P. Huovinen, E. Molnar, and D. H. Rischke. Influence of a temperature-dependent shear viscosity on the azimuthal asymmetries of transverse momentum spectra in ultrarelativistic heavy-ion collisions. *Phys. Rev.*, C86:014909, 2012.

[64] Bjorn Schenke, Sangyong Jeon, and Charles Gale. Higher flow harmonics from (3+1)D event-by-event viscous hydrodynamics. *Phys. Rev.*, C85:024901, 2012.

[65] Peter Brockway Arnold, Guy D. Moore, and Laurence G. Yaffe. Transport coefficients in high temperature gauge theories. 1. Leading log results. *JHEP*, 11:001, 2000.

[66] Joseph I. Kapusta. Viscous Properties of Strongly Interacting Matter at High Temperature. *Landolt-Bornstein*, 23:563–580, 2010.

[67] Peter Brockway Arnold, Caglar Dogan, and Guy D. Moore. The Bulk Viscosity of High-Temperature QCD. *Phys. Rev.*, D74:085021, 2006.

[68] Antonio Dobado and Silvia N. Santalla. Pion gas viscosity at low temperature and density. *Phys. Rev.*, D65:096011, 2002.

[69] Antonio Dobado and Felipe J. Llanes-Estrada. The Viscosity of meson matter. *Phys. Rev.*, D69:116004, 2004.

[70] Azwinndini Muronga. Shear viscosity coefficient from microscopic models. *Phys. Rev.*, C69:044901, 2004.

[71] Sean Gavin. Transport coefficients in ultra-relativistic heavy-ion collisions. *Nuclear Physics A*, 435(3-4):826–843, 1985.

[72] Madappa Prakash, Manju Prakash, R. Venugopalan, and G. Welke. Nonequilibrium properties of hadronic mixtures. *Phys. Rept.*, 227:321–366, 1993.

[73] P. Rehberg, S. P. Klevansky, and J. Hufner. Elastic scattering and transport coefficients for a quark plasma in SU-f(3) at finite temperatures. *Nucl. Phys.*, A608:356–388, 1996.

[74] P. Kovtun, Dan T. Son, and Andrei O. Starinets. Viscosity in strongly interacting quantum field theories from black hole physics. *Phys. Rev. Lett.*, 94:111601, 2005.

[75] A. Bazavov et al. Equation of state in (2+1)-flavor QCD. *Phys. Rev.*, D90:094503, 2014.

[76] Szabolcs Borsanyi, Zoltan Fodor, Sandor D. Katz, Stefan Krieg, Claudia Ratti, and Kalman Szabo. Fluctuations of conserved charges at finite temperature from lattice QCD. *JHEP*, 01:138, 2012.

[77] Harvey B. Meyer. A Calculation of the bulk viscosity in SU(3) gluodynamics. *Phys. Rev. Lett.*, 100:162001, 2008.

[78] Chihiro Sasaki and Krzysztof Redlich. Transport coefficients near chiral phase transition. *Nucl. Phys.*, A832:62–75, 2010.

[79] Rudy Marty, Elena Bratkovskaya, Wolfgang Cassing, Jrg Aichelin, and Hamza Berrehrah. Transport coefficients from the Nambu-Jona-Lasinio model for $SU(3)_f$. *J. Phys. Conf. Ser.*, 509:012052, 2014.

[80] Kerstin Paech and Scott Pratt. Origins of bulk viscosity in relativistic heavy ion collisions. *Phys. Rev.*, C74:014901, 2006. [Erratum: Phys. Rev.C93,no.5,059902(2016)].

[81] J. Chadwick. Possible Existence of a Neutron. *Nature*, 129:312, 1932.

[82] W. Heisenberg. On the structure of atomic nuclei. *Z. Phys.*, 77:1–11, 1932.

[83] Hideki Yukawa. On the Interaction of Elementary Particles I. *Proc. Phys. Math. Soc. Jap.*, 17:48–57, 1935. [Prog. Theor. Phys. Suppl.1,1(1935)].

[84] G. D. Rochester and C. C. Butler. Evidence for the Existence of New Unstable Elementary Particles. *Nature*, 160:855–857, 1947.

[85] Murray Gell-Mann. The Eightfold Way: A Theory of strong interaction symmetry. 1961.

[86] Yuval Ne'eman. Derivation of strong interactions from a gauge invariance. *Nucl. Phys.*, 26:222–229, 1961.

[87] Murray Gell-Mann. Symmetries of baryons and mesons. *Phys. Rev.*, 125:1067–1084, 1962.

[88] V. E. Barnes et al. Observation of a Hyperon with Strangeness -3. *Phys. Rev. Lett.*, 12:204–206, 1964.

[89] Murray Gell-Mann. A Schematic Model of Baryons and Mesons. *Phys. Lett.*, 8:214–215, 1964.

[90] G. Zweig. An SU(3) model for strong interaction symmetry and its breaking. Version 1. 1964.

[91] G. Zweig. An SU(3) model for strong interaction symmetry and its breaking. Version 2. In D.B. Lichtenberg and Simon Peter Rosen, editors, *DEVELOPMENTS IN THE QUARK THEORY OF HADRONS. VOL. 1. 1964 - 1978*, pages 22–101. 1964.

[92] F. E. Close. *An Introduction to Quarks and Partons*. 1979.

[93] E. Eichten, K. Gottfried, T. Kinoshita, K. D. Lane, and Tung-Mow Yan. Charmonium: The Model. *Phys. Rev.*, D17:3090, 1978.

[94] Andre Martin. A fit of upsilon and charmonium spectra. *Physics Letters B*, 93(3):338–342, 1980.

[95] C. Quigg and Jonathan L. Rosner. Quarkonium Level Spacings. *Phys. Lett.*, 71B:153–157, 1977.

[96] Xiao-tong Song and He-fen Lin. A New Potential Model for Heavy Quarkonium. *Z. Phys.*, C34:223, 1987.

[97] D. B. Lichtenberg, E. Predazzi, R. Roncaglia, M. Rosso, and J. G. Wills. Testing Static Quark - Anti-quark Potentials With Bottomonium. *Z. Phys.*, C41:615, 1989.

[98] M. Y. Han and Yoichiro Nambu. Three Triplet Model with Double SU(3) Symmetry. *Phys. Rev.*, 139:B1006–B1010, 1965.

[99] M. Gell-Mann. Quarks. *Acta Phys. Austriaca Suppl.*, 9:733–761, 1972.

[100] A. A. Slavnov. Ward identities in gauge theories. *Theoretical and Mathematical Physics*, 10(2):99–104, 1972.

[101] J.C. Taylor. Ward identities and charge renormalization of the yang-mills field. *Nuclear Physics B*, 33(2):436 – 444, 1971.

[102] C Becchi, A Rouet, and R Stora. Renormalization of gauge theories. *Annals of Physics*, 98(2):287 – 321, 1976.

[103] I. V. Tyutin. Gauge Invariance in Field Theory and Statistical Physics in Operator Formalism. 1975.

[104] P. Pascual and R. Tarrach. QCD: RENORMALIZATION FOR THE PRACTITIONER. *Lect. Notes Phys.*, 194:1–277, 1984.

[105] Gerard 't Hooft and M. J. G. Veltman. Regularization and Renormalization of Gauge Fields. *Nucl. Phys.*, B44:189–213, 1972.

[106] M. E. Peskin and D. V. Schroeder. *An Introduction to Quantum Field Theory.* Addison-Wesley, 1995.

[107] C. Itzykson and J.B. Zuber. *Quantum Field Theory.* McGraw-Hill, 1980.

[108] Christof Gattringer and Christian B. Lang. Quantum chromodynamics on the lattice. *Lect. Notes Phys.*, 788:1–343, 2010.

[109] Zoltan Fodor and Christian Hoelbling. Light Hadron Masses from Lattice QCD. *Rev. Mod. Phys.*, 84:449, 2012.

[110] S. Aoki et al. Review of lattice results concerning low-energy particle physics. *Eur. Phys. J.*, C77(2):112, 2017.

[111] F. J. Dyson. The S matrix in quantum electrodynamics. *Phys. Rev.*, 75:1736–1755, 1949.

[112] Julian S. Schwinger. On the Green's functions of quantized fields. 1. *Proc. Nat. Acad. Sci.*, 37:452–455, 1951.

[113] Julian S. Schwinger. On the Green's functions of quantized fields. 2. *Proc. Nat. Acad. Sci.*, 37:455–459, 1951.

[114] S. M. Dorkin, M. Viebach, L. P. Kaptari, and B. Kampfer. Extending the truncated Dyson-Schwinger equation to finite temperatures. 2015. [J. Mod. Phys.7,2071(2016)].

[115] Reinhard Alkofer and Lorenz von Smekal. The Infrared behavior of QCD Green's functions: Confinement dynamical symmetry breaking, and hadrons as relativistic bound states. *Phys. Rept.*, 353:281, 2001.

[116] B. A. Lippmann and Julian Schwinger. Variational Principles for Scattering Processes. I. *Phys. Rev.*, 79:469–480, 1950.

[117] E. E. Salpeter and H. A. Bethe. A Relativistic equation for bound state problems. *Phys. Rev.*, 84:1232–1242, 1951.

[118] Murray Gell-Mann and Francis Low. Bound states in quantum field theory. *Phys. Rev.*, 84:350–354, Oct 1951.

[119] Julian Schwinger. On the greens functions of quantized fields. i. *Proceedings of the National Academy of Sciences*, 37(7):452–455, 1951.

[120] Hideji Kita. Relativistic two-body problem*. *Progress of Theoretical Physics*, 7(2):217, 1952.

[121] John M. Cornwall, R. Jackiw, and E. Tomboulis. Effective Action for Composite Operators. *Phys. Rev.*, D10:2428–2445, 1974.

[122] C.H Llewellyn Smith. A relativistic formulation of the quark model for mesons. *Annals of Physics*, 53(3):521 – 558, 1969.

[123] C. H. Llewellyn-Smith. A relativistic formulation for the quark model for mesons. *Annals Phys.*, 53:521–558, 1969.

[124] Pieter Maris and Craig D. Roberts. Pi- and K meson Bethe-Salpeter amplitudes. *Phys. Rev.*, C56:3369–3383, 1997.

[125] L. X. Gutierrez-Guerrero, A. Bashir, I. C. Cloet, and C. D. Roberts. Pion form factor from a contact interaction. *Phys. Rev.*, C81:065202, 2010.

[126] R. L. S. Farias, G. Dallabona, G. Krein, and O. A. Battistel. Extension of the Nambu-Jona-Lasinio model at high densities and temperatures using an implicit regularization scheme. *Phys. Rev.*, C77:065201, 2008.

[127] R. Casalbuoni, Raoul Gatto, G. Nardulli, and M. Ruggieri. Aspects of the color flavor locking phase of QCD in the Nambu-Jona Lasinio approximation. *Phys. Rev.*, D68:034024, 2003.

[128] B. El-Bennich, O. Leitner, J. P. Dedonder, and B. Loiseau. The Scalar Meson f0(980) in Heavy-Meson Decays. *Phys. Rev.*, D79:076004, 2009.

[129] Edson O. da Silva, J. P. B. C. de Melo, Bruno El-Bennich, and Victo S. Filho. Pion and kaon elastic form factors in a refined light-front model. *Phys. Rev.*, C86:038202, 2012.

[130] Bruno El-Bennich, J. P. B. C. de Melo, and T. Frederico. A combined study of the pion's static properties and form factors. *Few Body Syst.*, 54:1851–1863, 2013.

[131] J. P. B. C. de Melo, K. Tsushima, Bruno El-Bennich, E. Rojas, and T. Frederico. Pion structure in the nuclear medium. *Phys. Rev.*, C90(3):035201, 2014.

[132] George H. S. Yabusaki, Ishtiaq Ahmed, M. Ali Paracha, J. P. B. C. de Melo, and Bruno El-Bennich. Pseudoscalar mesons with symmetric bound state vertex functions on the light front. *Phys. Rev.*, D92(3):034017, 2015.

[133] B. El-Bennich, J. P. B. C. de Melo, B. Loiseau, J. P. Dedonder, and T. Frederico. Modeling electromagnetic form-factors of light and heavy pseudoscalar mesons. *Braz. J. Phys.*, 38:465–471, 2008.

[134] B. El-Bennich, M. A. Ivanov, and C. D. Roberts. Flavourful hadronic physics. *Nucl. Phys. Proc. Suppl.*, 199:184–190, 2010.

[135] R. L. S. Farias, G. Dallabona, G. Krein, and O. A. Battistel. Cutoff-independent regularization of four-fermion interactions for color superconductivity. *Phys. Rev.*, C73:018201, 2006.

[136] R. L. S. Farias, G. Krein, G. Dallabona, and O. A. Battistel. Mesonic correlation functions at finite temperature in the NJL model. *Nucl. Phys.*, A790:332–335, 2007.

[137] Bruno El-Bennich, Gastao Krein, Lei Chang, Craig D. Roberts, and David J. Wilson. Flavor SU(4) breaking between effective couplings. *Phys. Rev.*, D85:031502, 2012.

[138] Bruno El-Bennich, M. Ali Paracha, Craig D. Roberts, and Eduardo Rojas. Couplings between the ρ and D- and D^*-mesons. *Phys. Rev.*, D95(3):034037, 2017.

[139] O. A. Battistel and G. Krein. Quark clustering and chiral symmetry breaking in nuclear matter. *Mod. Phys. Lett.*, A18:2255–2264, 2003.

[140] C. Patrignani et al. Review of Particle Physics. *Chin. Phys.*, C40(10):100001, 2016.

[141] Pieter Maris, Craig D. Roberts, and Peter C. Tandy. Pion mass and decay constant. *Phys. Lett.*, B420:267–273, 1998.

[142] Peter C. Tandy.

[143] Pieter Maris and Peter C. Tandy. Bethe-Salpeter study of vector meson masses and decay constants. *Phys. Rev.*, C60:055214, 1999.

[144] Damir Becirevic, Vittorio Lubicz, Francesco Sanfilippo, Silvano Simula, and Cecilia Tarantino. D-meson decay constants and a check of factorization in non-leptonic B-decays. *JHEP*, 02:042, 2012.

[145] J. I. Kapusta and Charles Gale. *Finite-temperature field theory: Principles and applications*. Cambridge University Press, 2011.

[146] Michel Le Bellac. *Thermal Field Theory*. Cambridge University Press, 2011.

[147] Craig D. Roberts and Sebastian M. Schmidt. Dyson-Schwinger equations: Density, temperature and continuum strong QCD. *Prog. Part. Nucl. Phys.*, 45:S1–S103, 2000.

[148] Axel Bender, David Blaschke, Yuri Kalinovsky, and Craig D. Roberts. Continuum study of deconfinement at finite temperature. *Phys. Rev. Lett.*, 77:3724–3727, 1996.

[149] S.K. Adhikari. *Variational Principles and the Numerical Solution of Scattering Problems*. A Wiley-Interscience publication. Wiley, 1998.

[150] T. Hatsuda and T. Kunihiro. Pion and σ Meson at Finite Temperature. *Prog. Theor. Phys. Suppl.*, 91:284–298, 1987.

[151] Yu. L. Kalinovsky, A. E. Radzhabov, and M. K. Volkov. Scalar sigma meson at finite temperature in nonlocal quark model. In *Round Table Discussion on Searching for the Mixed Phase of a Strongly Interacting Matter at JINR Nuclotron Dubna, Russia, July 7-9, 2005*, 2005.

[152] P. Maris, Craig D. Roberts, S. M. Schmidt, and P. C. Tandy. T - dependence of pseudoscalar and scalar correlations. *Phys. Rev.*, C63:025202, 2001.

[153] Sabyasachi Ghosh. A real-time thermal field theoretical analysis of Kubo-type shear viscosity: Numerical understanding with simple examples. *Int. J. Mod. Phys.*, A29:1450054, 2014.

[154] F. O. Gottfried and S. P. Klevansky. Thermodynamics of open and hidden charmed mesons within the NJL model. *Phys. Lett.*, B286:221–224, 1992.

[155] D. N. Zubarev. *Non-Equilibrium Statistical Thermodynamics*. Consultants Bureau, 1974.

[156] Ryogo Kubo. Statistical mechanical theory of irreversible processes. 1. General theory and simple applications in magnetic and conduction problems. *J. Phys. Soc. Jap.*, 12:570–586, 1957.

[157] Akio Hosoya, Masa-aki Sakagami, and Masaru Takao. Nonequilibrium Thermodynamics in Field Theory: Transport Coefficients. *Annals Phys.*, 154:229, 1984.

[158] Paul Romatschke. New Developments in Relativistic Viscous Hydrodynamics. *Int. J. Mod. Phys.*, E19:1–53, 2010.

[159] Tetsufumi Hirano, Naomi van der Kolk, and Ante Bilandzic. Hydrodynamics and Flow. *Lect. Notes Phys.*, 785:139–178, 2010.

[160] P. Chakraborty and J. I. Kapusta. Quasi-Particle Theory of Shear and Bulk Viscosities of Hadronic Matter. *Phys. Rev.*, C83:014906, 2011.

[161] S. Gavin. TRANSPORT COEFFICIENTS IN ULTRARELATIVISTIC HEAVY ION COLLISIONS. *Nucl. Phys.*, A435:826–843, 1985.

[162] Robert Lang, Norbert Kaiser, and Wolfram Weise. Shear viscosities from Kubo formalism in a large-N_c Nambu-Jona-Lasinio model. *Eur. Phys. J.*, A51(10):127, 2015.

[163] H. Arthur Weldon. Simple Rules for Discontinuities in Finite Temperature Field Theory. *Phys. Rev.*, D28:2007, 1983.

[164] Rudy Marty, Elena Bratkovskaya, Wolfgang Cassing, Jrg Aichelin, and Hamza Berrehrah. Transport coefficients from the Nambu-Jona-Lasinio model for $SU(3)_f$. *Phys. Rev.*, C88:045204, 2013.

[165] Sandeep Chatterjee and Kirtimaan A. Mohan. Including the Fermion Vacuum Fluctuations in the $(2+1)$ flavor Polyakov Quark Meson Model. *Phys. Rev.*, D85:074018, 2012.

[166] Abhijit Bhattacharyya, Paramita Deb, Sanjay K. Ghosh, Rajarshi Ray, and Subrata Sur. Thermodynamic Properties of Strongly Interacting Matter in Finite Volume using Polyakov-Nambu-Jona-Lasinio Model. *Phys. Rev.*, D87(5):054009, 2013.

[167] Sabyasachi Ghosh, Thiago C. Peixoto, Victor Roy, Fernando E. Serna, and Gasto Krein. Shear and bulk viscosities of quark matter from quark-meson fluctuations in the NambuJona-Lasinio model. *Phys. Rev.*, C93(4):045205, 2016.

[168] S. Plumari, A. Puglisi, F. Scardina, and V. Greco. Shear Viscosity of a strongly interacting system: Green-Kubo vs. Chapman-Enskog and Relaxation Time Approximation. *Phys. Rev.*, C86:054902, 2012.

[169] Robert Lang and Wolfram Weise. Shear viscosity from Kubo formalism: NJL model study. *Eur. Phys. J.*, A50:63, 2014.

[170] P. Zhuang, J. Hufner, S. P. Klevansky, and L. Neise. Transport properties of a quark plasma and critical scattering at the chiral phase transition. *Phys. Rev.*, D51:3728–3738, 1995.

[171] Frithjof Karsch, Dmitri Kharzeev, and Kirill Tuchin. Universal properties of bulk viscosity near the QCD phase transition. *Phys. Lett.*, B663:217–221, 2008.

[172] Antonio Dobado and Juan M. Torres-Rincon. Bulk viscosity and the phase transition of the linear sigma model. *Phys. Rev.*, D86:074021, 2012.

[173] J. Haidenbauer, G. Krein, Ulf-G. Meissner, and A. Sibirtsev. Anti-D N interaction from meson-exchange and quark-gluon dynamics. *Eur. Phys. J.*, A33:107–117, 2007.

[174] J. Haidenbauer, G. Krein, Ulf-G. Meissner, and A. Sibirtsev. Charmed meson rescattering in the reaction anti-p d —¿ anti-D N. *Eur. Phys. J.*, A37:55–67, 2008.

[175] J. Haidenbauer, G. Krein, Ulf-G. Meissner, and L. Tolos. DN interaction from meson exchange. *Eur. Phys. J.*, A47:18, 2011.

[176] C. E. Fontoura, G. Krein, and V. E. Vizcarra. $\bar{D}$N interaction in a color-confining chiral quark model. *Phys. Rev.*, C87(2):025206, 2013.

[177] Kazuo Tsushima, Ding-Hui Lu, Anthony William Thomas, K. Saito, and R. H. Landau. Charmed mesic nuclei. *Phys. Rev.*, C59:2824–2828, 1999.

[178] C. Garcia-Recio, J. Nieves, and L. Tolos. D mesic nuclei. *Phys. Lett.*, B690:369–375, 2010.

[179] C. Garcia-Recio, J. Nieves, L. L. Salcedo, and L. Tolos. D^- mesic atoms. *Phys. Rev.*, C85:025203, 2012.

[180] Su Houng Lee and C. M. Ko. Charmonium in nuclear matter. *Phys. Rev.*, C67:038202, 2003.

[181] Gastao Krein. SU(4)-flavor symmetry breaking in hadron couplings. *PoS*, ConfinementX:144, 2012.

[182] Gasto Krein. Charmed hadrons in matter and SU(4) flavor symmetry. *EPJ Web Conf.*, 73:05001, 2014.

[183] C. E. Fontoura, J. Haidenbauer, and G. Krein. SU(4) flavor symmetry breaking in D-meson couplings to light hadrons. *Eur. Phys. J.*, A53(5):92, 2017.

[184] Alfonso Ballon-Bayona, Gastao Krein, and Carlisson Miller. Strong couplings and form factors of charmed mesons in holographic QCD. *Phys. Rev.*, D96(1):014017, 2017.